兰州理工大学

科研成果汇总

学　　号：	211081101008
研 究 生：	周　勃
导　　师：	李二超　教授
研究方向：	综合能源系统优化控制
论文题目：	计及共享储能的多区域综合能源系统鲁棒优化调度研究
学　　科：	控制理论与控制工程
学　　院：	电气工程与信息工程学院
入学时间：	2021 年 9 月

目 录

机构：兰州理工大学 电气工程与信息工程学院

姓名：周勃　[211081101008]

著者要求对其在国内外学术出版物所发表的科技论著被以下数据库收录情况进行查证。

检索范围：

- 科学引文索引（Science Citation Index Expanded）：1900年-2024年

检索结果：

检索类型	数据库	年份范围	总篇数	第一作者篇数
SCI-E 收录	SCI-EXPANDED	2024 - 2025	4	4

委托人声明：

本人委托兰州理工大学图书馆查询论著被指定检索工具收录情况，经核对检索结果，附件中所列文献均为本人论著，特此声明。

作　　者（签字）：周勃

完成人（签字）：刘婧

完　成　日　期：2024年11月5日

完成单位（盖章）：兰州理工大学图书馆信息咨询与学科服务部

（本检索报告仅限校内使用）

图书馆

文献检索报告
SCI-E 收录

报告编号：**R2024-1059 SCI-E 收录**

数据库：科学引文索引 (Science Citation Index Expanded) 时间范围：**2024年至2025年**	作者姓名：周勃 作者单位：兰州理工大学 电气工程 与信息工程学院	检索人员：刘婧 检索日期：**2024年11月5日**

检索结果：被 **SCI-E** 收录文献 **4** 篇

#	作者	地址	标题	来源出版物	文献类型	入藏号
1	**Zhou, B**; Li, ER	[Zhou, Bo; Li, Erchao] Lanzhou Univ Technol, Coll Elect Engn & Informat Engn, Lanzhou 730050, Peoples R China.	Multi-Regional Integrated Energy Economic Dispatch Considering Renewable Energy Uncertainty and Electric Vehicle Charging Demand Based on Dynamic Robust Optimization	***ENERGIES*** 2024, 17 (11): 2453.	J Article	WOS:0012 452776000 01
2	**Zhou, B**; Li, ER	[Zhou, Bo; Li, Erchao] Lanzhou Univ Technol, Coll Elect Engn & Informat Engn, Lanzhou 730050, Peoples R China.	Dynamic Robust Optimization Method Based on Two-Stage Evaluation and Its Application in Optimal Scheduling of Integrated Energy System	***APPLIED SCIENCES-BASEL*** 2024, 14 (12): 4997.	J Article	WOS:0012 545275000 01
3	**Zhou, B**; Li, ER	[Zhou, Bo; Li, Erchao] Lanzhou Univ Technol, Coll Elect & Informat Engn, Lanzhou 730050, Peoples R China.	An Improved Dynamic Robust Optimization Algorithm and Its Application in Optimal Scheduling of Integrated Energy System Considering Carbon Emission Reduction	***IEEE ACCESS*** 2024, 12: 115642-115656.	J Article	WOS:0013 034267000 01
4	**Zhou, B**; Li, EC	[Zhou, Bo; Li, Erchao] Lanzhou Univ Technol, Coll Elect & Informat Engn, Lanzhou 730050, Peoples R China.	Research on robust optimal operation strategy of regional integrated energy system considering heating network transmission model	***ELECTRIC POWER SYSTEMS RESEARCH*** 2025, 238: 111046.	J Article	WOS:0013 124497000 01
					合计	4

Multi-Regional Integrated Energy Economic Dispatch Considering Renewable Energy Uncertainty and Electric Vehicle Charging Demand Based on Dynamic Robust Optimization

Bo Zhou * and Erchao Li

College of Electrical Engineering and Information Engineering, Lanzhou University of Technology,
Lanzhou 730050, China; lecstarr@163.com
* Correspondence: zhoubo@lut.edu.cn

Abstract: Aiming at the problem of source-load uncertainty caused by the increasing penetration of renewable energy and the large-scale integration of electric vehicles (EVs) into modern power system, a robust optimal operation scheduling algorithm for regional integrated energy systems (RIESs) with such uncertain situations is urgently needed. Based on this background, aiming at the problem of the irregular charging demand of EV, this paper first proposes an EV charging demand model based on the trip chain theory. Secondly, a multi-RIES optimization operation model including a shared energy storage station (SESS) and integrated demand response (IDR) is established. Aiming at the uncertainty problem of renewable energy, this paper transforms this kind of problem into a dynamic robust optimization with time-varying parameters and proposes an improved robust optimization over time (ROOT) algorithm based on the scenario method and establishes an optimal scheduling mode with the minimum daily operation cost of a multi-regional integrated energy system. Finally, the proposed uncertainty analysis method is verified by an example of multi-RIES. The simulation results show that in the case of the improved ROOT proposed in this paper to solve the robust solution of renewable energy, compared with the traditional charging load demand that regards the EVs as a whole, the EV charging load demand based on the trip chain can reduce the cost of EV charging by 3.5% and the operating cost of the multi-RIES by 11.7%. With the increasing number of EVs, the choice of the starting point of the future EV trip chain is more variable, and the choice of charging methods is more abundant. Therefore, modeling the charging demand of EVs under more complex trip chains is the work that needs to be studied in the future.

Keywords: integrated energy system; electric vehicle; energy storage system; robust optimization; renewable uncertainty; optimal scheduling

1. Introduction

In the face of increasingly serious energy and environmental problems, building an energy-sustainable and environmentally friendly development strategy is a key issue of common concern in the world today [1,2]. A regional integrated energy system (RIES), which is based on a renewable energy source (RES) and combined cooling heating and power (CCHP), can improve energy efficiency due to its complementary characteristics between energy sources and energy ladder utilization characteristics [3,4]. However, with the increasing penetration of RES and the massive access of electric vehicles (EVs) as loads to RIES, the RIES faces more uncertainties due to the RES's inherent randomness and volatility and EVs' irregular charging time and charging power. Based on the above background, it is of great theoretical and practical significance to study the RIES optimal scheduling method considering the uncertainty of RESs and EVs [5].

Large-scale EV access to a power grid will bring problems such as increased network loss and decreased power quality to the power grid [6]. In reference [7], a model considering advanced support vector machine (SVM) and hybrid electric vehicle (EV) charging demand

is proposed, and the influence of hybrid EV charging on the whole system is studied. Considering the dual attributes of EVs with load and energy storage equipment, reference [8,9] proposed that the orderly participation of EVs in grid activities can reduce the load peak–valley gap and improve the scheduling flexibility. Reference [10] proposes that EVs, as a flexible energy storage carrier, can smooth the energy fluctuations caused by the uncertainty of RESs, and through the guidance of electricity price, EVs can improve the consumption rate of the RES to a certain extent. For the coordinated scheduling problem of EVs in integrated energy system, reference [11] proposed an EV charging behavior framework based on time-of-use (TOU) electricity price guidance to attract EVs users to charge during the valley price period. On the basis of the TOU electricity price, reference [12] proposes that when the load is at the peak, the EVs can be used as a power source to discharge to the system to a smooth load curve. Example results show that a certain scale of EVs can be used as a backup power source to alleviate the system operating pressure during peak periods. Reference [13] also proposes a decentralized EV scheduling strategy based on the TOU electricity price. In reference [14], an optimization model with the objective of minimizing household energy consumption is established for EV home users with self-use energy storage equipment. Experimental results show that the reasonable use of EV charging and discharging can reduce the cost of energy consumption. However, most of the current research only focuses on the charging and discharging behavior of an EV at a fixed time of place and does not fully consider the characteristics of the non-fixed-time random charging of an EV during use, which is very common in the use of EV.

Due to the unpredictability of the natural environment in which RES equipment is located, there is a high uncertainty in RES output, which is one of the main reasons for the uncertainty of the power supply side. In order to solve the uncertainty of RES, reference [15] proposed a prediction method based on a deep learning approach (DLA) from the perspective of prediction. Reference [16] by assigning the probability to chance constraint of each constraint event, the complex combinatorial chance constraint is transformed into a severalty chance constraint for solution. Reference [17] uses the method of support vector machine to identify zero-probability events, improve the average distribution of intersection probability, and improve the reliability of the consequences. In reference [18], an algorithm based on Wasserstein Gan with gradient penalty (WGAN-GP) is proposed to delineate the scenarios of renewable energy. In reference [19], the uncertainty problem is modeled by improving the generative adversarial network. In reference [20], they propose a two-stage distributed robust optimization algorithm and integrate a data-driven approach to deal with these uncertainty problems. In reference [21], a two-stage model is established to solve the uncertainty of a RES and the economy of power grid operation, and experimental results show that this model can achieve system robustness while reducing operating costs.

At present, most of the research on the charging behavior of an EV connected to the power grid regards the EV as a whole part and conducts charging and discharging behavior at a fixed time, while ignoring the randomness of the individual charging behavior of the EV; meanwhile, most of the research on the uncertainty of RESs based on scenario method does not consider whether data after scenario reduction are robust. Aiming at these problems in current research, in this paper, the charging demand model of EV is established based on the trip chain theory, and an improved robust optimization over time (ROOT) algorithm based on the scenario method is proposed to solve the uncertainty problem of RESs. The main contributions are as follows:

1. Aimed at the randomness of EV charging behavior, a charging demand model of an EV based on trip chain theory is proposed;
2. Aimed at the RES uncertainty problem, an improved robust optimization over time algorithm based on the scenario method is proposed;
3. Based on the existing comprehensive demand response, a cold–heat–electric alternative integrated demand response (IDR) model is proposed.

The rest of this paper is structured as follows. Section 2 introduces the basic structure of the RIES, IDR and shared energy storage station (SESS). In Section 3, the EV charging demand model based on the trip chain theory is established. In Section 4, the algorithm for solving the uncertainty of RES is proposed. In Section 5, the optimization model is established. Section 6 presents example analysis and finally, the conclusions are given in Section 7.

2. Structure Modeling of RIES Based on SESS and IDR

2.1. Overall Framework of RIES

The structure of RIES is shown in Figure 1. It is known from Figure 1 that the RIES includes several CCHPs in different regions, and each CCHP is connected to the external power network, gas network and water network. Each CCHP provides cold, heat and electricity energy supply for their respective energy users. At the same time, a power transmission node is established at each CCHP, which is connected to the SESS through the node. Because there is no direct electrical interaction between each CCHP in this region, CCHP can only interact with the external power grid (EPG) or SESS through the power network.
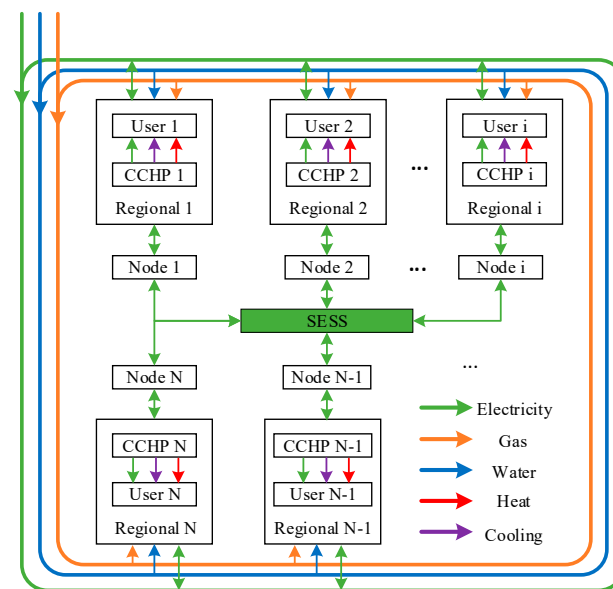

Figure 1. The structure of RIES with SESS.

For any CCHP $i(i \in N)$ shown in Figure 1, its internal structure is shown in Figure 2. It is known from Figure 2 that CCHP is mainly composed of the following components: energy supply, energy conversion, energy demand and energy exchange. The energy supply part comprises a wind turbine (WT), photovoltaic (PV), gas turbine (GT) and gas boiler (GB), and EPG, which is connected to the CCHP via a transformer. The energy conversion part comprises a waste heat boiler (WHB), electric boiler (EB), absorption chiller (AC), heat exchanger (HE), electrical chiller (EC) and electric storage (ES). The energy demand part comprises electrical, cooling and heating loads. The energy exchange part mainly comprises the SESS, EV, other CCHPs, external energy market and carbon market, etc. The CCHP receives the natural gas and the electric energy provided by the EPG and RES included in the energy supply and converts it into the energy needed by the user through the energy coupling device of the energy conversion, and finally provides it to the energy demand. At the same time, the CCHP also participates in other forms of energy interaction mentioned in the energy exchange. This paper mainly studies the interaction between the CCHP, EV and SESS. The detailed modeling work of the equipment in CCHP can be found in reference [22], which will not be introduced in this paper.
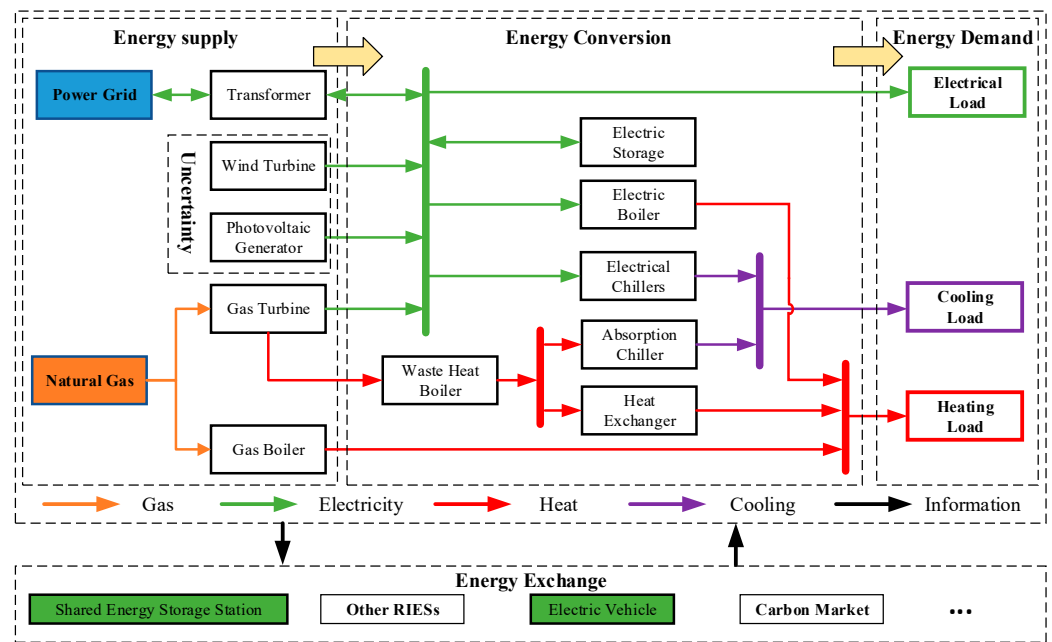
Figure 2. The structure of the CCHP.

2.2. Modeling of SESS

An SESS usually refers to a model in which a public energy storage device provides energy storage services to multiple users [23,24]. An SESS utilizes the difference and complementarity of load curves of different users, and through the integration and optimization, to improve the utilization of energy storage equipment, the level of RES consumption and the user's benefit, so as to realize value creation [25–27]. An SESS should satisfy the following constraints.

2.2.1. Power Continuity Constraint

Under the action of the user's charging and discharging behavior, the internal energy of SESS should remain continuous.

$$E_t^{SESS} = \left(1 - \eta_{SESS}^{loss}\right)E_{t-1}^{SESS} + (\eta_{SESS}^{abs}P_t^{SESS,abs} - \frac{1}{\eta_{SESS}^{relea}}P_t^{SESS,relea})\Delta t, \tag{1}$$

where E_t^{SESS} and E_{t-1}^{SESS} are the state of charge (SOC) of the SESS at time t and $t-1$, respectively; $P_t^{SESS,abs}$ and $P_t^{SESS,relea}$ are the charge and discharge power at time t, respectively; η_{SESS}^{loss}, η_{SESS}^{abs} and η_{SESS}^{relea} are the self-discharge, charge and discharge efficiency, respectively; and Δt is the scheduling time interval.

2.2.2. SOC Constraints

The SOC of SESS cannot exceed the design parameters of its equipment.

$$\begin{cases} \sigma_{SESS}^{\min}E_{\max}^{SESS} \leq E_t^{SESS} \leq \sigma_{SESS}^{\max}E_{\max}^{SESS} \\ E_{start}^{SESS} = \sigma_{SESS}^{init}E_{\max}^{SESS} = E_{end}^{SESS} \end{cases}, \tag{2}$$

where $E_{\max}^{SESS}$, E_{start}^{SESS} and E_{end}^{SESS} are the maximum, initial and final SOC of the SESS, respectively; $\sigma_{SESS}^{\min}$, $\sigma_{SESS}^{\max}$ and σ_{SESS}^{init} are the lower limit, upper limit and initial coefficient of the SOC, respectively.

2.2.3. Charge and Discharge Constraints

There can be no simultaneous charging and discharging behavior between the SESS and the user.

$$\begin{cases} 0 \le P_t^{SESS,abs} \le P_{\max}^{SESS} U_{abs}^{SESS} \\ 0 \le P_t^{SESS,relea} \le P_{\max}^{SESS} U_{relea}^{SESS} \\ U_{abs}^{SESS} + U_{relea}^{SESS} \le 1 \\ U_{abs}^{SESS} \in \{0,1\} U_{relea}^{SESS} \in \{0,1\} \end{cases}, \tag{3}$$

where $P_{\max}^{SESS}$ is the maximum power of the SESS; U_{abs}^{SESS} and U_{relea}^{SESS} are the charging and discharging state bits of the SESS at time *t*, respectively.

2.3. Modeling of IDR

An IDR is an important means of RIES load demand management [28]. It aims to guide power users and load aggregators to adjust energy consumption strategies through market-oriented means, actively participate in power grid valley filling, and improve the reliability of power system operation. This paper divides the IDR load into a reducible load (RL), transferable load (TL) and substituted load (SL).

2.3.1. Modeling of RL

Energy users determine whether the current load is a RL by comparing the changes in energy prices during the scheduling period. RL can be described as follows:

$$\Delta P_{RL,i}^e = \Delta P_{RL,i}^{e0} \left[\sum_{j=1}^{24} \mathbf{E}_{RL}(i,j) \frac{\rho_j - \rho_j^0}{\rho_j^0} \right], \tag{4}$$

where $\Delta P_{RL,i}^e$ is the variation in RL after IDR; $\Delta P_{RL,i}^{e0}$ is the initial RL; $\mathbf{E}_{RL}(i,j)$ is the price elasticity matrix of the RL; ρ_j is the energy price at time *j*; and ρ_j^0 is the initial energy price at time *j*.

The constraint of RL is as follows:

$$0 \le \Delta P_{RL,i}^e \le \Delta P_{RL,\max}^e, \tag{5}$$

where $\Delta P_{RL,\max}^e$ is the maximum value of $\Delta P_{RL,i}^e$.

2.3.2. Modeling of TL

TL refers to those loads the access time of which users can flexibly adjust according to their demand price. The TOU energy price is used as the signal to guide users to transfer the load from the peak price period to valley price period. TL can be described as follows:

$$\Delta P_{TL,i}^e = \Delta P_{TL,i}^{e0} \left[\sum_{j=1}^{24} \mathbf{E}_{TL}(i,j) \frac{\rho_j - \rho_j^0}{\rho_j^0} \right], \tag{6}$$

where $\Delta P_{TL,i}^e$ is the variation in the TL after IDR; $\Delta P_{TL,i}^{e0}$ is the initial TL; $\mathbf{E}_{TL}(i,j)$ is the price elasticity matrix of the TL.

The constraint of the TL is as follows:

$$0 \le \Delta P_{TL,i}^e \le \Delta P_{TL,\max}^e, \tag{7}$$

where $\Delta P_{TL,\max}^e$ is the maximum value of $\Delta P_{TL,i}^e$.

2.3.3. Modeling of SL

For those loads that can be directly supplied by electric energy or cold/heat energy, when the electricity price per unit of energy supply is less than the price of cold/heat energy, electric energy is used to substitute cold/heat energy; otherwise, cold/heat energy is used to substitute electric energy. SL can be described as follows:

$$\begin{cases} \Delta P_t^{s,e} = -\varepsilon_{e,h(c)} \Delta P_t^{s,c(h)} \\ \varepsilon_{e,c(h)} = v_e \varphi_e / v_{c(h)} \varphi_{c(h)} \end{cases}, \tag{8}$$

where $\Delta P_t^{s,e}$ and $\Delta P_t^{s,c(h)}$ are the substituted electrical load and corresponding substituted cold/heat load, respectively; $\varepsilon_{e,c(h)}$ is the electro-cold/heat substitution coefficient; v_e and $v_{c(h)}$ are unit calorific values of electric and cold/heat, respectively; and φ_e and $\varphi_{c(h)}$ are the energy efficiency of electric and cold/heat, respectively.

The constraints of SL are as follows:

$$\begin{cases} \Delta P_{\min}^{s,e} \leq \Delta P_t^{s,e} \leq \Delta P_{\max}^{s,e} \\ \Delta P_{\min}^{s,c(h)} \leq \Delta P_t^{s,c(h)} \leq \Delta P_{\max}^{s,c(h)} \end{cases}, \tag{9}$$

where $\Delta P_{\min}^{s,e}$ and $\Delta P_{\max}^{s,e}$ are the minimum and maximum substitution values of the substituted electrical load, respectively; $\Delta P_{\min}^{s,c(h)}$ and $\Delta P_{\max}^{s,c(h)}$ are the minimum and maximum substitution values of the substituted cold/heat load.

3. EV Modeling Based on Trip Chain Theory

3.1. Basic Theory of EV Trip Chain

The trip chain simulates a series of behavioral characteristics during the period from the initial point to the terminal point [29]. The EV trip chain is defined as a space–time chain formed by linking the time series and spatial state of the EV travel process, with the residence of the EV user as the starting point and terminal point. Figure 3 is the schematic diagram of the EV trip chain.
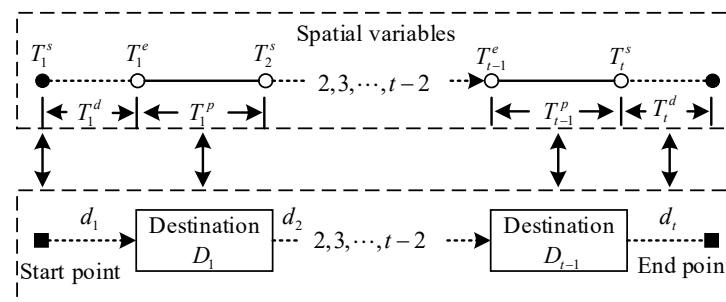

Figure 3. Schematic diagram of the EV trip chain.

The variables describing the spatial transfer of EV are called spatial variables, including destination D_t and driving distance d_t. The variables describing the change in the EV driving and stopping state are called time variables, including the start time of driving T_t^s, end time of driving T_t^e, driving time T_t^d and parking time T_t^p.

Based on the actual EV usage environment, it is known that EV travel behavior has the memoryless nature of Markov chains. That is, the destination $D_{EST}(i)$ of an EV driving at time i is only related to the last driving destination $D_{EST}(i-1)$, and is not related to any of the travel destinations $D_{EST}(n), n \in [1, \cdots, i-2]$. Based on this fact, the trip chain of EV can be regarded as a special class of Markov chain. The state of an EV at time i is E_i, and the state at the next moment is E_j. According to the Markov chain theory, the probability from E_i to E_j is as follows:

$$P(E_i \rightarrow E_j) = P(E_j | E_i) = p_{ij}, \tag{10}$$

where p_{ij} is the probability of EV transferring from the current state to the next state. Based on (1), the space transition probability matrix of EV can be expressed as follows:

$$p(t_i) = \begin{bmatrix} p_{11}(t_i) & \cdots & p_{1n}(t_i) \\ \vdots & \ddots & \vdots \\ p_{n1}(t_i) & \cdots & p_{nn}(t_i) \end{bmatrix} \forall \begin{cases} 0 \le p_{ij} \le 1, p_{ii} = 0 \\ \sum_{j=1}^{n} p_{ij} = 1 \end{cases} \quad i, j = 1, 2, \cdots, n, \quad (11)$$

In order to construct a reasonable EV trip chain, based on the data of the national household travel survey (NHTS), the NHTS divides the parking places of vehicles within one day into three types: home, work and other, and according to the data of the NHTS, the probability of EV in different parking places at the initial state ($t = 1$) is shown in Table 1.

Table 1. The probability of an EV in a different parking place at the initial state.

Initial Places D_{EST}	Home	Work	Other
Probability p	0.9810	0.0027	0.0163

3.2. Modeling of EV Trip Chain

According to the trip chain theory, the following models can be established. The probability distribution function (PDF) of T_t^s is shown as follows:

$$f(T_1^s) = \frac{1}{\sqrt{2\pi}\sigma} \exp\left[-(T_1^s - \mu)^2 / 2\sigma^2\right], \quad (12)$$

where μ and σ are the mathematical expectation of and variance in PDF, respectively.

The T_t^d obeys the normal distribution, and its PDF is as follows:

$$f\left(T_t^d\right) = \frac{1}{T_t^d \sigma \sqrt{2\pi}} \exp -\left\{ \left[\ln\left(T_t^d\right) - \mu_i\right]^2 / \left(2\sigma_i^2\right) \right\}, \quad (13)$$

The d_t can be calculated by driving time T_t^d and average speed v_{ave}. The average driving speed is affected by many factors, such as real-time traffic conditions. According to <China's major urban traffic analysis report>, the average speed v_{ave} of automobiles in Lanzhou is 35.17 km/h. Similarly, T_t^e can be obtained by summing T_t^s and T_t^d.

The PDF of the home area parking time T_t^{hp}, working area parking time T_t^{wp} and other area parking time T_t^{op} are shown as follows:

- The PDF of the home area parking time:

$$T_t^{hp} = \frac{1.153}{195.787} \left(\frac{t_{s\_i}}{195.787}\right)^{1.153-1} e^{-(t_{s\_i}/195.787)^{1.153}}, \quad (14)$$

- The PDF of the working area parking time:

$$\begin{cases} z = \left(T_t^{wp} - 438.445\right)/164.506 \\ T_t^{wp} = \dfrac{\exp\left[-(1-0.234z)^{4.27}\right](1-0.234z)^{3.27}}{164.506} \end{cases}, \quad (15)$$

- The PDF of the other area parking time:

$$\begin{cases} z = \left(T_t^{wp} - 438.445\right)/164.506 \\ T_t^{op} = \dfrac{\exp\left[-(1-0.234z)^{4.27}\right](1-0.234z)^{3.27}}{164.506} \end{cases}, \quad (16)$$

The spatial variable is determined by the actual engineering application environment, and the time variable is obtained by (12)~(16). Based on the above data, a complete EV trip

chain can be constructed to obtain the EV charging load demand of each charging station in a scheduling day.

4. Uncertainty Analysis of Renewable Energy Based on Scenario Method and Improved Robust Optimization over Time

In the actual engineering environment, there are many uncertain factors affecting RES. Therefore, from the perspective of cybernetics, this paper regarded a WT and PV as a kind of time-varying factor, transformed the uncertainty of an RES into a kind of dynamic optimization problem with time-varying parameters, and focused on the robustness of output data in the time domain. ROOT is a new algorithm for solving dynamic optimization problems with time-varying parameters. Its central idea is to find a time–domain robust solution and make the solution applicable to a variety of changing environments to improve the stability and robustness of the system operation. Therefore, the ROOT algorithm is more feasible than the traditional optimization algorithm in practical engineering problems [30,31]. At the same time, this paper used the Latin hypercube sampling (LHS) and backward reduction (BR) scenario method as a pre-method to establish the renewable energy output curve, which can make the time-varying factors transformed by the wind power output curve and the photovoltaic processing curve contained in the established dynamic optimization problem as close as possible to the actual output of renewable energy and obtain a more realistic time–domain robust solution.

4.1. Scene Analysis Method

The scene analysis method mainly includes two parts: scene generation and scene reduction. Scene generation refers to the large-scale scenarios with uncertain characteristics obtained by sampling according to the PDF or statistical characteristics of the research object, which can be represented by the set $S = \{S_1, S_2, \cdots, S_N\}$. In this paper, LHS was used as a method for scene generation. Scene reduction reduces the number of similar scenes by analyzing the data set of set S, obtains the expected number of scenes, and reduces computational complexity. In this paper, BR was used as a method for scene reduction. The set $K = \{K_1, K_2, \cdots, K_M\}$, composed of a small number of classical scenes, was obtained by BR, which can represent the random variables of the original scene to a large extent. The process is shown in Figure 4.
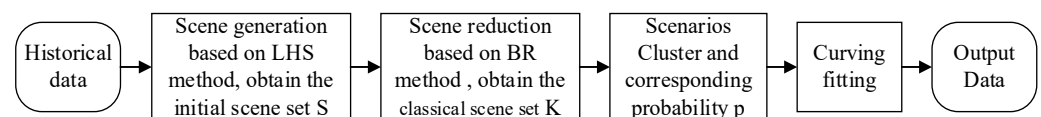

Figure 4. Process of scenario analysis.

4.1.1. Scene Generation Based on LHS

LHS can divide a large interval into several fixed intervals, generates a probability value P_m in each interval $[m/l, (m+1)/l]$, then reorders the intervals according to the probability value of each interval. LHS was used to sample multiple renewable uncertain data at the hourly level, and the sample set was constructed by using sampling results.

4.1.2. Scene Reduction Based on BR

In order to merge the similar scenes more effectively, a scene reduction model based on BR was constructed to process the large amount data. We defined the stochastic scenario $w_m = (obj_{m,1}, obj_{m,2}, \cdots, obj_{m,t}, \cdots, obj_{m,T})$, where $obj_{m,t}$ is the reduced object at time t in m-th scene; then, we defined the probability of the occurrence of scenario w_n as p_n. The distance between w_m and w_n can be described as follows:

$$d(w_m, w_n) = \sqrt{\sum_{t=0}^{T}(w_{m,t} - w_{n,t})^2}, \tag{17}$$

The objective of BR is to minimize the probabilistic distance between the set of scenes before reduction and the set of scenes retained after reduction, which can be described as follows:

$$F^{BR} = \min\sum_{i=1}^{J} p_i d\left(w_i, w_j\right) j \notin J, \tag{18}$$

where J is the set of deleted scenes for scene reduction.

4.1.3. Curving Fitting

According to the number of scenarios $Cluster_i$ obtained from the scenario reduction and probability of occurrence of the corresponding scenarios p_i, it is possible to calculate optimal RES output fitting curve $P_{i,t,opt}^{WT/PV}$, which can be described as follows:

$$P_{i,t,opt}^{WT/PV} = \sum_{c=1}^{C} (Cluster_i \times p_i), \tag{19}$$

where C is the number of scenes after scene reduction, which is specified by the decision maker. Then, we could fit curve $P_{i,t,opt}^{WT/PV}$, and the algebraic expression could be obtained. The specific steps of the scene analysis method proposed in this paper are shown in Figure 5.
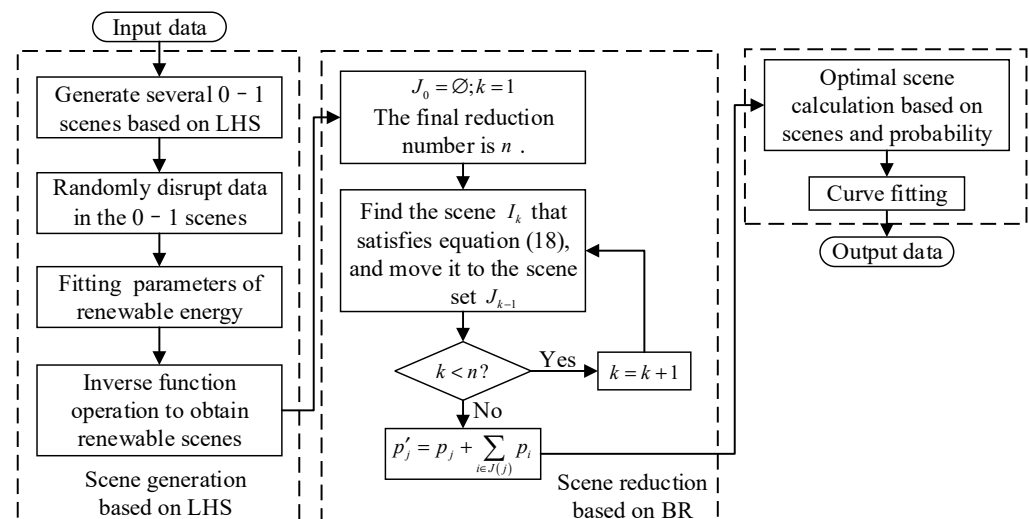

Figure 5. The specific steps of scenario analysis.

4.2. Uncertainty Analysis of Renewable Energy Based on the Scenario Method and Improved Robust Optimization over Time

4.2.1. Description of Renewable Uncertainty Problem

The optimal scheduling result of the RIES is based on the establishment of robustness, and robustness requires RIES to be able to maintain stability under different operating environments. Therefore, this paper considered predicting the minimum output of the RES. According to the fitting curve of RES output obtained by LHS and BR, the optimization problem with time-varying parameters was established as follows:

$$P_{i,t}^{RG} = \min f\left(P_{i,t}^{WT} + P_{i,t}^{PV}\right), \tag{20}$$

where $P_{i,t}^{RG}$ is the output of renewable generation; f is the objective function; and $P_{i,t}^{WT}$ and $P_{i,t}^{PV}$ are the output of the WT and PV, respectively, and are both time-varying parameters. Suppose that $P_{i,t}^{WT}$ and $P_{i,t}^{PV}$ are constants that remain constant, and each change only occurs at the scheduling time point. That is, in a fixed period of time $[0, T]$, the optimization problem described by (17) can be re-formulated as follows: with the change in parameters

$P_{i,t}^{WT}$ and $P_{i,t}^{PV}$, it is divided into a sequence of functions composed of multiple static functions. These can be described as follows:

$$\left\langle f\left(P_{i,1}^{WT}, P_{i,1}^{PV}\right), \ldots, f\left(P_{i,t}^{WT}, P_{i,t}^{PV}\right), \ldots, f\left(P_{i,T}^{WT}, P_{i,T}^{PV}\right)\right\rangle, \tag{21}$$

From the above analysis, it can be seen that for the dynamic optimization problem with time-varying parameters shown in (21), ROOT has good engineering application value because it can find the robust solutions of the time-varying elements of the WT and PV in the time domain of the dynamic optimization problem. Therefore, ROOT was introduced to solve the problem. However, most ROOT algorithms need to use future predicted fitness values to find solutions with better robustness. However, the existing methods ignore the influence of prediction error on the robustness of the solution, and the prediction error is large, so it is difficult to find a better robust solution. In order to reduce the influence of prediction error on the robustness of the solution, this paper makes full use of the change trend of the fitness value of the solution in the historical moment and the future moment and guides the algorithm to select the better solution of survival time (ST) and average fitness (AF) [32] in the solution space. At the same time, by analyzing the characteristic quantity of the change in the fitness value of the solution, the limitation of the prediction error on the robustness optimization is reduced.

4.2.2. Improved ROOT

This paper introduces two new evaluation metrics: feasible direction (FD) and stability degree (SD), to reduce the influence of the error of predicted value on the robustness evaluation of ROOT solution. Based on these new evaluation metrics, a ROOT based on the characteristics change in fitness value (ROOT-CCFV) was proposed, so that the optimal solution obtained by ROOT-CCFV could have better robustness in multiple dynamic environments.

- Feasible direction

The FD $R^{FD}(x, t, p, q)$ is used to describe the change trend of function.

$$R^{FD}(x, t, p, q) = \frac{1}{p + q + 1} \sum_{i=t-p}^{t+q} |f(x, \alpha_{i+1}) - f(x, \alpha_i)|, \tag{22}$$

where x is the decision variable, t is the current moment; p is the number of historical environments; q is the number of future environments; and α is the time-varying parameter. The magnitude of FD is proportional to the change in objective function value: a large FD indicates that current objection function value changes with more magnitude at that moment.

- Stability degree

The SD $R^{SD}(x, t, p, q)$ is used to describe the stability of the predicted value.

$$\begin{aligned} R^{SD}(x, t, p, q) &= \frac{f(x, \alpha_j) - [\max f(x, \alpha_i) + \min f(x, \alpha_i)]}{\eta} \\ s.t. \ \ i &\in [1, p], j \in [t+1, q], \eta \in [1, +\infty) \end{aligned}, \tag{23}$$

where η is the fluctuation threshold. When the SD is positive, it means that the objective function of the solution in the current environment is not smaller than the mean value curve of the known objective function.

- ROOT-CCFV

In ROOT-CCFV, the FD and SD of the solutions are firstly judged, and the better solution is selected, then the robustness of the selected solutions is evaluated by ST and AF, and finally the optimal robust solution satisfying the actual requirements is obtained. The algorithm flow based on scenario method and ROOT-CCFV is shown in Figure 6.
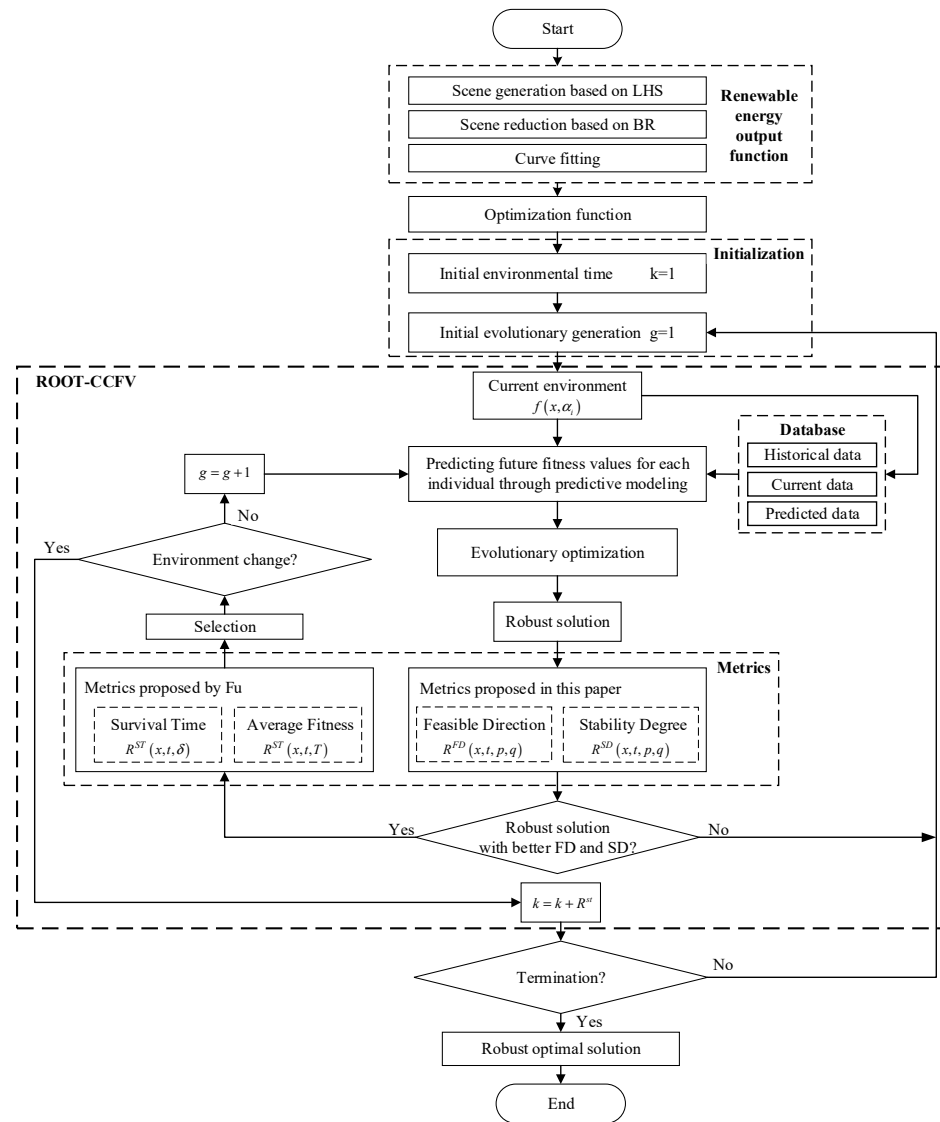
Figure 6. Process of ROOT-CCFV based on the scenario method.

5. Optimal Scheduling Model Considering EV and Renewable Energy Uncertainty

5.1. Optimization Objective

The objective functions are expressed as follows:

$$\min C_{IES} = C_{grid} + C_{gas} + C_{om} + C_{sess}, \tag{24}$$

where C_{grid} and C_{gas} are the electrical energy transaction expenditure and gas energy transaction expenditure with EPG, respectively; C_{om} is the operation and maintenance expenditure of RIES; and C_{sess} is the energy transaction expenditure with SESS.

$$C_{grid} = \sum_{i=1}^{N} \sum_{t=1}^{T} \left(c_{b,t}^{gird} P_{i,t}^{Grid,buy} - c_{s,t}^{gird} P_{i,t}^{Grid,sell} \right) \Delta t, \tag{25}$$

where N is the number of CCHP; i is the ith CCHP; T is the length of the scheduling period; t is the time period t; $c_{b,t}^{gird}$ is the purchase price of electricity energy from the EPG; $P_{i,t}^{Grid,buy}$ is the purchase power of electricity; $c_{s,t}^{gird}$ is the price of electricity energy sold to the EPG; and $P_{i,t}^{Grid,sell}$ is the sale power of electricity.

$$C_{gas} = \sum_{i=1}^{N} \sum_{t=1}^{T} c_{gas} \left[P_{i,t}^{GT} / \left(\eta_i^{GT} H_{ng} \right) + H_{i,t}^{GB} / \left(\eta_i^{GB} H_{ng} \right) \right] \Delta t, \tag{26}$$

where c_{gas} is the price of natural gas; $P_{i,t}^{GT}$ and $H_{i,t}^{GB}$ are the electrical and heat power output of the GT and GB, respectively; η_i^{GT} and η_i^{GB} are the efficiencies of the GT and GB, respectively; and H_{ng} is the heating value of natural gas.

$$C_{om} = \sum_{i=1}^{N} \sum_{t=1}^{T} \left(K_{om}^{Elec} P_{i,t}^{Elec} + K_{om}^{Heat} H_{i,t}^{Heat} + K_{om}^{Cold} C_{i,t}^{Cold} \right) \Delta t, \tag{27}$$

where K_{om}^{Elec}, K_{om}^{Heat} and K_{om}^{Cold} are the operating and maintenance expenditure of electric energy equipment, heat energy equipment and cold energy equipment, respectively; $P_{i,t}^{Elec}$, $H_{i,t}^{Heat}$ and $C_{i,t}^{Cold}$ are the output of electric power, heat power and cold power of various types of energy equipment, respectively.

$$C_{sess} = \sum_{i=1}^{N} \sum_{t=1}^{T} \left(c_{b,t}^{sess} P_{i,t}^{SESS,cha} - c_{s,t}^{sess} P_{i,t}^{SESS,dis} \right) \Delta t, \tag{28}$$

where $c_{b,t}^{sess}$ is the purchase price of electricity energy from the SESS; $c_{s,t}^{sess}$ is the price of electricity energy sold to the SESS.

5.2. Operational Constraints

From the system structure shown in Figures 1 and 2, the constraints can be categorized into CCHP equipment constraints, SESS equipment constraints and coupling constraints between CCHP and the SESS, as shown in Table 2.

Table 2. Details of operational constraints.

Constraint Type	CCHP	SESS	Coupling Relationship
Equality constraints	1. Power bus energy balance constraints 2. Electric storage energy relationship constraints	Energy continuity constraint	CCHP-SESS energy coupling constraint
Inequality constraints	1. Equipment operating power constraints 2. Electric storage charging/discharging power constraints	1. Charging/discharging power constraints 2. Capacity constraints	/

CCHP constraints are detailed in references [22,33], and SESS constraints are detailed in Section 2.2. Compared with an RIES without an SESS, the RIES with an SESS increases the energy coupling link between CCHP and the SESS, as follows:

$$\sum_{i=1}^{N} \left(P_{i,t}^{SESS,dis} - P_{i,t}^{SESS,cha} \right) = P_t^{SESS,relea} - P_t^{SESS,abs}, \tag{29}$$

where $P_{i,t}^{SESS,cha}$ and $P_{i,t}^{SESS,dis}$ are the charging and discharging of the ith CCHP using the SESS at time period t.

In particular, the heat energy emitted by the WHB in CCHP constructed in this paper simultaneously supplies the AC and HE, so it is necessary to add the heat energy balance constraint between the WHB, AC and HE, as follows:

$$H_{i,t}^{HE} / \eta_{he} + C_{i,t}^{AC} / \eta_{ac} = H_{i,t}^{GT} \gamma_{gt} \eta_{whb}, \tag{30}$$

where $H_{i,t}^{HE}$ is the heat output power of the HE; η_{he} is the efficiency of the HE; $C_{i,t}^{AC}$ is the cold output power of the AC; η_{ac} is the energy efficiency ratio of the AC; $H_{i,t}^{GT}$ is the heat

output power of the GT; γ_{gt} is the thermoelectric ratio of the GT; and η_{whb} is the efficiency of the WHB.

5.3. Optimization Method

After introducing the RES power data obtained based on ROOT-CCFV into the optimal scheduling model, the model became a mixed-integer linear programming (MILP) model. The decision variables were the output of each piece of equipment in CCHPs, the input and output of the SESS and the purchase and sale of energy from the EPG. At present, the MILP model has a mature solution algorithm and can be directly solved by CPLEX 12.10, GUROBI 9.5.1 and other commercial software. In this paper, YALMIP20230622 + CPLEX12.10 was used to simulate and solve the optimal scheduling problems.

6. Case Study

6.1. Simulation System

We took a comprehensive area as an example, as shown in Figure 7. The area was divided into four sub-regions: the residential area (RA), commercial area (CA), industrial area (IA) and office area (OA). Each sub-region had CCHP, and each CCHP was interconnected with the SESS and EPG through the regional power gird to form an RIES.
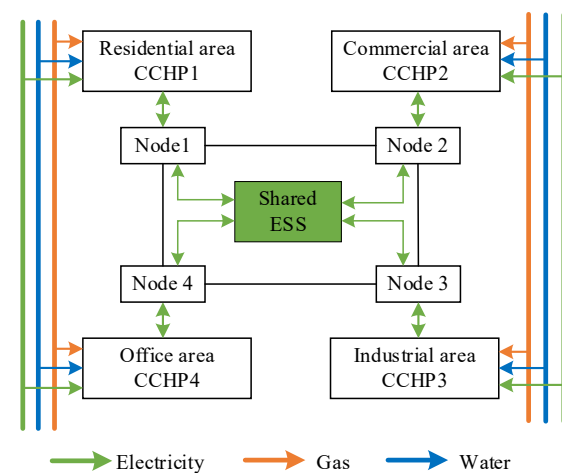

Figure 7. Structure partition diagram of RIES.

Among them, the RA and OA are not separately configured with an ES, and the CA and IA are configured with independent ES. The parameters of each piece of equipment in CCHP are shown in Tables A1 and A2. The historical output curve of the RES and historical load curve in each region are shown in Figure 8.
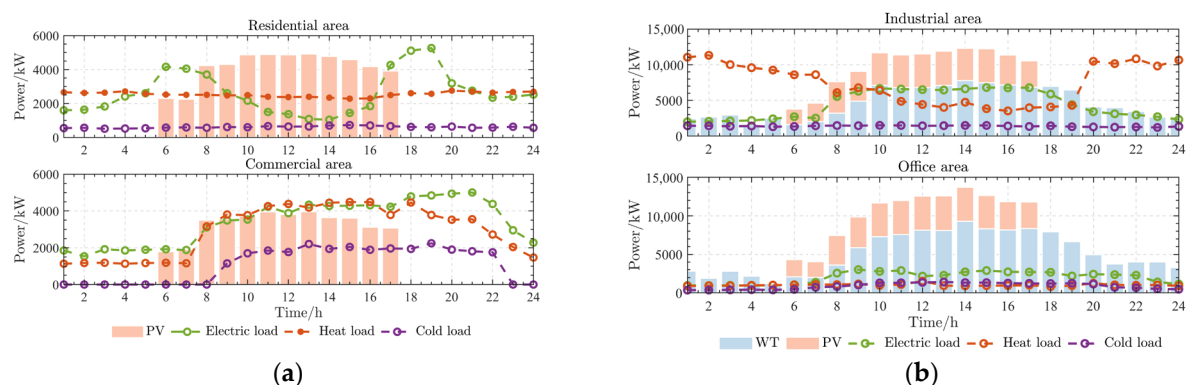

(**a**) (**b**)

Figure 8. The historical output curve of the RES and historical load curve in each region. (**a**) The output and load data of the RA and CA. (**b**) The output and load data of the IA and OA.

The parameters of the SESS are shown in Table A3, and the TOU price of EPG and the SESS are shown in Tables A4 and A5. The price of natural gas was 2.46 CNY/m^3, and the calorific value of natural gas was 9.78 kWh/m^3. The scheduling period of each typical day was 24 h.

6.2. Simulation Results and Analysis

6.2.1. Analysis of Charging Demand of EV

This paper considered the most important travel purpose of EV, supposing that EVs drive up to four times a day and the last drive is to return to the RA. The spatial transfer probability of the driving can be found in reference [29]. While ignoring traffic congestion and short-term parking for non-main travel purposes, the EV can only be charged after reaching the travel destination. This paper assumed that this region contained 2000 EVs, the initial SOC of each EV was a random number of 0.6~0.8, the power consumption per kilometer was a random number of 0.1~0.25 kWh, the EV battery capacity was a random number of 25~35 kWh, and the maximum charging power of charging piles in each area was 5 kW. The relationship between T_t^d and d_t is referred to in [34]. According to Section 3, the EV charging demand in each region could be obtained, as shown in Figure 9.
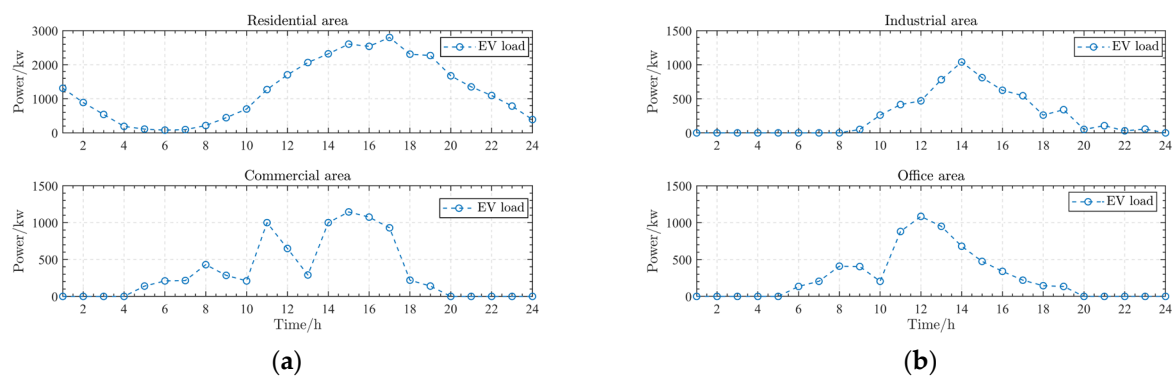

Figure 9. The charging demand of EV in each region. (**a**) The charging demand of the RA and CA. (**b**) The charging demand of the IA and OA.

As can be seen from Figure 9, the RA bears the largest demand of EV charging. The charging valley was 05:00–07:00, and the charging peak was 16:00–18:00, which is in line with the regularity of commuting and traveling for most users. Combined with Figure 7, it can be seen that the IA was the farthest from the RA, so the IA had EV charging demand start from 09:00, while the CA and OA had EV charging demand at an earlier time node. Since it was assumed that the EVs return to the RA for the last trip, the other areas assumed charging demand after 20:00 tended to zero. From the above analysis, it can be seen that the method proposed in this paper can reflect the complex driving, parking rules and charging demand of EV in the daytime, so that each region can obtain a value closer to the actual EV charging demand, so as to better carry out the optimal scheduling work.

6.2.2. Analysis of the Effectiveness of ROOT-CCFV

Because each peak of the improved moving peak benchmark (mMPB) can change autonomously, we could test the effectiveness of the dynamic optimization algorithms when facing the dynamic environment well. This paper used mMPB as the test function to verify the effectiveness of ROOT-CCFV compared with other ROOT algorithms. The parameter setting of mMPB is detailed in reference [31]. We compared the methods in references [31,32,35,36]. The results of the average time of robust solutions under different algorithms are shown in Figure 10 and Table 3.
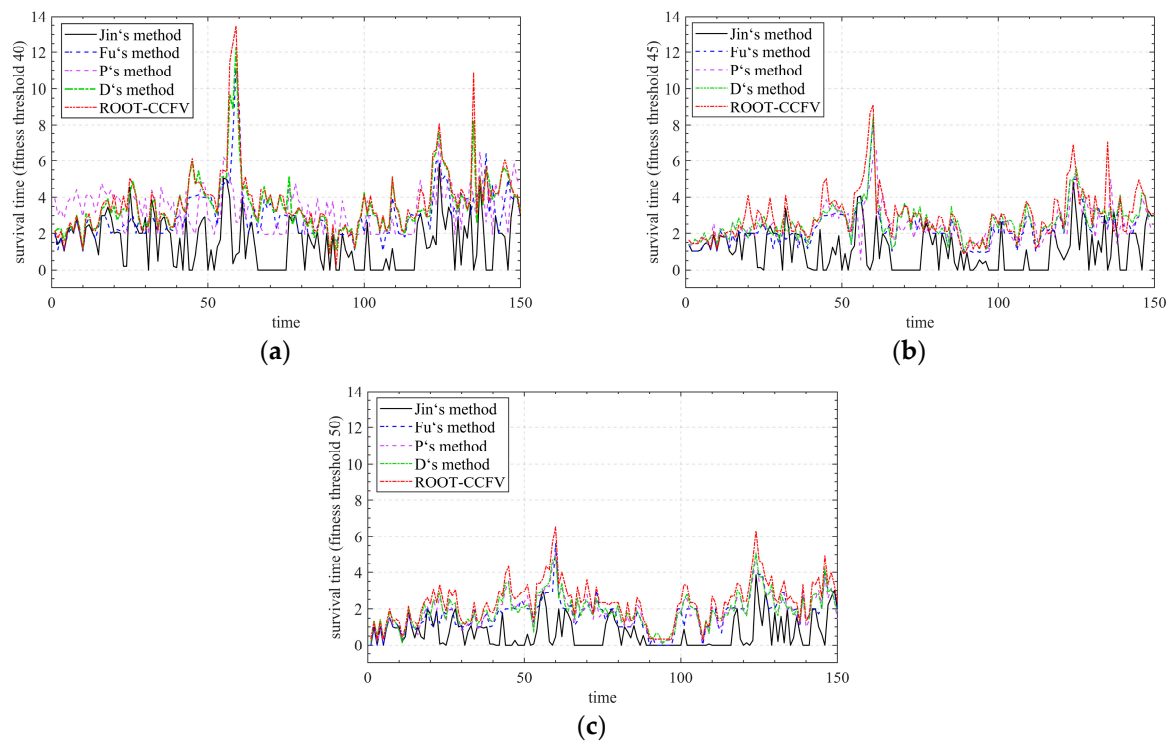
Figure 10. The survival time of different algorithms under different fitness thresholds. (**a**) Fitness threshold = 40. (**b**) Fitness threshold = 45. (**c**) Fitness threshold = 50.

Table 3. The average survival time of robust solutions under different algorithms.

Algorithm	Fitness Threshold		
	40	**45**	**50**
Jin's ROOT [31]	1.53	1.11	0.69
Fu's ROOT [32]	3.03	2.39	1.69
P's ROOT [35]	3.35	2.46	1.82
D's ROOT [36]	3.62	2.65	1.95
ROOT-CCFV	3.75	2.94	2.17

From Figure 10 and Table 2, it can be seen that the robustness of the solution obtained by ROOT-CCFV is better than other existing ROOT methods proposed in references [29,30,33] when dealing with mMPB under different fitness thresholds. Taking the fitness threshold of 40 as an example, the average survival time of ROOT-CCFV under the current fitness threshold was 145.1%, 23.8%, 11.9% and 3.6% higher than that of Jin's ROOT, Fu's ROOT, P's ROOT and D's ROOT, respectively.

6.2.3. Analysis of RES Uncertainty under ROOT-CCFV Based on Scene Method

This section took the WT in the IA as an example to illustrate. Figure 11 shows the process of the scene analysis method based on LHS and BR, where Figure 11a is the generated wind speed in multiple scenarios based on LHS; based on BR, we reduced the large-scale scene and calculated the probability of each scene after reduction, as shown in Figure 11b; the output power of the WT in typical scenarios by (16) is shown in Figure 11c; and Figure 11d fits the typical wind power output power curve obtained by the scenario method.
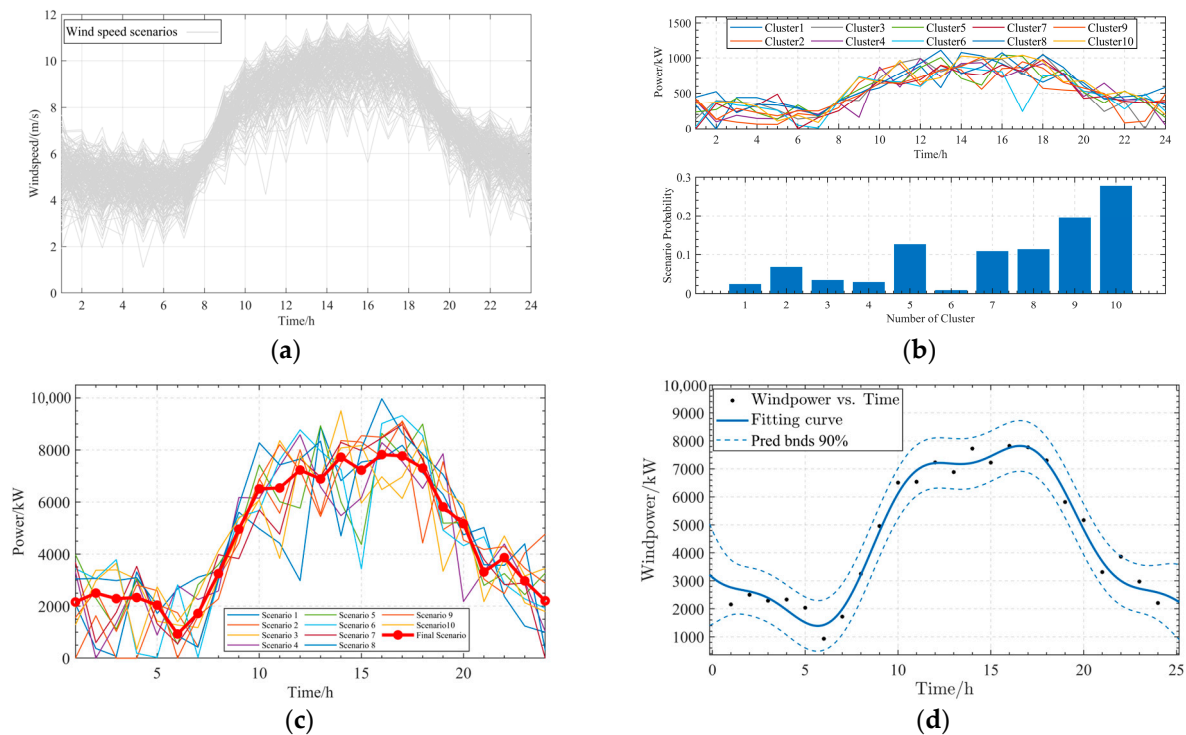
Figure 11. Process of scene analysis method. (**a**) Scene generation based on LHS. (**b**) Scene reduction based on BR. (**c**) Calculated typical outpower power. (**d**) Curving fitting.

Based on the fitting curve of the RES in each region, the ROOT-CCFV was used to solve the optimal robust solution of the RES power output in each region. In order to verify the robustness of ROOT-CCFV, the algorithm was compared with stochastic optimization (SO) and fuzzy optimization (FO). The confidence interval of FO was set to 0.95. The robust solutions of RES output power under different algorithms are shown in Figures 12 and 13.

It can be seen from Figures 12 and 13 that due to the robustness requirements for the stable operation of a RIES, the uncertainty prediction curves of the RES are slightly smaller than the actual RES output curve. Compared with the other two comparison algorithms, the prediction curve of ROOT-CCFV based on the scene method was closest to the actual output curve. Compared with SO, the curve of ROOT-CCFV was smoother. This is because under the ROOT-CCFV strategy, when the RES changes dynamically, the algorithm can obtain a more robust solution through R^{FD} and R^{SD}. Compared with FO, ROOT-CCFV can make the RIES obtain better economy under the premise of ensuring the robustness of optimal scheduling.
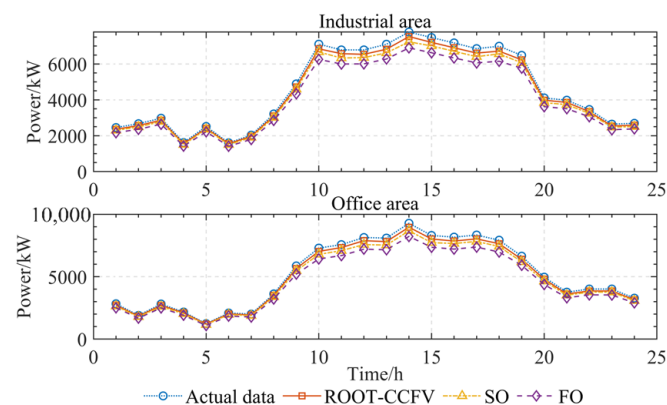

Figure 12. Robust solutions of the WT under different algorithms in the IA and OA.
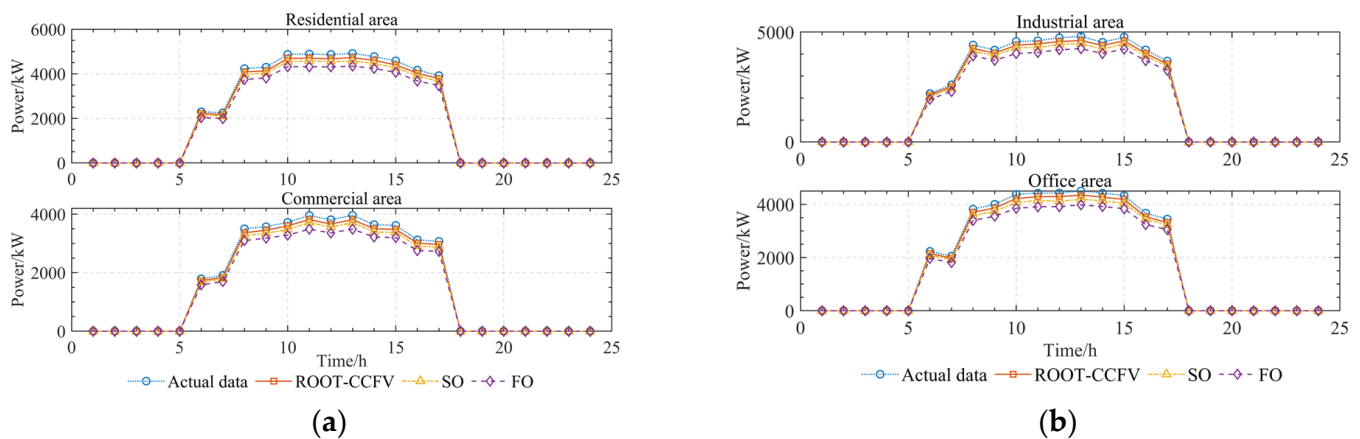
Figure 13. Robust solutions of PV under different algorithms in each region. (**a**) Robust solutions of PV in the RA and CA. (**b**) Robust solutions of PV in the IA and OA.

6.2.4. Analysis of SESS Capacity Configuration Considering EV Charging Demand

In order to study the influence of different EV charging models and RES uncertain calculation methods on SESS capacity configuration, the following four modes were set up.

Mode 1: The charging load of an EV was considered as a whole and it was charged only at RI; meanwhile, the SO was used to calculate the output power of the RES.

Mode 2: The charging loads of an EV were based on the trip chain proposed in this paper; meanwhile, the SO was used to calculate the output power of the RES.

Mode 3: The charging load of EV was considered as a whole and charged only at RI; meanwhile, the ROOT-CCFV was used to calculate the power output of an RES.

Mode 4: The charging loads of an EV were based on the trip chain proposed in this paper; meanwhile, the ROOT-CCFV was used to calculate the output power of the RES.

It was stipulated that the electric energy charged into an SESS is positive, indicating that each region charges the electric energy into SESS, the release of electric energy is negative, and indicating that each region is retrieving electric energy from SESS. The capacity configuration result of the SESS and the charging expenditure of the EV under different modes is shown in Table 4.

Table 4. Capacity configuration of SESS and charging expenditure of EV under different modes.

Mode	Capacity Configuration	Charging Expenditure
Mode 1	18,180.31 kWh	21,916.43 ¥
Mode 2	17,511.84 kWh	21,120.63 ¥
Mode 3	19,433.79 kWh	20,895.32 ¥
Mode 4	18,919.55 kWh	20,262.24 ¥

Comparing the results of mode 1 and mode 2, and mode 3 and mode 4, respectively, it can be seen that under the same RES algorithm, the traditional EV charging model has a greater demand for SESS capacity and charging expenditure than the EV charging model based on the trip chain. This is because under the traditional EV charging, RI bears huge load pressure. In order to reduce the operating cost of the entire RIES, it is necessary to maintain sufficient SESS capacity to provide a power supply for RI, and a large number of EV charging loads are concentrated in RI, resulting in higher charging expenditure. Similarly, under the same RES algorithm, it can be seen that the charging expenditure of the EV charging model based on the trip chain was 3.6% and 3.1% lower than that of the traditional EV charging model, respectively. Therefore, the EV charging model proposed in this paper has better energy economy.

Comparing the results of mode 1 and mode 3, and mode 2 and mode 4, respectively, it can be seen that under the same EV charging model, the SESS capacity configuration under ROOT-CCFV was higher than that under SO. This is because under the premise of ensuring

robustness, ROOT-CCFV can obtain a value closer to the actual RES output power through its strategy than SO. In order to reduce the operating expenditure, the RIES chooses to store the surplus RES in the SESS and retrieve it from the SESS to the load during the peak load period, so as to achieve the purpose of reducing the interaction cost with EPG during peak period. Therefore, more SESS capacity configuration is required in the case of ROOT-CCFV.

Upon further study of the influence of different scales of the EV charging load on SESS capacity configuration and the RIES operating cost, based on the EV trip chain charging demand model in this paper, the total electric load of the four regions without the EV was 229,220 kW on a typical scheduling day. Assuming that the scale of the EV charging load was equal to 15%/20%/25%/30%/35% of the total electric load, the results of the SESS capacity configuration and RIES operating cost are shown in Table 5.

Table 5. The result of capacity configuration and operation cost under different EV load scales.

EV Load Scale	Mode 2		Mode 4	
	Capacity Configuration	Operation Cost	Capacity Configuration	Operation Cost
15% of Total load	17,232.17 kWh	CNY 110,462.33	18,746.26 kWh	CNY 103,908.74
20% of Total load	16,634.31 kWh	CNY 119,153.54	18,296.35 kWh	CNY 110,280.87
25% of Total load	16,278.97 kWh	CNY 127,855.19	17,767.79 kWh	CNY 116,781.45
30% of Total load	15,728.46 kWh	CNY 136,542.37	17,373.30 kWh	CNY 122,976.14
35% of Total load	15,395.42 kWh	CNY 145,246.72	16,899.01 kWh	CNY 129,187.59

From Table 5, as the scale of the EV load continues to increase, the optimal configuration capacity of the SESS continues to decrease, and the operating cost of the RIES continues to increase. For the SESS, this is because when the EV load is large, each region needs to provide more power to the EV, and there is no more surplus RES stored in SESS, resulting in a reduction in the required capacity of SESS. For RIES, this is because each region needs to produce more electric power to meet the demand for the EV load.

6.2.5. Analysis of Optimal Scheduling Results of the RIES Considering the EV Charging Demand

Based on the four modes set out in Section 6.2.4, the influence of different EV charging models and the RES uncertainty calculation methods on RIES operating costs were studied. The details of RIES operation costs under different modes are shown in Table 6.

Table 6. The details of RIES operating costs under different modes.

Details of Operating Cost	Mode 1	Mode 2	Mode 3	Mode 4
Electrical energy transaction expenditure	CNY 37,380.93	CNY 31,740.59	CNY 35,694.37	CNY 30,477.46
Gas energy transaction expenditure	CNY 60,872.21	CNY 57,072.09	CNY 55,624.14	CNY 51,773.44
Operation and maintenance expenditure	CNY 24,931.91	CNY 20,431.22	CNY 23,788.59	CNY 19,118.81
Energy transaction expenditure with the SESS	CNY 3143.58	CNY 3021.33	CNY 3332.67	CNY 3219.21
Total cost	CNY 126,319.63	CNY 112,265.17	CNY 118,439.77	CNY 104,548.92

It can be seen from Table 6 that in the mode of the same use of ROOT-CCFV, the operating cost of the RIES under the EV charging demand based on the trip chain was 11.7% lower than that under the traditional EV charging demand model. In the same mode of using the EV charging demand based on the trip chain, the operating cost of the RIES under ROOT-CCFV was 6.9% lower than that of the RIES under SO. In summary, compared with the traditional EV charging demand modeling method, the EV charging demand model based on the trip chain can help the RIES obtain a capacity configuration result that is more in line with the actual energy demand, thereby reducing the operating

cost of the RIES. Similarly, compared with SO, ROOT-CCFV can obtain more robust RES output power, reduce the interaction cost between the RIES and EPG, and thus reduce the operating cost of the RIES. Taking mode 4 as an example, the optimal scheduling results of each region in the RIES were analyzed and are described as follows.

The RIES electrical load optimization scheduling results are shown in Figure 14. It can be seen from Figure 14a that since the RA and CA only contain PV, the RA and CA purchase the required electrical energy from the EPG when PV has less output power or no output power. At the same time, when the EPG price is high, the RA and CA will also start the GT for power generation. From Figure 14b, it can be seen that because the IA and OA contain abundant RESs, excess power can be sold to EPG or stored in the SESS when the RES meets its own load demand. The IA and OA start the GT power generation to make up for the electric load gap only when the RES output power is not enough to meet their own load in the morning and evening.
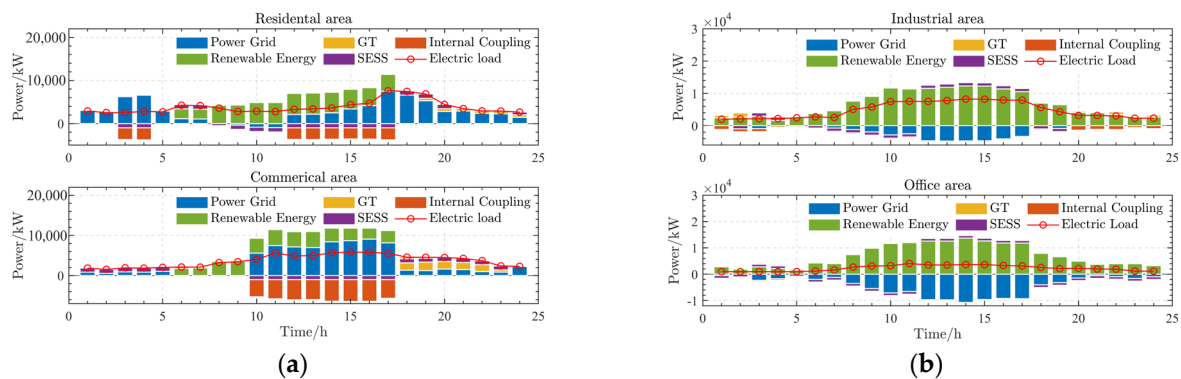

Figure 14. Electric load optimization scheduling results of the RIES. (**a**) Electric optimal scheduling of the RA and CA. (**b**) Electric optimal scheduling of the IA and OA.

The RIES electrical load optimization scheduling results are shown in Figure 15. From Figure 15, we can see that the GB is the main equipment to provide heat power for each region. It can be seen from Figure 15a that when the PV equipment starts to work during the 10:00–17:00 period, the RA and CA choose PV to provide electricity for the EB to provide the required heat energy in order to better reduce operating costs. From Figure 15b, it can be seen that for the IA and OA, their RES was mainly sold to the EPG for revenue, so their heat load was mainly provided by the GB.

Figure 15. Heat load optimization scheduling results of the RIES. (**a**) Heat optimal scheduling of the RA and CA. (**b**) Heat optimal scheduling of the IA and OA.

The RIES cold load optimization scheduling results are shown in Figure 15. From Figure 16, we can see that the EC was the main equipment to provide heat power for each region. It can be seen from Figure 16a and previous analysis that the GT needs to provide power for the RA and CA when PV energy stops. At this time, the high-temperature waste

heat generated by the GT was transmitted through the WHB, part of which was transmitted to the HE and converted into heat energy to meet the heat load demand, and part of which was transmitted to the AC and converted into cold energy to meet the cold load demand. For the IA and OA, from Figure 16b we can see that because they contain very rich RES, they mainly met their own demand for cooling load through the EC.

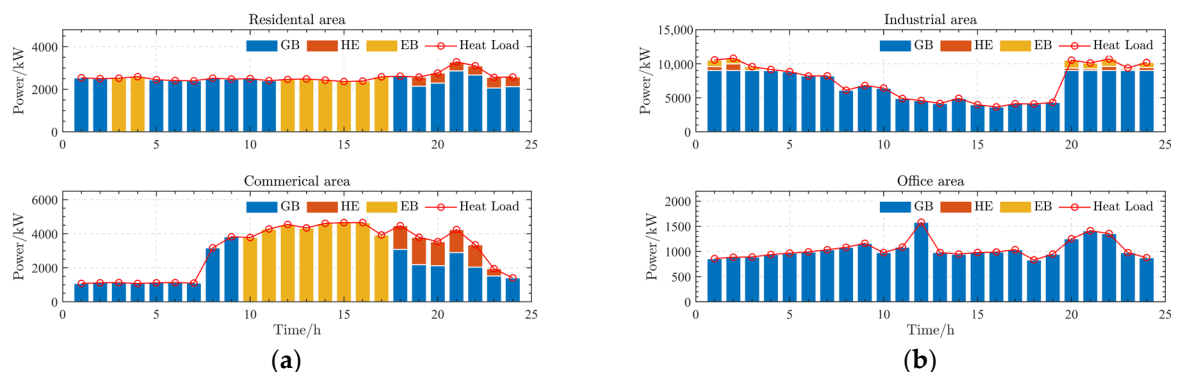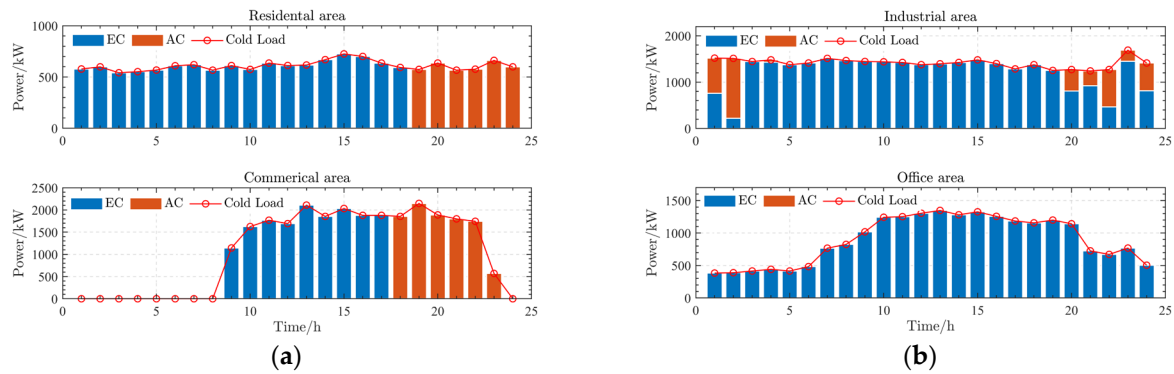**Figure 16.** Cold load optimization scheduling results of the RIES. (**a**) Cold optimal scheduling of the RA and CA. (**b**) Cold optimal scheduling of the IA and OA.

6.2.6. Analysis of IDR

The IDR optimization results are shown in Figures 17–19. The RL according to the EPG price, in the period of a high electricity price, cut part of the load. The TL transferred the load in the high-energy-price period to the low-energy-price period, and reduced the operating costs while causing the load curve to tend to be smooth. When the electricity price per unit energy supply was higher than the price of cold/heat energy price, SL converted part of the cold/heat energy into electric load. The IDR model established in this paper makes the load curve smoother and realizes peak load shifting. In order to verify the effect of the IDR in RIES optimal scheduling, the following mode were set.

Mode 5: based on mode 4 without considering the IDR.

Mode 6: based on mode 4 considering the IDR.

The details of RIES operating costs before and after considering the IDR are shown in Table 7. From Table 7, it can be seen that when the RIES considers the IDR model proposed in this paper, its optimal operating cost decreases from CNY 104,548.92 without considering the IDR model to CNY 99,502.61; the optimal operating cost decreases by 4.8%. In summary, the IDR model proposed in this paper can effectively reduce the operating cost of the RIES.
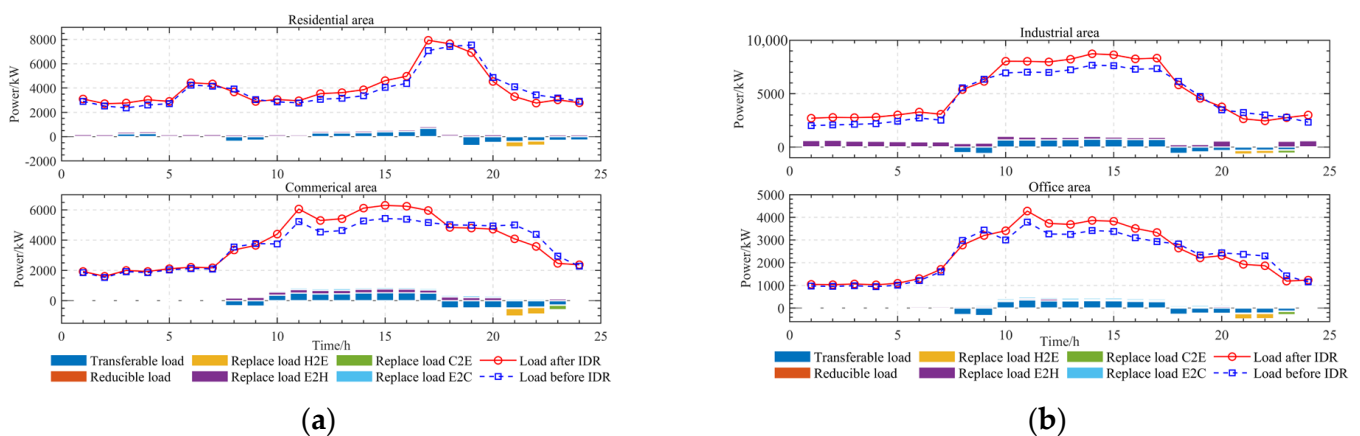

Figure 17. Electric load IDR optimization results of the RIES. (**a**) Electric load IDR results of the RA and CA. (**b**) Electric load IDR results of the IA and OA.
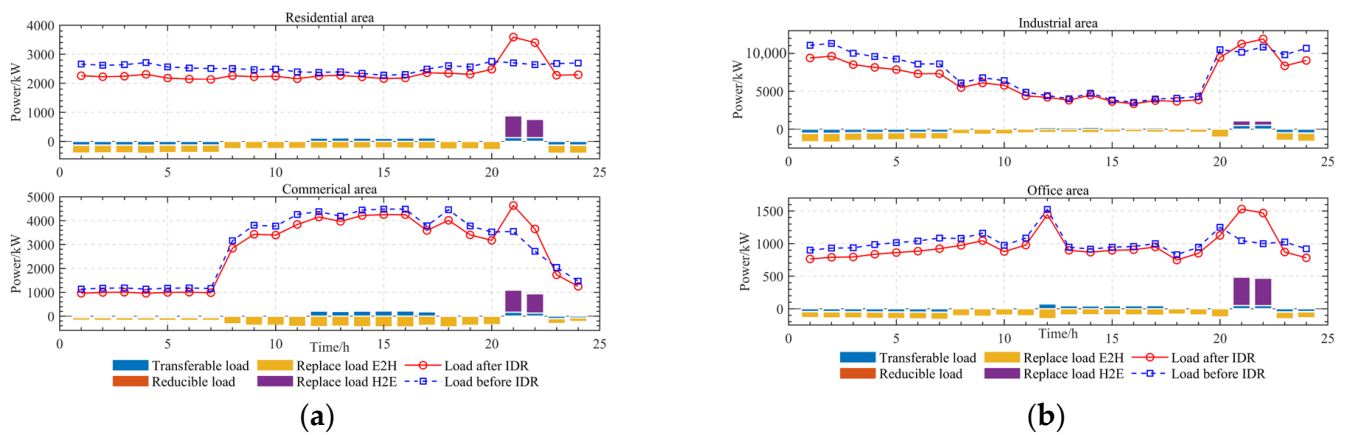
Figure 18. Heat load IDR optimization results of the RIES. (**a**) Heat load IDR results of the RA and CA. (**b**) Heat load IDR results of the IA and OA.
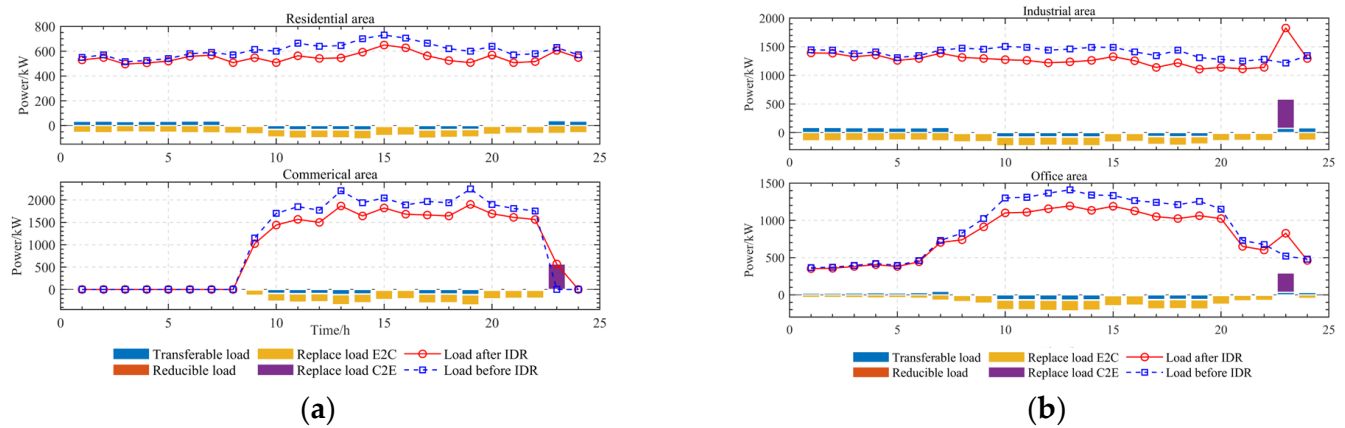

Figure 19. Cold load IDR optimization results of the RIES. (**a**) Cold load IDR results of the RA and CA. (**b**) Cold load IDR results of the IA and OA.

Table 7. The details of RIES operating costs before and after the IDR.

Details of Operating Cost	Mode 5	Mode 6
Electrical energy transaction expenditure	CNY 30,477.46	CNY 29,569.46
Gas energy transaction expenditure	CNY 51,773.44	CNY 48,846.58
Operation and maintenance expenditure	CNY 19,118.81	CNY 17,910.47
Energy transaction expenditure with SESS	CNY 3219.21	CNY 3176.10
Total cost	CNY 104,548.92	CNY 99,502,61

7. Conclusions

Aiming at the optimal scheduling problem of an RIES with EVs, this paper first established a charging demand load mode of EV based on the trip chain theory; meanwhile, it established a multi-energy IDR model. Aiming at the uncertainty problem of an RES, firstly, the above problem was transformed into a class of dynamic robust optimization problems with time-varying parameters, and then a ROOT-CCFV algorithm based on a scenario method was proposed to solve this kind of problem. By establishing an RIES model containing four regions and conducting case studies, the following conclusions can be drawn:

1. The ROOT-CCFV algorithm can better solve the dynamic optimization problem with time-varying parameters and obtain a more robust solution. Compared with the existing algorithms, in the mMPB test environment, the average survival time of the robust solution obtained by the ROOT-CCFV algorithm was increased by 46.1%

on average. The proposed ROOT-CCFV algorithm provides a solution for solving dynamic optimization problems in the future.

2. The reasonable modeling of an EV charging demand model can effectively reduce the capacity configuration cost of an SESS and the optimal operation cost of an RIES in this region. And the larger the EV load in the region, the less the SESS capacity required in the region. Under the same RES uncertainty solving algorithm, compared with the traditional EV charging model, the EV charging model based on the trip chain proposed in this paper can reduce the cost of its own charging expenditure by 3.5%, and at the same time reduce the operating cost of an RIES by 11.7%.

3. The alternative IDR model proposed in this paper can realize the coupling of electric heating and cold energy, and effectively reduce the operation cost of an RIES. When the IDR model proposed in this paper is considered in RIES optimal scheduling, the operating cost can be reduced by 4.8%.

Data Availability Statement: The data that support the findings of this study are available from the corresponding author upon reasonable request.

Appendix A

Table A1. Capacity parameters of equipment in each CCHP/(kWh).

Equipment	RA	CA	IA	OA
PV	2000	4000	8000	2000
WT	/	/	6000	3000
ES	/	1000	2000	/
GT	2000	5000	8000	3000
WHB	5000	5000	8000	5000
GB	5000	5000	8000	5000
EH	5000	5000	8000	5000
EC	5000	5000	8000	5000
AC	5000	5000	8000	5000
HE	4000	4000	4000	4000

Table A2. Efficiency parameters of equipment in each CCHP.

Equipment	RA	CA	IA	OA
Efficiency of GT	0.35	0.35	0.35	0.35
Heat-to-electric ratio of GT	2.3	2.3	2.3	2.3
Efficiency of WHB	0.73	0.73	0.73	0.73
Efficiency of GB	0.85	0.85	0.85	0.85
Efficiency of EH	0.98	0.98	0.98	0.98

Table A2. *Cont.*

Equipment	RA	CA	IA	OA
Efficiency of EC	4	4	4	4
Efficiency of AC	1.2	1.2	1.2	1.2
Efficiency of HE	0.9	0.9	0.9	0.9
Maximum charging of ES	/	200 kW	400 kW	/
Maximum discharging of ES	/	200 kW	400 kW	/
Charging efficiency of ES	/	0.95	0.95	/
Discharging efficiency of ES	/	0.95	0.95	/
Self-discharging efficiency of ES	/	0.04	0.04	/
Initial energy storage of ES	/	200 kWh	400 kWh	/
Maximum energy storage of ES	/	900 kWh	1800 kWh	/
Minimum energy storage of ES	/	200 kWh	400 kWh	/

Table A3. Equipment parameters of an SESS.

Parameter	Value	Parameter	Value
Charging efficiency	0.95	Initial state of SOC	0.50
Discharging efficiency	0.95	Maximum state of SOC	0.90
Self-discharging efficiency	0.04	Minimum state of SCO	0.20
		Maximum charge/discharge power to each region	1000 kW

Table A4. TOU electricity price of EPG (CNY/kWh).

RA				CA/IA/OA			
Price Types	Time Interval	Purchase Price	Sale Price	Price Types	Time Interval	Purchase Price	Sale Price
Peak time	07:00–09:00 18:00–24:00	0.759	0.415	Peak time	07:00–09:00 17:00–23:00	0.8650	0.415
Usual time	00:00–02:00 04:00–07:00 09:00–11:00 17:00–18:00	0.510	0.415	Usual time	23:00–00:00 00:00–07:00	0.5843	0.415
Valley time	02:00–04:00 11:00–17:00	0.261	0.415	Valley time	09:00–17:00	0.3036	0.415

Table A5. TOU electricity price of an SESS (CNY/kWh).

Price Types	Time Interval	Purchase Price	Sale Price
Peak time	08:00–09:00, 19:00–24:00	0.725	0.435
Usual time	00:00–02:00, 05:00–07:00 10:00–11:00, 18:00–18:00	0.475	0.435
Valley time	03:00–04:00, 12:00–17:00	0.271	0.435

References

1. European Commission. *Horizon 2020 Work Programme 2018–2020: 10. Secure, Clean and Efficient Energy*; Official Publications of the European Communities: Luxembourg, 2018.
2. Zhou, S.; Han, Y.; Mahmoud, K.; Darwish, M.M.; Lehtonen, M.; Yang, P.; Zalhaf, A.S. A novel unified planning model for distributed generation and electric vehicle charging station considering multi-uncertainties and battery degradation. *Appl. Energy* **2023**, *348*, 121566. [CrossRef]
3. Zhang, N.; Sun, Q.; Yang, L.; Li, Y. Event-Triggered Distributed Hybrid Control Scheme for the Integrated Energy System. *IEEE Trans. Ind. Inform.* **2021**, *18*, 835–846. [CrossRef]

4. Liu, L.; Yao, X.; Qi, X.; Han, Y. Low-carbon economy configuration strategy of electro-thermal hybrid shared energy storage in multiple multi-energy microgrids considering power to gas and carbon capture system. *J. Clean. Prod.* **2023**, *428*, 139366. [CrossRef]

5. Li, Y.; Han, M.; Yang, Z.; Li, G. Coordinating Flexible demand response and renewable uncertainties for scheduling of community integrated energy systems with an electric vehicle charging station: A bi-level approach. *IEEE Trans. Sustain. Energy* **2021**, *12*, 2321–2331. [CrossRef]

6. Gan, L.; Chen, X.; Yu, K.; Zheng, J.; Du, W. A probabilistic evaluation method of household EVs dispatching potential considering users' multiple travel needs. *IEEE Trans. Ind. Appl.* **2020**, *56*, 5858–5867. [CrossRef]

7. Lan, T.; Jermsittiparsert, K.; Alrashood, S.T.; Rezaei, M.; Al-Ghussain, L.; Mohamed, M.A. An Advanced Machine Learning Based Energy Management of Renewable Microgrids Considering Hybrid Electric Vehicles' Charging Demand. *Energies* **2021**, *14*, 569. [CrossRef]

8. Taibi, E.; del Valle, C.F.; Howells, M. Strategies for solar and wind integration by leveraging flexibility from electric vehicles: The Barbados case study. *Energy* **2018**, *164*, 65–78. [CrossRef]

9. Mwasilu, F.; Justo, J.J.; Kim, E.-K.; Do, T.D.; Jung, J.-W. Electric vehicles and smart grid interaction: A review on vehicle to grid and renewable energy sources integration. *Renew. Sustain. Energy Rev.* **2014**, *34*, 501–516. [CrossRef]

10. Rassaei, F.; Soh, W.S.; Chua, K.C. Demand response for residential electric vehicles with random usage patterns in smart grids. *IEEE Trans. Sustain. Energy* **2015**, *6*, 1367–1376. [CrossRef]

11. Tan, J.; Wang, L. Real-Time charging navigation of electric vehicles to fast charging stations: A hierarchical game approach. *IEEE Trans. Smart Grid* **2015**, *8*, 846–856. [CrossRef]

12. Li, G.; Wu, D.; Hu, J.; Li, Y.; Hossain, M.S.; Ghoneim, A. HELOS: Heterogeneous load scheduling for electric vehicle-integrated microgrids. *IEEE Trans. Veh. Technol.* **2016**, *66*, 5785–5796. [CrossRef]

13. Yu, M.; Hong, S.H. A real-time demand-response algorithm for smart grids: A stackelberg game approach. *IEEE Trans. Smart Grid* **2015**, *7*, 879–888. [CrossRef]

14. Wang, D.; Guan, X.; Wu, J.; Li, P.; Zan, P.; Xu, H. Integrated energy exchange scheduling for multimicrogrid system with electric vehicles. *IEEE Trans. Smart Grid* **2015**, *7*, 1762–1774. [CrossRef]

15. Husein, M.; Chung, I.-Y. Day-Ahead Solar Irradiance Forecasting for Microgrids Using a Long Short-Term Memory Recurrent Neural Network: A Deep Learning Approach. *Energies* **2019**, *12*, 1856. [CrossRef]

16. Huang, Y.; Wang, L.; Guo, W.; Kang, Q.; Wu, Q. Chance constrained optimization in a home energy management system. *IEEE Trans. Smart Grid* **2016**, *9*, 252–260. [CrossRef]

17. Baker, K.; Bernstein, A. Joint chance constraints in AC optimal power flow: Improving bounds through learning. *IEEE Trans. Smart Grid* **2019**, *10*, 6376–6385. [CrossRef]

18. Zhang, Y.; Ai, Q.; Xiao, F.; Hao, R.; Lu, T. Typical wind power scenario generation for multiple wind farms using conditional improved Wasserstein generative adversarial network. *Int. J. Electr. Power Energy Syst.* **2020**, *114*, 105388. [CrossRef]

19. Li, Y.; Wang, B.; Yang, Z.; Li, J.; Chen, C. Hierarchical stochastic scheduling of multi-community integrated energy systems in uncertain environments via Stackelberg game. *Appl. Energy* **2021**, *308*, 118392. [CrossRef]

20. Li, Y.; Han, M.; Shahidehpour, M.; Li, J.; Long, C. Data-driven distributionally robust scheduling of community integrated energy systems with uncertain renewable generations considering integrated demand response. *Appl. Energy* **2023**, *335*, 120749. [CrossRef]

21. Yang, J.; Su, C. Robust optimization of microgrid based on renewable distributed power generation and load demand uncertainty. *Energy* **2021**, *223*, 120043. [CrossRef]

22. Huang, S.; Lu, H.; Chen, M.; Zhao, W. Integrated energy system scheduling considering the correlation of uncertainties. *Energy* **2023**, *283*, 129011. [CrossRef]

23. Kalathil, D.; Wu, C.; Poolla, K.; Varaiya, P. The sharing economy for the electricity storage. *IEEE Trans. Smart Grid* **2017**, *10*, 556–567. [CrossRef]

24. Dai, R.; Esmaeilbeigi, R.; Charkhgard, H. The utilization of shared energy storage in energy systems: A comprehensive review. *IEEE Trans. Smart Grid* **2021**, *12*, 3163–3174. [CrossRef]

25. Kang, C.; Liu, J.; Zhang, N. A new form of energy storage in future power system: Cloud energy storage. *Autom. Electr. Power Syst.* **2017**, *41*, 2–8.

26. Walker, A.; Kwon, S. Analysis on impact of shared energy storage in residential community: Individual versus shared energy storage. *Appl. Energy* **2020**, *282*, 116172. [CrossRef]

27. Liu, N.; Tan, L.; Sun, H.; Zhou, Z.; Guo, B. Bilevel Heat–Electricity Energy Sharing for Integrated Energy Systems with Energy Hubs and Prosumers. *IEEE Trans. Ind. Inform.* **2021**, *18*, 3754–3765. [CrossRef]

28. Jabir, H.J.; Teh, J.; Ishak, D.; Abunima, H. Impacts of Demand-Side Management on Electrical Power Systems: A Review. *Energies* **2018**, *11*, 1050. [CrossRef]

29. Tang, D.; Wang, P. Probabilistic modeling of nodal charging demand based on spatial-temporal dynamics of moving electric vehicles. *IEEE Trans. Smart Grid* **2015**, *7*, 627–636. [CrossRef]

30. Yu, X.; Jin, Y.; Tang, K.; Yao, X. Robust optimization over time—A new perspective on dynamic optimization problems. In Proceedings of the 2010 IEEE Congress on Evolutionary Computation, Barcelona, Spain, 18–23 July 2010; pp. 3998–4003.

31. Jin, Y.; Tang, K.; Yu, X.; Sendhoff, B.; Yao, X. A framework for finding robust optimal solutions over time. *Memetic Comput.* **2013**, *5*, 3–18. [CrossRef]

32. Fu, H.; Sendhoff, B.; Tang, K.; Yao, X. Finding Robust Solutions to Dynamic Optimization Problems. In Proceedings of the 16th European Conference on Applications of Evolutionary Computation, Vienna, Austria, 3–5 April 2013; pp. 616–625.

33. Cao, M.; Shao, C.; Hu, B.; Xie, K.; Li, W.; Peng, L.; Zhang, W. Reliability Assessment of Integrated Energy Systems Considering Emergency Dispatch Based on Dynamic Optimal Energy Flow. *IEEE Trans. Sustain. Energy* **2021**, *13*, 290–301. [CrossRef]

34. Lee, T.-K.; Bareket, Z.; Gordon, T.; Filipi, Z.S. Stochastic modeling for studies of real-world PHEV usage: Driving schedule and daily temporal distributions. *IEEE Trans. Veh. Technol.* **2012**, *61*, 1493–1502. [CrossRef]

35. Novoa-Hernandez, P.; Pelta, D.A.; Corona, C.C. Approximation Models in Robust Optimization Over Time—An Experimental Study. In Proceedings of the 2018 IEEE Congress on Evolutionary Computation (CEC), Rio de Janeiro, Brazil, 8–13 July 2018; pp. 1–6. [CrossRef]

36. Yazdani, D.; Nguyen, T.T.; Branke, J. Robust Optimization over Time by Learning Problem Space Characteristics. *IEEE Trans. Evol. Comput.* **2018**, *23*, 143–155. [CrossRef]

Article

Dynamic Robust Optimization Method Based on Two-Stage Evaluation and Its Application in Optimal Scheduling of Integrated Energy System

Bo Zhou * and Erchao Li

College of Electrical Engineering and Information Engineering, Lanzhou University of Technology,
Lanzhou 730050, China; lecstarr@163.com
* Correspondence: zhoubo@lut.edu.cn

Abstract: As an emerging energy allocation method, shared energy storage devices play an important role in modern power systems. At the same time, with the continuous improvement in renewable energy penetration, modern power systems are facing more uncertainties from the source side. Therefore, a robust optimization algorithm that considers both shared energy storage devices and source-side uncertainty is needed. Responding to the above issues, this paper first establishes an optimal model of a regional integrated energy system with shared energy storage. Secondly, the uncertainty problem is transformed into a dynamic optimization problem with time-varying parameters, and a modified robust optimization over time algorithm combined with scenario analysis is proposed to solve such optimization problems. Finally, an optimal scheduling objective function with the lowest operating cost of the system as the optimization objective is established. In the experimental part, this paper first establishes a dynamic benchmark test function to verify the validity of proposed method. Secondly, the multi-mode actual verification of the proposed algorithm is carried out through a regional integrated energy system. The simulation results show that the modified robust optimization over time (ROOT) algorithm could find solutions with better robustness in the same dynamic environment based on the two-stage evaluation strategy. Compared with the existing algorithms, the average fitness and survival time of the robust solution obtained by the modified ROOT algorithm are increased by 94.41% and 179.78%. At the same time, the operating cost of the system is reduced by 11.65% by using the combined optimization scheduling method proposed in this paper.

Keywords: dynamic optimization problem; shared energy storage system; renewable uncertainty; regional integrated energy system; dynamic robust optimization

1. Introduction

In-depth development of an RES is a considerable way to reduce carbon emissions in power systems [1]. An RIES based on the CCHP is a crucial way to improve energy efficiency and promote the consumption of the RES. Vigorously developing a CCHP-based RIES is a momentous means for China to achieve "carbon peak and carbon neutrality" [2]. On the other hand, an RIES contains an RES, which makes the overall power generation output curve intermittent, random and volatile. An ESS is considered an important method to suppress the internal uncertainty of the new power system due to its generation–use electrolytic coupling effect [3]. Although energy storage has great potential, it still faces problems such as a high investment cost and long return period, which limits the development of ESSs [4].

Based on the above background, SESSs proposed by the combination of sharing economy and ESS technology have become the focus of attention of experts and scholars [5]. References [6,7] introduce the basic principle, operation mechanism, pricing strategy and evaluation method of SESSs in detail and put forward suggestions for the next research

direction of SESSs. Zhao et al. [8] proved that the rational allocation of SESSs can effectively reduce the storage–use bilateral operation cost by establishing a double level optimal configuration model. Based on the problem of energy community configuration sharing energy storage, Chang et al. [9] proposed a community configuration framework and set up three energy storage device allocation methods. The test results show that the reasonable arrangement of SESSs in the community can save configuration access and use costs. Liu et al. [10] studied the role of SESSs in new energy consumption trends and low-carbon operation. Huang et al. [11] applied SESSs to multi-microgrid grid-connected systems, and an optimal scheduling strategy was proposed to improve the local consumption of RESs. Reference [12] reduced the total energy cost and peak–valley difference rate of the entire power grid through the virtualized SESS scheduling strategy. Currently, the academic community generally believes that the participation of SESSs in the optimal scheduling of RIESs is crucial for the stability and efficiency of system operation, which needs to be further studied and discussed. However, due to the access of the RES, the RIES has great uncertainty, which has a certain risk impact on the participation of the SESS in operation of the RIES. Therefore, it is necessary to consider the uncertainty of RIESs when studying SESSs, which is the focus of this paper.

From the perspective of control theory, the optimization problem considering RES uncertainty can be regarded as a kind of dynamic optimization problem with time-varying parameters. And ROOT can provide dynamic solutions according to specific time-varying fitness functions [13]. Yu et al. [14] proposed the dynamic optimization algorithm concept of ROOT for the first time. The main idea is to search for a set of dynamic robust solutions which can be used by multiple continuous dynamic environments. Jin et al. [15] proposed a framework of ROOT and introduced the implementation method of each module in the framework. Fu et al. [16] proposed a method for characterizing and analyzing environmental changes in ROOT. Based on the concept of robustness, Fu et al. [17] proposed two new robustness metrics. A new semi-ROOT was introduced by Yazdani et al. [18], which can find a better solution when the current solution is acceptable. Novoa-Hernández et al. [19] proposed the idea of using an approximate model to analyze ROOT. Fox et al. [20] studied different prediction methods of the ROOT algorithm. Zhang et al. [21] studied the prediction model under the ROOT framework. Guzmán-Gaspar et al. [22] made an empirical comparison between the DE algorithm and random sampling method and analyzed the feasibility and effectiveness of the differential evolution algorithm to solve the modified ROOT problem in dynamic environments by using the survival time method. Yazdani et al. [23] proposed a multi-population ROOT and introduce two metrics, one of which is to estimate the robust estimation component of the promising region, and the other is the dual-mode computing resource allocation component considering various factors such as robustness. Chen et al. [24] proposed a new dynamic optimization method based on the environment-driven method and ROOT and selected different algorithms to solve different problems. The current research of ROOT is generally based on the AF or ST concept to find a solution with better robustness. Therefore, the accuracy of the predicted solution needs to be improved, and how to improve the accuracy is the focus of this paper.

In order to supplement the shortcomings of the current research, this paper establishes the model of multi-district RIESs considering SESS access and establishes an objective function with the optimal RIES daily operating cost. Aiming to address the uncertainty of RESs, a modified ROOT algorithm combined with scenario analysis is proposed from the perspective of optimal control. The contribution and novelty of this study are as follows:

1. Aiming to resolve the dynamic optimization problem, the ROOT-TSE-PCCG is proposed. FD, SD and SFV are introduced as new evaluation metrics to improve the prediction accuracy of ROOT, and the above three new evaluation metrics are used as the first-stage evaluation index of the robust solution set. On this basis, the ST and AF are introduced as the second-stage evaluation index. Finally, through the two-stage evaluation method, the optimal robust solutions of the dynamic optimization problem are obtained.

2. To address the problem of uncertainty in RESs, this paper proposes an algorithm that integrates the modified ROOT based on a two-stage evaluation with scenario analysis methods. By using LHS to generate the scene of the RES output power curve, then using BR to reduce the scene of the generated multiple scenes, and fitting the final power curve conversion, the RES uncertainty problem is transformed into a dynamic optimization problem with time-varying parameters. The modified ROOT method based on two-stage evaluation and scene analysis is used to solve the above optimization model, and the dynamic environment robust solution of RES output power is obtained.

The rest of this paper is structured as follows: Section 2 introduces the structure of the RIES with an SESS. In Section 3, the modified ROOT algorithm combined with scenario analysis is proposed. Section 4 establishes the system optimization objective and discusses the constraints. Section 5 analyzes the methodology of this paper through an arithmetic example and Section 6 gives the conclusions obtained.

2. Structure Modeling of RIES Considering SESS

2.1. Structure of Multi-District RIES

The structure of the whole system is shown in Figure 1. This paper stipulates that the bidirectional energy interaction objects of the CCHP in the region are the EPG and SESS, and the purpose of energy interaction is to build an interconnected power network in the region.
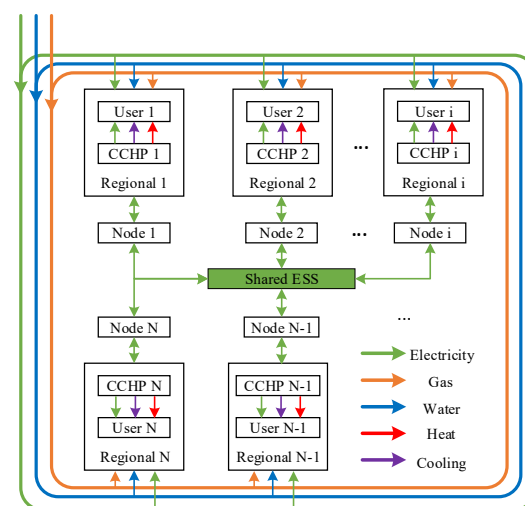
Figure 1. The framework of the multi-district RIES.

The internal structure diagram of the CCHP contained in Figure 1 is shown in Figure 2. It can be seen from Figure 2 that the CCHP can be divided into source side, converter module and load side. The source side consists of a WT, PV cell, GT and GB. The converter modules consist of a WHB, ES, EB, EC, AC and HE. The load side consist of electrical, cooling and heating loads. Due to the limited space, and because the mathematical modeling work of various types of equipment contained in the CCHP is very mature, the modeling work of this paper is no longer discussed, and the mathematical model of each equipment can be found in [25,26].
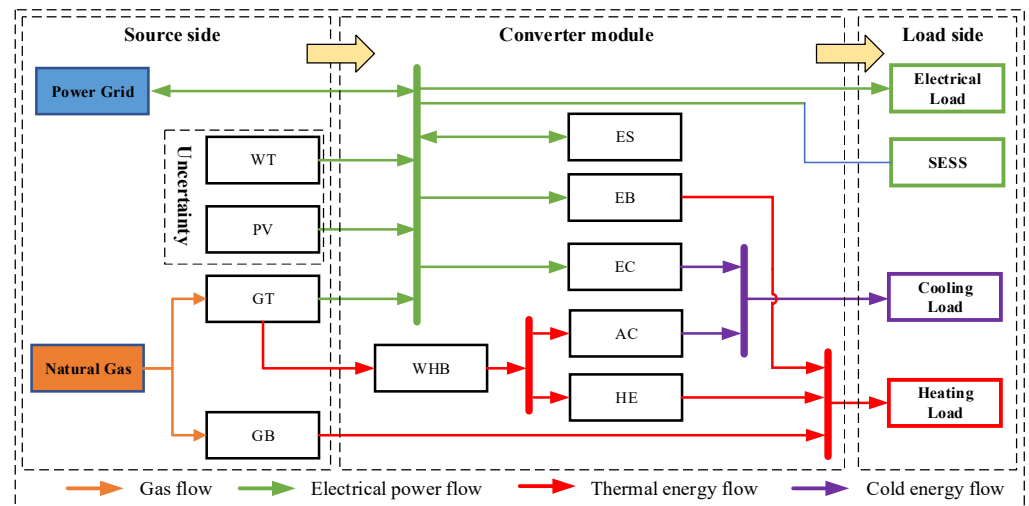
Figure 2. The framework of the CCHP.

2.2. Modeling of SESS

The operator establishes an SESS among user groups for unified operation and management and provides energy storage services for multiple users in the same distribution network area [6,27]. At the same time, operators make use of the differences in the electricity consumption behavior of users at different moments and of different users at the same time to allocate energy storage resources, thus further improving the utilization rate of energy storage equipment and achieving the purpose of increasing the system's operating income [28,29]. In summary, the mathematical model of the SESS runtime should meet the following conditions.

2.2.1. Constraint of State of Charge of SESS [30]

During the normal operation of the SESS, the electric energy contained in it should not mutate.

$$E_t^{SESS} = \left(1 - \eta_{SESS}^{loss}\right)E_{t-1}^{SESS} + \left(\eta_{SESS}^{abs}P_t^{SESS,abs} - \frac{1}{\eta_{SESS}^{relea}}P_t^{SESS,relea}\right)\Delta t, \qquad (1)$$

2.2.2. Capacity Constraints of SESS

The normal operation of the SESS should conform to the physical parameters of its equipment.

$$\begin{cases} \sigma_{SESS}^{\min}E_{max}^{SESS} \leq E_t^{SESS} \leq \sigma_{SESS}^{\max}E_{max}^{SESS} \\ E_{start}^{SESS} = \sigma_{SESS}^{init}E_{\max}^{SESS} = E_{end}^{SESS} \end{cases}, \qquad (2)$$

2.2.3. Charge and Discharge Power Constraints of SESS

When the SESS is in normal operation, it cannot have both charging behavior and discharging behavior at the same time with any single user.

$$\begin{cases} 0 \leq P_t^{SESS,abs} \leq P_{\max}^{SESS}U_{abs}^{SESS} \\ 0 \leq P_t^{SESS,relea} \leq P_{\max}^{SESS}U_{relea}^{SESS} \\ U_{abs}^{SESS} + U_{relea}^{SESS} \leq 1 \\ U_{abs}^{SESS} \in \{0,1\}U_{relea}^{SESS} \in \{0,1\} \end{cases}, \qquad (3)$$

3. Uncertainty Analysis Method of RES

3.1. Problem Description

The robustness of the RIES optimal operation requires that the system can maintain stable operation in the case of large fluctuations. At the same time, the robust RIES

optimal scheduling results have practical engineering application significance. Therefore, considering the actual engineering situation, when the external RES available energy is the smallest, the stability of the system is the worst. Therefore, based on the theoretical requirements of robustness requirements, this paper sets the optimization goal as the minimum output of the RES. It is assumed that the output of the WT is $P_{i,t}^{WT}$ and the output of the PV cell is $P_{i,t}^{PV}$. Obviously, both $P_{i,t}^{WT}$ and $P_{i,t}^{PV}$ are time-varying parameters [31]. Therefore, the expression of the optimization problem with $P_{i,t}^{WT}$ and $P_{i,t}^{PV}$ parameters is as follows:

$$P_{i,t}^{RG} = \min f\left(P_{i,t}^{WT} + P_{i,t}^{PV}\right), \tag{4}$$

where f is the objective function. It is assumed that $P_{i,t}^{WT}$ and $P_{i,t}^{PV}$ change only at the specified time point of the specified scheduling conversion. In other words, within a fixed time period $[0, T]$, the minimization problem described in (4) can be expressed by the changing behavior of definitions $P_{i,t}^{WT}$ and $P_{i,t}^{PV}$ as follows: the function sequence consisting of a set of static functions consisting of multiple subintervals $P_{i,t}^{WT}$ and $P_{i,t}^{PV}$ represents the optimization problem (4), which is described as follows:

$$\left\langle f\left(P_{i,1}^{WT}, P_{i,1}^{PV}\right), \ldots, f\left(P_{i,t}^{WT}, P_{i,t}^{PV}\right), \ldots, f\left(P_{i,T}^{WT}, P_{i,T}^{PV}\right)\right\rangle, \tag{5}$$

For the optimization problem defined by (5), ROOT is a novel algorithm used to solve this problem due to its ability to provide dynamic solutions according to specific time-varying fitness functions [15]. In order to better apply ROOT to obtain a more robust solution, this paper first uses the scenario method to obtain the typical output curve of renewable energy, fits the output curve and then substitutes the fitted result into the ROOT algorithm for calculation. At the same time, the existing ROOT algorithm finds a new robust solution according to its future predicted fitness value. However, the error of predicting the future fitness value is often too large, which makes it difficult to find a better robust solution. Aiming to solve the problems existing in the ROOT algorithm, this paper proposes a modified ROOT algorithm.

3.2. Scenario Analysis Method

In order to make the time-varying parameters of the WT and PV cell contained in the established dynamic optimization problem closer to the model reality, this paper chooses the LHS and BR scenario method as the pre-method to modify the ROOT calculation method, so as to ensure that the dynamic optimization algorithm can obtain a more robust solution in the time domain. The scenario generation method is a way to analyze the uncertainty of power systems by constructing deterministic scenarios, including scene generation and scene restoration. Scene generation refers to the generation of a large number of scenes with uncertain features based on the PDF of the research object, which is represented by the set $S = \{S_1, S_2, \ldots, S_N\}$. Here, LHS is used to generate typical scenarios. Through the analysis of the generated scene data set S, BR is used here to filter the scenes with high similarity, and finally, the scene of set $K = \{K_1, K_2, \ldots, K_M\}$ with the highest expected value is obtained. Set K can replace the large-scale low-probability scene of the original production with a small-scale high-probability scene. The process of scene analysis is shown in Figure 3.
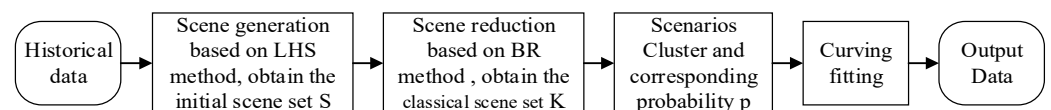

Figure 3. Process of scenario analysis.

3.3. Modified Robust Optimization over Time

The accuracy of the existing algorithm depends on the amount of statistical data, that is, the statistical data required to cover the past and current fitness values of the search space. However, in the problem of high dimension or large search space, as much data as possible are needed to obtain a more accurate approximation, which is difficult to achieve in practical engineering. Therefore, based on the spatial characteristics of the solution of the dynamic robust optimization problem, this paper finds three important metrics that affect the search robust optimal prediction: the sum of feasible direction, stability degree and floating value. Based on the three new metrics, ROOT-TSE-PCCG is proposed.

3.3.1. Feasible Direction

The FD is used to describe the change trend of the objective function, which is as follows:

$$R^{fd}(x,t,u,v) = \frac{1}{u+v+1} \sum_{i=t-u}^{i=t+v} |f(x,\varphi_{i+1}) - f(x,\varphi)|, \tag{6}$$

where u and v are the number of historical and future environments, respectively; t is the current moment; R^{fd} determines the FD of the objective function value (OFV) by calculating the sum of the objective function change value under p historical environments, q future environments and current t and then taking the average value.

In the process of evolutionary optimization of the algorithm, the change trajectory of the corresponding solution can be obtained according to the change in the OFV of each solution in the whole dynamic environment. Taking the single-objective maximization problem as an example, 2 solutions are selected in 100 continuous dynamic environments based on whether the FD is considered. The trajectory of the OFV obtained is shown in Figure 4; both solutions are higher than the set threshold $_\delta$. From Figure 1, it can be seen that in the A, B and C regions, the prediction error between the OFV and the actual value of the two is the same, but the solution considering the FD can judge the change trend of the optimal robust solution through the existing robust solution and the predictive robust solution, and better track the change direction of the optimal solution, so the overall error is small. Without considering the solution of the FD, the change trend of the optimal robust solution cannot be judged in time; so, the tracking effect of the optimal robust solution is general, and the overall error is large. Based on the above analysis, it can be seen that the introduction of the FD into the prediction solution helps to obtain a robust solution with better robustness.
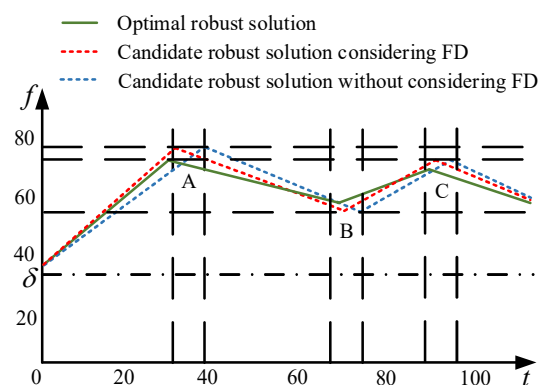

Figure 4. Robust solution of OFV change curve based on FD.

3.3.2. Stability Degree

The SD is used to describe the stability of the predicted value, which is as follows:

$$R^{SD}(x,t,u,v) = \left| \frac{f(x,\varphi_j) - [\max f(x,\varphi_i) + \min f(x,\varphi_i)]}{\eta} \right|,$$

$$s.t.i \in [1,u], j \in [t+1,v], \eta \in [1,+\infty) \tag{7}$$

where δ is the fluctuation threshold.

The trajectory of the OFV obtained is shown in Figure 5; both solutions are higher than the set threshold δ. As shown in Figure 5, it can be seen that the candidate robust solution considering the SD can judge its change range and offset the degree by the size of the value of the SD that is constantly updated. If the SD of the OFV is large, the prediction accuracy is poor at this time, and the robust solution obtained may not be accurate enough. If the SD of the OFV is small, the prediction accuracy is good at this time, and the accuracy of the robust solution obtained is high. From the above analysis, it can be seen that the value of the SD is also an important metric to guide the algorithm to find a solution with better robustness.
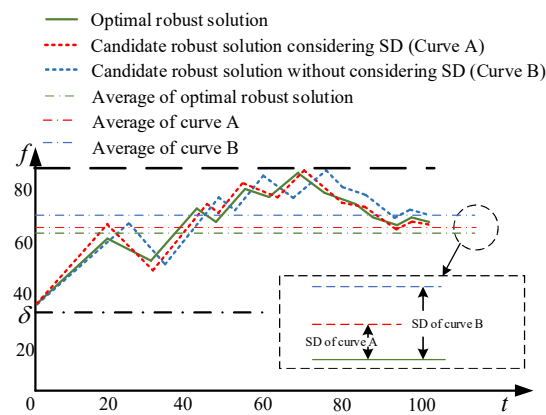
Figure 5. Robust solution of OFV change curve based on SD.

3.3.3. Sum of Floating Value

The SFV of the objective function in the adjacent environment can represent the change state of the OFV corresponding to the solution, which is as follows:

$$R^{SFV}(x,t,u,v) = \sum_{i=t-u}^{i=t+v} (f(x,\varphi_{i+1}) - f(x,\varphi_i)), \tag{8}$$

The trajectory of the OFV obtained is shown in Figure 6; both solutions are higher than the set threshold δ. As can be seen from Figure 6, the candidate robust solution considering the SFV can continuously predict the change state of the optimal robust solution at the next moment by updating the positive and negative values of the SFV, so as to better track the function value at a future moment so that the error of the robust solution is kept in a small interval. From the tracking curves of the A and B regions in Figure 3, it can be seen that the optimal robust solution cannot be effectively tracked without considering the candidate robust solution of the SFV when the optimization problem is in a state of fluctuation in a dynamic environment, thus increasing the prediction error of the algorithm. From the above analysis, it can be seen that the SFV is also an important metric in selecting the optimal robust solution.
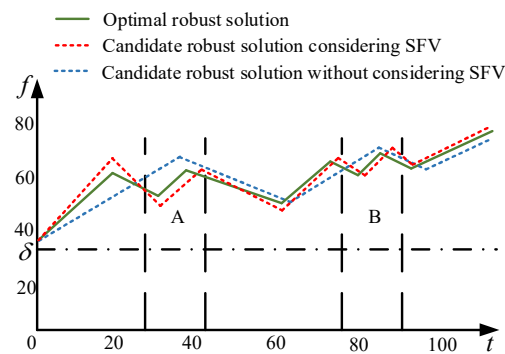
Figure 6. Robust solution of OFV change curve based on SFV.

3.4. Analysis Method of Renewable Energy Uncertainty Problem

Based on the above analysis, this paper introduces three new metrics on the basis of the existing ROOT algorithm and proposes the ROOT-TSE- PCCG algorithm. The algorithm flow chart is shown in Figure 7. The algorithm design idea of this paper can be reflected by the algorithm flow chart shown in Figure 7. Firstly, the typical output curve of the RES is calculated by using the pre-scene analysis method. On the basis of the output curve fitting results, $P_{i,t}^{WT}$ and $P_{i,t}^{PV}$ are rewritten as time-varying parameters and brought into the dynamic optimization problem shown in (4). Secondly, the proposed ROOT-TSE- PCCG algorithm is used to solve the dynamic optimization problem. Finally, the robust solution set is evaluated by using the two-stage evaluation method to obtain the optimal robust solution to the dynamic optimization problem.
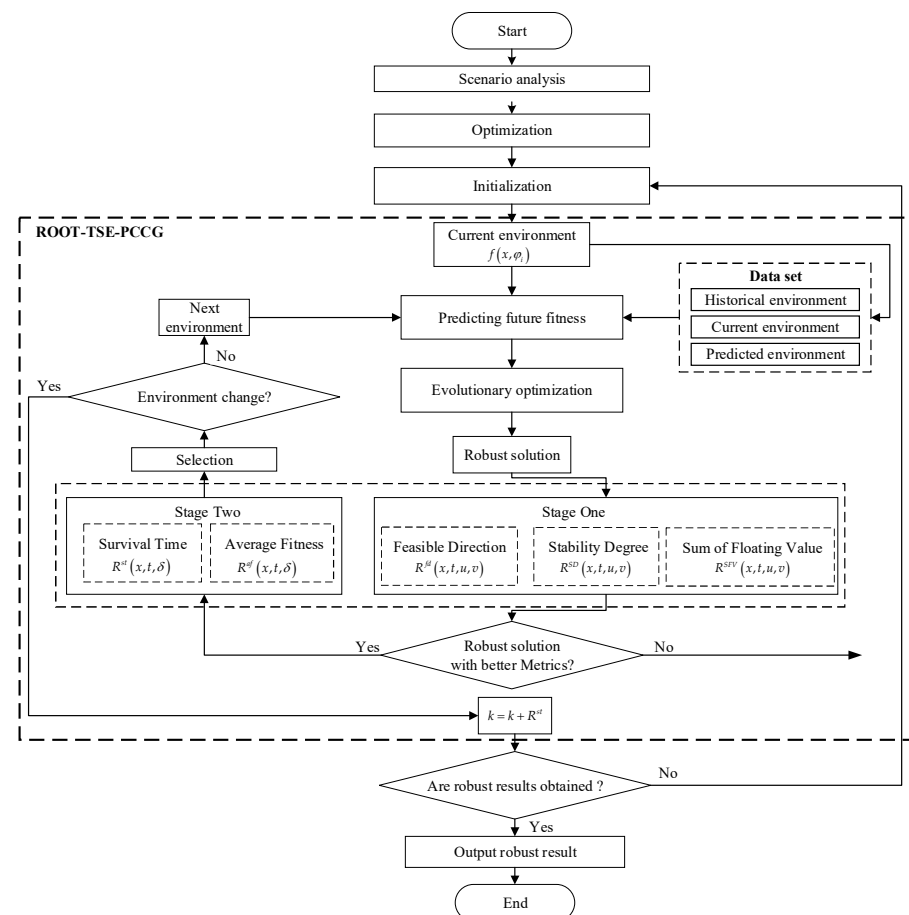
Figure 7. Flow chart of ROOT-TSE-PCCG.

4. Optimal Scheduling Model

4.1. Optimization Objective

The objective function is shown below.

$$\min C_{IES} = C_{grid} + C_{gas} + C_{om} + C_{sess},\tag{9}$$

where C_{grid} and C_{gas} are the electrical energy transaction expenditure and gas energy transaction expenditure of the EPG, respectively; C_{om} is the operation and maintenance expenditure of the RIES; C_{sess} is the energy transaction expenditure of the SESS.

$$C_{grid} = \sum_{n=1}^{N}\sum_{t=1}^{T}\left(c_{b,t}^{gird}P_{n,t}^{Grid,buy} - c_{s,t}^{gird}P_{n,t}^{Grid,sell}\right)\Delta t,\tag{10}$$

$$C_{gas} = \sum_{i=1}^{N}\sum_{t=1}^{T}c_{gas}\left[P_{i,t}^{GT}/\left(\eta_i^{GT}H_{ng}\right) + H_{i,t}^{GB}/\left(\eta_i^{GB}H_{ng}\right)\right]\Delta t,\tag{11}$$

$$C_{om} = \sum_{i=1}^{N}\sum_{t=1}^{T}\left(K_{om}^{Elec}P_{i,t}^{Elec} + K_{om}^{Heat}H_{i,t}^{Heat} + K_{om}^{Cold}C_{i,t}^{Cold}\right)\Delta t,\tag{12}$$

$$C_{sess} = \sum_{i=1}^{N}\sum_{t=1}^{T}\left(c_{b,t}^{sess}P_{i,t}^{SESS,cha} - c_{s,t}^{sess}P_{i,t}^{SESS,dis}\right)\Delta t,\tag{13}$$

4.2. Optimization Constraints

For the multi-district RIES shown in Figure 1, the constraints can be categorized into CCHP constraints, SESS constraints and coupling constraints between the CCHP and SESS, as shown in Table 1.

Table 1. Optimization constraints of multi-district RIES.

Constraint Type	CCHP	SESS	Coupling Relationship
Equality constraints	1. Power bus energy balance constraints 2. Electric storage energy relationship constraints	1. Energy continuity constraint	1. CCHP-SESS energy coupling constraint
Inequality constraints	1. Equipment operating power constraints 2. Electric storage charging/discharging power constraints	1. Charging/discharging power constraints 2. Capacity constraints	/

The constraints of the CCHP and SESS can be found in references [26,31] and Section 2.2, respectively. At the same time, according to Table 1, the direct energy coupling constraints of the CCHP and SESS should be considered. That is to say, from the perspective of the coupling system and engineering practice, the cumulative value of the energy interaction of all users using the SESS for charging and discharging behavior at a certain scheduling moment should be equal to the energy input/output of the SESS itself at this moment, and the energy source of each charging and discharging behavior of the SESS should be the cumulative value of user charging/discharging behavior.

$$\sum_{i=1}^{N}\left(P_{i,t}^{SESS,dis} - P_{i,t}^{SESS,cha}\right) = P_t^{SESS,relea} - P_t^{SESS,abs},\tag{14}$$

For the CCHP established in this paper, as shown in Figure 2, it is also necessary to meet the waste heat balance constraints of the waste heat boiler, as shown below.

$$H_{i,t}^{HE}/\eta_{he} + C_{i,t}^{AC}/\eta_{ac} = H_{i,t}^{GT}\gamma_{gt}\eta_{whb},\tag{15}$$

4.3. Optimization Method

After substituting the RES power data obtained based on the scenario analysis method, the model is transformed into an MILP model. In this paper, the commercial solver CPLEX12.8 and YALMIP toolbox are used to solve the model in Matlab R2021a [32].

5. Case Study

5.1. Simulation System

We take a more common comprehensive area as an example, as shown in Figure 8. As shown in Figure 8, the RIES established in this paper consists of four sub-districts: RA, CA, IA and OA [33,34]. Each sub-district has a self-built CCHP, and each sub-district is connected to the energy transmission line between the EPG and SESS.
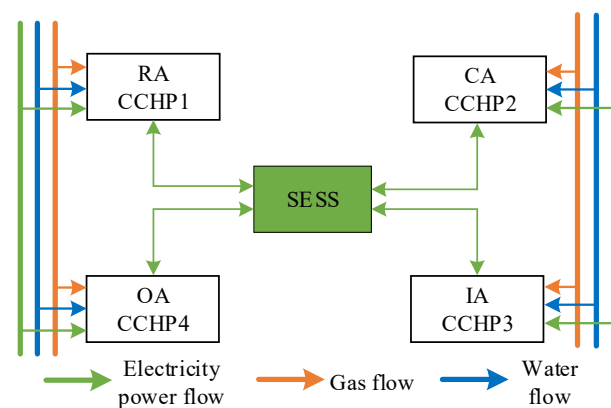
Figure 8. Structure of multi-district RIES.

Tables A1 and A2 in Appendix A describe the parameters of the energy equipment contained in each region. Table A3 in Appendix A describes the operating parameters of the SESS equipment in this paper. Tables A4 and A5 in Appendix A describe the time-of-use electricity prices of the EPG and SESS, respectively. The equipment efficiency parameters of the ES installed in the CA and IA are the same as those of the SESS equipment. At the same time, the price and calorific value of natural gas are 2.46 CNY/m^3 and 9.78 kWh/m^3, respectively. For security considerations in real life, the RA and CA are not equipped with a WT. Figure 9 shows the typical RES output curve and typical electrical, heat and cold load curves in each region.

(**a**)

(**b**)
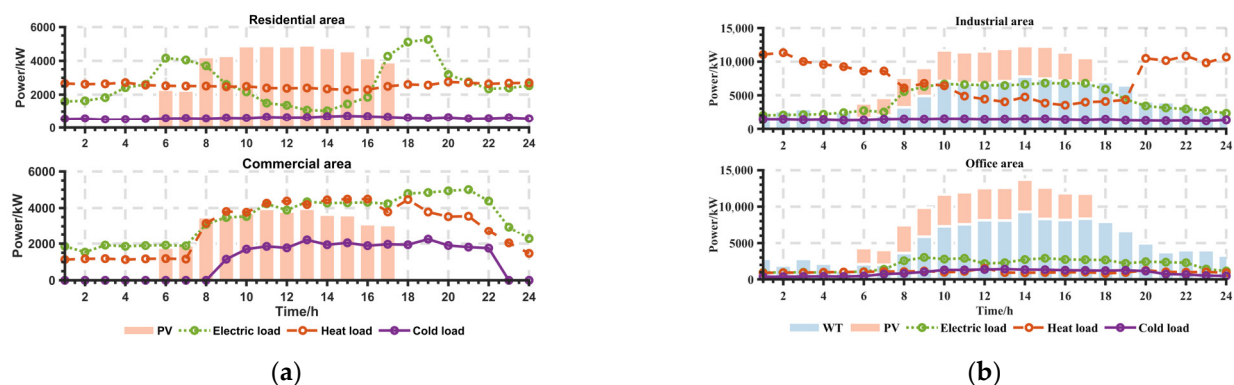
Figure 9. The typical output curve of RESs and the typical load curve in each region. (**a**) The output and load data of the RA and CA. (**b**) The output and load data of the IA and OA.

From Figure 9, the OA is a multi-power-type district; the RD and ID are a flat-power-type district; the CA is a power-shortage-type district. And the scheduling time T of each typical day is 24 h.

5.2. Analysis of the Validity of Modified ROOT

To test the performance of ROOT-TSE-PCCG, all experiments in this paper are conducted on mMPB [16], which can be described as follows:

$$F_t\left(\vec{X}\right) = \max_{i=1}^{i=m}\left\{H_t^i - W_t^i \times \|\vec{X} - \vec{C}_t^i\|_2\right\},\qquad(16)$$

where $F_t\left(\vec{X}\right)$ is the objective function; H_t^i, W_t^i and $\vec{C}_t^i$ are the height, width and central position of the *i-th* peak function, respectively; $\vec{X}$ is the decision variable; m is the total number of peaks. In order to remain dynamic, t is added to 1 after Δe in a certain period of time, and Δe is measured by the number of fitness evaluations. The dynamic changes in H_t^i, W_t^i and $\vec{C}_t^i$ are as follows:

$$H_{t+1}^i = H_t^i + height\_severity^i \times N(0,1),\qquad(17)$$

$$W_{t+1}^i = W_t^i + width\_severity^i \times N(0,1),\qquad(18)$$

$$\vec{C}_{t+1}^i = \vec{C}_t^i + \vec{v}_{t+1}^i,\qquad(19)$$

$$\vec{v}_{t+1}^i = \frac{s \times ((1-\lambda) \times \vec{r} + \lambda \times \vec{v}_t^i)}{\|(1-\lambda) \times \vec{r} + \lambda \times \vec{v}_t^i\|},\qquad(20)$$

where $N(0,1)$ is a random number of Gaussian distributions with a mean of zero and a variance of one. The height and width of each peak are initialized according to its own set of *height_severity^i* and *width_severity^i*, and the above two parameters are randomly selected in *height_severity_range* and *width_severity_range*. The parameter setting of mMPB is shown in reference [18]. The comparison algorithms are proposed in reference [16] and reference [18]. The experiment is tested under the condition that mMPB changes randomly 150 times, and each comparison algorithm runs independently 30 times to take the average value. The experimental results are shown in Figure 10.

It can be seen from Figure 10a,b that as the fitness threshold set by the dynamic optimization problem increases, the ST obtained by each dynamic optimization problem decreases. The larger the fitness threshold set, the higher the robustness of the robust solution obtained by the dynamic optimization problem in dealing with time-varying parameters. It can be seen that when the fitness threshold is set to 40, the robust solution obtained by the dynamic optimization algorithm has high robustness in the current external environment. However, when the fitness threshold is set to 50, some solutions with low robustness cannot adapt to the changing environment, resulting in a continuous decrease in the ST of the robust solutions obtained by each ROOT algorithm.

Similarly, from Figure 10c,d, it can be seen that the average robustness of the robust solution obtained by the dynamic optimization problem is also reduced with the increase in the set threshold. The larger the threshold setting of the time window, the higher the robustness of the robust solution obtained by the dynamic optimization problem when dealing with time-varying parameters. When time window value is set to 2, the robust solution obtained by dynamic optimization problem can adapt to the two minimum dynamic environments. When the time window value is set to 6, the robust solution obtained by requiring the previous time window to be 2 can satisfy more changing environments. At this time, some robust solutions cannot adapt to the changing environment of the outside world, resulting in a decrease in the average robustness of the robust solutions obtained by each ROOT algorithm.
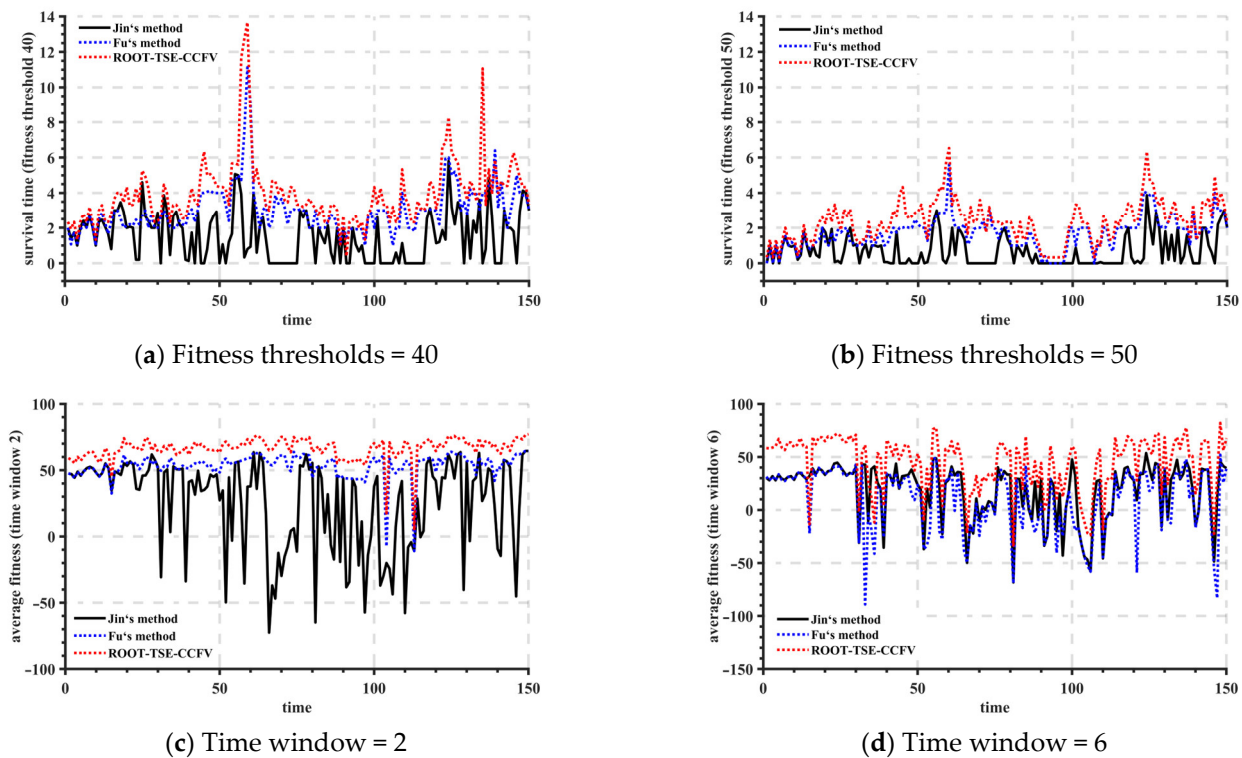
(**a**) Fitness thresholds = 40

(**b**) Fitness thresholds = 50

(**c**) Time window = 2

(**d**) Time window = 6

Figure 10. The average robustness of different ROOT algorithms with different setting of fitness thresholds and time windows.

In the case of mMPB, the robustness results of the average ST and the average AF of different algorithms are shown in Table 2. The robustness of the proposed algorithm in terms of the average ST and the average AF is significantly improved compared with the comparison algorithm. From Table 2 and Figure 10, it can be seen that in general, with the increase in the threshold set by the decision maker, the average robust performance of each dynamic optimization algorithm shows a downward trend. At the same time, from the experimental results in the mMPB environment, it can be seen that the average robustness of the proposed algorithm has achieved good robustness results in any case.

Table 2. Comparison of average ST and AF of different ROOT algorithms under mMPB.

Algorithm	Fitness Threshold		Time Window	
	40	**50**	**2**	**6**
Jin's ROOT	1.54	0.69	25.95	18.64
Fu's ROOT	3.03	1.72	53.58	9.17
ROOT-TSE-PCCG	3.97	2.39	68.71	44.63

5.3. Analysis of SESS Capacity Configuration and RIES Operation Cost

In order to study the influence of different RES uncertainty calculation methods on SESS capacity configuration and the role of the SESS in RIES optimal scheduling, SO is introduced as a comparison algorithm for solving RES uncertainty, and the following four modes are set up.

Mode 1: Calculation of RES output power using SO without considering the participation of the SESS in the optimized scheduling.

Mode 2: Calculation of RES output power using SO, and the SESS is considered to participate in optimal scheduling.

Mode 3: Calculation of RES output power using ROOT-TSE-PCCG without considering the participation of the SESS in the optimized scheduling.

Mode 4: Calculation of RES output power using ROOT-TSE-PCCG, and the SESS is considered to participate in optimal scheduling.

In the subsequent analysis, it is stipulated that the power is positive when the electric energy is charged into the SESS. At this time, it means that each sub-region charges its own electric energy into the SESS, and the power is negative when the electric energy is released by the SESS. At this time, it means that the electric energy in each region is recovering from the energy storage system. The results of SESS capacity configuration and RIES operation cost under different conditions are shown in Table 3.

Table 3. The details of SESS capacity configuration and RIES operating cost under different modes.

Details of Operating Cost	Mode 1	Mode 2	Mode 3	Mode 4
Electrical energy transaction expenditure	18,410.47 CNY	15,122.97 CNY	17,410.43 CNY	14,225.04 CNY
Gas energy transaction expenditure	78,229.09 CNY	71,094.58 CNY	74,161.40 CNY	66,716.22 CNY
Operation and maintenance expenditure	6055.71 CNY	6117.08 CNY	5963.88 CNY	6120.32 CNY
Energy transaction expenditure with SESS	/	3571.85 CNY	/	3666.71 CNY
Capacity configuration of SESS	/	15,352.76 kWh	/	15,761.51 kWh
Total cost	102,695.27 CNY	95,906.49 CNY	97,535.71 CNY	90,728.29 CNY

By comparing mode 1 and mode 3, it can be seen that compared with SO, ROOT-TSE-PCCG can obtain a more robust solution due to the introduction of three metrics R^{fd}, R^{SD} and R^{SFV}. Therefore, when solving the dynamic optimization problem considering RES uncertainty, the total cost of the system can be reduced. Compared with mode 1, the total operating cost of mode 3 decreased by 5.02%. By comparing mode 2 and mode 4, it can be seen that the RES robust solutions obtained by different algorithms also have an impact on the capacity configuration of the SESS. Since the solution obtained by ROOT-TSE-PCCG is more robust, the required SESS capacity configuration is higher in this case, and the capacity configuration of the SESS under mode 4 is 2.66% higher than that under mode 2. In summary, ROOT-TSE-PCCG can better solve the RES uncertainty problem and obtain a more robust solution so that the RIES can operate under more economical and stable conditions. By comparing mode 3 and mode 4, it can be seen that when the RIES configures the SESS, the total operating cost of the system is further reduced. Although the cost of interaction between the RIES and SESS is increased, due to the complementary effect of the SESS by coordinating the power load curve of each region, the energy that cannot be absorbed by the rich areas of RESs can be reasonably stored and allocated to the areas in need. Therefore, the electricity and gas purchase costs of the whole RIES are reduced, of which the electricity purchase cost is reduced by 18.30% and the gas purchase cost is reduced by 10.04%. In summary, the rational allocation of SESSs is also an important means to enhance the stability of RIES operation and reduce operating costs.

5.4. Analysis of SESS-Optimized Operation Results

Taking the established mode 2 and mode 4 as an example, the optimal scheduling operation results of the SESS are calculated, and the optimal energy interaction results between each region and the SESS in each scheduling day are shown in Figure 11. In Figure 11, when the value represented by a vertical column is positive (the vertical column is above the left horizontal axis y = 0 kW), it means that the sub-region corresponding to the vertical column is charging electricity power into the SESS. Otherwise, it means that the sub-region corresponding to the vertical column retrieves electricity power from the SESS. The red curve represents the change curve of the state of charge at each scheduling moment of the SESS, and the value of the state of charge corresponds to the value of the right *y* axis.

(**a**) Operation results of SESS under mode 2   (**b**) Operation results of SESS under mode 4
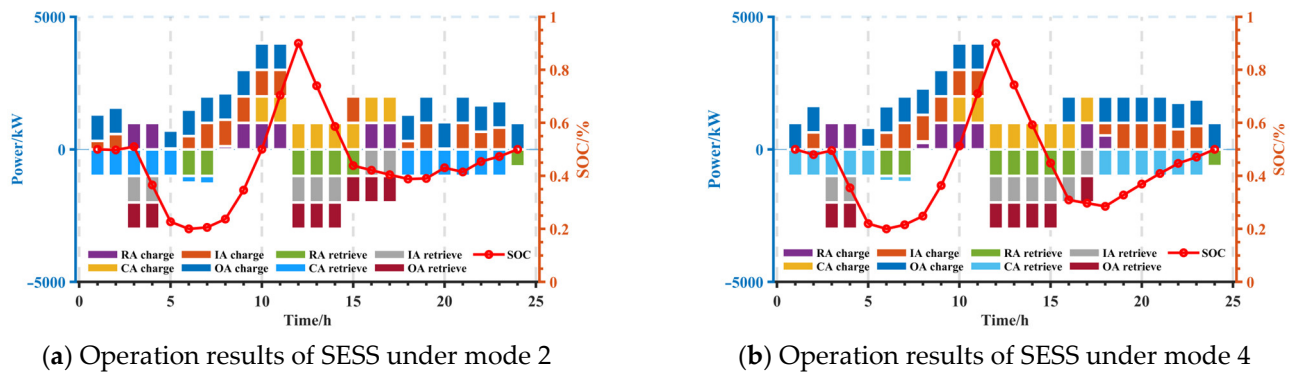
Figure 11. The optimized operation results of the SESS under different modes.

It can be seen from Figure 11 that the SOC curves of the SESS under mode 2 and mode 4 are similar, because whether it is SO or ROOT-TSE-PCCG, the above algorithms calculate the robust output based on the uncertainty of historical data of RESs and do not produce large offset changes. At the same time, due to the different robust solutions obtained by different algorithms, the interaction strategy between each region and the SESS in the 15:00–20:00 time period is different. Combined with Figure 9, it can be seen that the OA mainly charges power into the SESS because it contains abundant RESs, and its own load is small. The RA, IA and CA are mainly powered from the SESS. It is worth noting that due to the large power load demand of the CA in the evening peak period, the CA purchases a large amount of power from the SESS during the 18:00–23:00 period. While meeting its own power load, it reduces the interaction with the EPG to achieve the purpose of reducing operating costs.
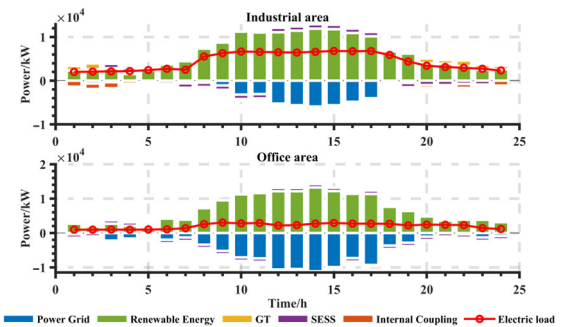
5.5. Analysis of Optimal Scheduling Results of RIES Considering SESS

We take mode 4 as an example to analyze the optimal scheduling result for each region in the RIES.

The optimal scheduling results of power load in each region of the RIES are shown in Figure 12. On the whole, RESs in all regions can participate in the actual power load supply; so, the optimal scheduling strategy can complete the consumption of RESs. At the same time, the area with abundant RESs sells a large amount of electric energy to the EPG to reduce the operation cost of the whole system. Similarly, abundant electric energy can also be stored in the SESS to ensure the rational utilization of renewable energy in the RIES. Specifically, it can be seen from Figure 12a that the RA and CA only contain a PV cell, which belongs to the RES-deficient area. Therefore, when the RA has no PV output during 03:00–04:00 and 18:00–24:00, it is necessary to purchase electricity from the EPG to meet its own demand for power load. When the output power of the PV cell is large at 09:00–11:00, most of the users of the RA have moved to other areas to consolidate their lives. At this time, their own power load is small, so they can be charged to the SESS to improve their own electricity sales revenue and complete the consumption of RESs. For the CA, since the power load and heat load are at the peak stage during the period of 10:00–17:00, and during this period, the CA's own photovoltaic power generation cannot meet the load's demand for electricity, the CA mainly purchases electricity from the EPG during this period. In the rest of the time period, due to the comprehensive consideration of the coupling supply of cold and heat energy, some of the electricity is supplied through a GT. From Figure 12b, it can be seen that the IA has abundant RESs and its own power load is low; so, the IA can sell rich power resources to the EPG to earn profits. Similarly, while the OA region is rich in RESs, its own power load is lower than that of the IA, so it can sell a large amount of power to the EPG.
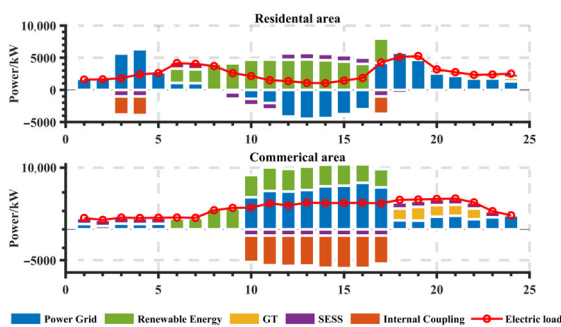
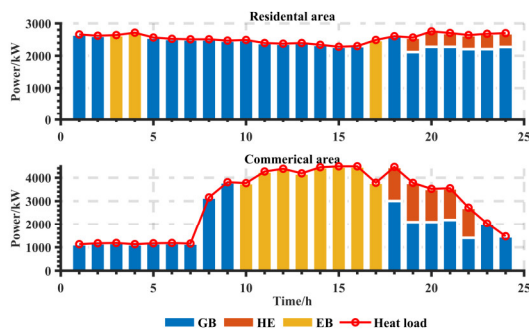(**a**) Electric optimal scheduling of RA and CA

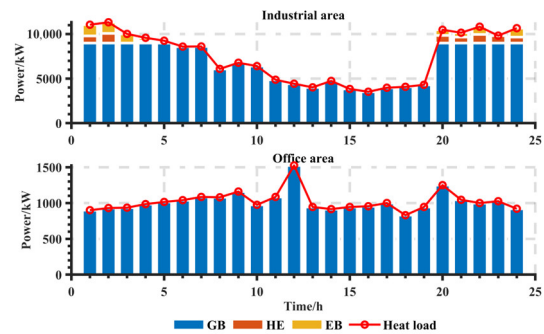
(**b**) Electric optimal scheduling of IA and OA

Figure 12. Electric load optimization scheduling results of RIES.

The optimal scheduling results of the RIES heat load are shown in Figure 13. On the whole, the thermal energy generated by the GB is the main source used to meet the thermal load in the region, accounting for 86.58% of the total cooling load supply, and the remaining thermal energy supply is completed by the HE and EB. The following is a detailed analysis of the thermal energy supply model for each region from Figure 14. Figure 13a shows the electric energy purchased from the EPG in the RA and CA areas. The RA and CA areas are mainly used to supply power to the EB, and the EB converts electric energy into heat energy to heat the area. In particular, because the electric load and heat load in the CA area are at their peak during 10:00–17:00 and the external electricity price is at the valley stage, the CA is mainly provided for by the EB during this period. It can be seen from Figure 13b that the IA and OA use the GB as the only device that provides more than 80% of thermal energy in a day. In particular, the IA only uses the EB and HE to provide a small amount of heat energy during the morning and evening due to electricity prices. The reason for the above results is that gasoline prices remain unchanged for a day. At the same time, in the process of the GB directly providing heat to the load, the energy from the conversion steps involved is less and the energy loss is lower.

Figure 14 shows the optimal scheduling results of the multi-region RIES cooling load. On the whole, the cold energy generated by the EC is the main source used to meet the cooling load in the region, accounting for 84.38% of the total cooling load supply, and the remaining cold energy supply is completed by the AC. The following is a detailed analysis of the cold energy supply mode in each region from Figure 14. From diagram (a), it can be seen that since there is no PV power supply in the RA area during 19:00–24:00, the EPG is in the peak stage of electricity prices, so the RA will use the GT to produce the required electricity, and the GT will produce high-temperature waste heat when running. In order to give full play to the advantages of the CCHP, improve energy utilization and reduce operating costs while ensuring the cascading utilization of energy, at this time, high-temperature waste heat passes through the heat pipe. Part of the heat energy is transmitted to the HE to continue to generate heat energy with a controllable success rate, and the other part of the heat energy is transmitted to the AC to convert high-temperature waste heat into cold power to the user. Thus, this is more economical to meet the user's demand for cold power. Similarly, the optimal operation result of the CA is similar to that of the RA, that is, when there is no RES available, the AC is used to absorb high-temperature waste heat to provide the cooling load. It can be seen from Figure 14b combined with Figure 9b above that both the IA and OA are RES-rich areas. On the one hand, in order to consume their own RESs and reduce the rate of wind and light abandonment, and on the other hand, in order to reduce the expenditure of purchasing natural gas from the EPG and reduce the operating cost, the cooling load generated by the EC is mainly used to meet the needs of their users for the cooling load.

(**a**) Heat optimal scheduling of RA and CA

(**b**) Heat optimal scheduling of IA and OA

Figure 13. Heat load optimization scheduling results of RIES.
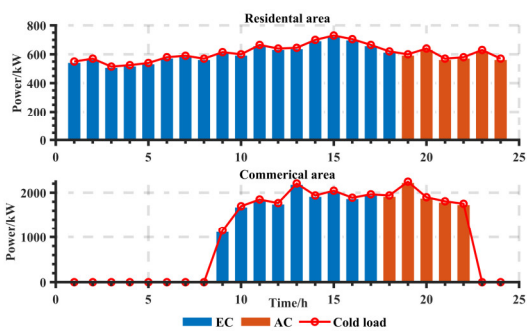
(**a**) Cold optimal scheduling of RA and CA

(**b**) Cold optimal scheduling of IA and OA
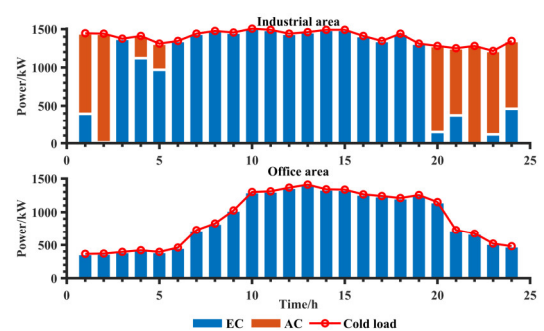
Figure 14. Cold load optimization scheduling results of RIES.

6. Conclusions

In this paper, the following work is carried out for the multi-area RIES optimal scheduling problem with an SESS, considering RES uncertainty. Firstly, a multi-area RIES system model considering SESS access is established. At the same time, the working state of SESS access of the RIES is considered from three aspects and the corresponding constraints are proposed. Secondly, PV cells and a WT are regarded as time-varying parameters, and a dynamic optimization problem model considering time-varying parameters is established. For such problems, this paper also proposes a ROOT-TES-PCPG algorithm combined with a scene analysis method to solve them. Finally, the proposed method is verified by establishing a practical example model. Based on the proposed different models, the following conclusions can be obtained through the results.

1. For the dynamic robust optimization problem considering time-varying parameters, the improved ROOT algorithm based on the two-stage evaluation proposed in this paper has a better judgment effect on the predicted solution in the future, so that the robustness of the solution obtained by the overall algorithm is better. In the mMPB test environment, compared with the results of the existing ROOT algorithm, the solution AF index and ST index obtained by ROOT-TSE-PCPG are increased by 94.41% and 179.78, respectively. Therefore, the algorithm proposed in this paper provides a new method for calculating the optimal robust solution of dynamic optimization problems in practical engineering and has certain practical application value.

2. When there are uncertainties such as a WT and PV cells in the RIES system, the ROOT-TSE-PCPG based on the scenario analysis method proposed in this paper can be used to analyze the uncertainty of RESs through the robust control method. At the same time, the method proposed in this paper can effectively reduce the operating cost of the RIES. The application of the proposed method in the optimal scheduling problem can reduce the operating cost of the whole system by 5.32% on average. Similarly,

when there are multiple sub-energy regions in the system, the rational allocation of SESSs can make the energy consumption of the whole system more stable and the energy interaction more scientific, so as to achieve the purpose of reducing the operating cost of the system. The rational allocation of SESSs can reduce the operating cost of the whole system by an average of 6.81%, while considering the above two factors in the optimal scheduling problem can reduce the operating cost of the system by 11.65%. At the same time, the SESS also acts as an energy transmission line, which can transmit electricity from RES-rich areas to RES-deficient areas.

At present, although several SESS demonstration parks have been put into operation in China, they are still in the development stage. As China continues to move toward the goal of 'carbon peak carbon neutrality', the method proposed in this paper will provide a reference for the operation of SESSs in the future. At the same time, with the increasing uncertainty factors on the source-load side of the RIES, the operation cost and economy requirements of RIES optimal scheduling will be higher in the future, and the operation optimization objectives will be more diversified. Therefore, how to model and solve the dynamic robust optimization problem with multiple optimization objectives and uncertain time-varying parameters is an issue that needs to be studied in the future.

Nomenclature

Acronym			
AC	Absorption chiller	mMPB	Modified moving peaks benchmark
AF	Average fitness	OA	Office area
BR	Backward reduction	OFV	Objective function value
CA	Commercial area	PDF	Probability density function
CCHP	Combined cooling heating and power	PV	Photovoltaic
DE	Differential evolution	RES	Renewable energy source
ESS	Energy storage system	RIES	Regional integrated energy system
EPG	External power grid	ROOT	Robust optimization over time
EB	Electric boiler	ROOT-TSE-PCCG	ROOT based on two-stage evaluation of problem characteristic change guidance
EC	Electrical chiller	RA	Residential area
ES	Energy storage	SOC	State of charge
FD	Feasible direction	SD	Stability degree
GT	Gas turbine	SFV	Sum of floating value
GB	Gas boiler	ST	Survival time
HE	Heat exchanger	SO	Stochastic optimization
IA	Industrial area	SESS	Shared energy storage station
LHS	Latin hypercube sampling	WT	Wind turbine
MILP	Mixed integer linear programming	WHB	Waste heat boiler

Variables		Parameters	
t	Scheduling time	$\eta_{SESS}^{loss}/\eta_{SESS}^{abs}/\eta_{SESS}^{relea}$	Self-discharge/charge/discharge efficiency of SESS
Δt	Scheduling time period	$\sigma_{SESS}^{min}/\sigma_{SESS}^{max}/\sigma_{SESS}^{init}$	Minimum/maximum/initial coefficient of SOC
n	Number of CCHP	$c_{b,t}^{gird}/c_{s,t}^{gird}$	Electricity purchase/sale price with EPG
E_t^{SESS}	State of charge of SESS	$c_{b,t}^{sess}/c_{s,t}^{sess}$	Electricity purchase/sale price with SESS
$P_t^{SESS,abs}/P_t^{SESS,relea}$	Charge/discharge power of SESS	c_{gas}	Price of natural gas
$E_{max}^{SESS}/E_{start}^{SESS}/E_{end}^{SESS}$	Maximum/initial/final SOC	$\eta_n^{GT}/\eta_n^{GB}/\eta_{he}/\eta_{ac}/\eta_{whb}$	Efficiency of GT/GB/HE/AC/WHB
P_{max}^{SESS}	Maximum power of SESS	H_{ng}	Heating value of natural gas
$U_{abs}^{SESS}/U_{relea}^{SESS}$	Charging/discharging state bit of SESS	$K_{om}^{Elec}/K_{om}^{Heat}/K_{om}^{Cold}$	Operating and maintenance expenditure of electric/heat/cold energy equipment
$P_{n,t}^{Grid,buy}/P_{n,t}^{Grid,sell}$	Electricity purchase/sale power with EPG	γ_{gt}	Thermoelectric ratio of GT
$P_{n,t}^{GT}/H_{n,t}^{GT}$	Electrical/heat power of GT		
$H_{n,t}^{GB}$	Heat power of GB		
$P_{n,t}^{SESS,cha}/P_{n,t}^{SESS,dis}$	Charging/discharge power of CCHP		
$C_{n,t}^{AC}$	Cold power of AC		
$P_{n,t}^{RG}$	Electrical power of RES		
$H_{n,t}^{HE}$	Heat power of HE		

Appendix A

Table A1. Capacity parameters (kWh).

Equipment	RA	CA	IA	OA
PV	2500	4500	8500	2500
WT	/	/	6500	3500
GT	2500	5500	8500	3500
GB	5500	5500	8500	5500
WHB	5500	5500	8500	5500
ES	/	1500	2500	/
EH	5500	5500	8500	5500
EC	5500	5500	8500	5500
HE	4500	4500	8500	4500
AC	5500	5500	8500	5500

Table A2. Efficiency parameters.

Equipment	RA	CA	IA	OA
Efficiency of GT	0.35	0.35	0.35	0.35
Heat-to-electricity ratio of GT	2.3	2.3	2.3	2.3
Efficiency of WHB	0.74	0.74	0.74	0.74
Efficiency of GB	0.86	0.86	0.86	0.86
Efficiency of EH	0.98	0.98	0.98	0.98
Efficiency of EC	4	4	4	4
Efficiency of AC	1.2	1.2	1.2	1.2

Table A2. *Cont.*

Equipment	RA	CA	IA	OA
Efficiency of HE	0.9	0.9	0.9	0.9
Maximum charge power of ES	/	250 kW	500 kW	/
Maximum discharge power of ES	/	250 kW	500 kW	/
Capacity of ES	/	1000 kWh	2000 kWh	/

Table A3. Equipment parameters of SESS.

Parameter	Value	Parameter	Value
Charging efficiency	0.95	Initial state of SOC	0.50
Discharging efficiency	0.95	Maximum state of SOC	0.90
Self-discharging efficiency	0.04	Minimum state of SOC	0.20
Maximum discharge power	1000 kW	Maximum charge power	1000 kW

Table A4. Time-of-use electricity price of EPG (CNY/kWh).

Price Types	Time Interval	Purchase Price	Sale Price
Peak time	06:00–08:00 17:00–23:00	0.763	0.420
Usual time	04:00–06:00 10:00–16:00	0.521	0.420
Valley time	23:00–00:00 0:00–03:00	0.253	0.420

Table A5. Time-of-use electricity price of SESS (CNY/kWh).

Price Types	Time Interval	Purchase Price	Sale Price
Peak time	08:00–09:00 19:00–24:00	0.725	0.435
Usual time	00:00–02:00 05:00–07:00 10:00–11:00 18:00–18:00	0.475	0.435
Valley time	03:00–04:00 12:00–17:00	0.271	0.435

References

1. Hou, Q.; Du, E.; Zhang, N.; Kang, C. Impact of High Renewable Penetration on the Power System Operation Mode: A Data-Driven Approach. *IEEE Trans. Power Syst.* **2019**, *35*, 731–741. [CrossRef]
2. Chen, X.; McElroy, M.B.; Kang, C. Integrated Energy Systems for Higher Wind Penetration in China: Formulation, Implementation and Impacts. *IEEE Trans. Power Syst.* **2017**, *33*, 1309–1319. [CrossRef]
3. Usaola, J. Renewables and Advanced Storage in Power Systems: The Iberian Case. *Appl. Sci.* **2022**, *12*, 3373. [CrossRef]
4. Xiao, J.W.; Yang, Y.B.; Cui, S.; Liu, X.K. A new energy storage sharing framework with regard to both storage capacity and power capacity. *Appl. Energy* **2022**, *307*, 118171. [CrossRef]
5. Zhang, S.; Li, Y.; Du, E.; Fan, C.; Wu, Z.; Yao, Y.; Liu, L.; Zhang, N. A review and outlook on cloud energy storage: An aggregated and shared utilizing method of energy storage system. *Renew. Sustain. Energy Rev.* **2023**, *185*, 113606. [CrossRef]
6. Dai, R.; Esmaeilbeigi, R.; Charkhgard, H. The Utilization of Shared Energy Storage in Energy Systems: A Comprehensive Review. *IEEE Trans. Smart Grid* **2021**, *12*, 3163–3174. [CrossRef]
7. Yong, X.; Wu, Y.; Zhou, J.; Tao, Y.; Chen, W. Prospects and barriers analysis framework for the development of energy storage sharing. *Sustain. Cities Soc.* **2023**, *89*, 104368. [CrossRef]
8. Zhao, D.; Wang, H.; Huang, J.; Lin, X. Virtual Energy Storage Sharing and Capacity Allocation. *IEEE Trans. Smart Grid* **2019**, *11*, 1112–1123. [CrossRef]
9. Chang, H.-C.; Ghaddar, B.; Nathwani, J. Shared community energy storage allocation and optimization. *Appl. Energy* **2022**, *318*, 119160. [CrossRef]

10. Liu, L.; Yao, X.; Qi, X.; Han, Y. Low-carbon economy configuration strategy of electro-thermal hybrid shared energy storage in multiple multi-energy microgrids considering power to gas and carbon capture system. *J. Clean. Prod.* **2023**, *428*, 139366. [CrossRef]

11. Huang, P.; Lovati, M.; Zhang, X.; Bales, C. A coordinated control to improve performance for a building cluster with energy storage, electric vehicles, and energy sharing considered. *Appl. Energy* **2020**, *268*, 114983. [CrossRef]

12. Jo, J.; Park, J. Demand-Side Management with Shared Energy Storage System in Smart Grid. *IEEE Trans. Smart Grid* **2020**, *11*, 4466–4476. [CrossRef]

13. Yazdani, D.; Nguyen, T.T.; Branke, J. Robust Optimization over Time by Learning Problem Space Characteristics. *IEEE Trans. Evol. Comput.* **2018**, *23*, 143–155. [CrossRef]

14. Yu, X.; Jin, Y.; Tang, K.; Yao, X. Robust optimization over time—A new perspective on dynamic optimization problems. In Proceedings of the IEEE Congress on Evolutionary Computation, Barcelona, Spain, 18–23 July 2010; pp. 1–6.

15. Jin, Y.; Tang, K.; Yu, X.; Sendhoff, B.; Yao, X. A framework for finding robust optimal solutions over time. *Memetic Comput.* **2013**, *5*, 3–18. [CrossRef]

16. Fu, H.; Sendhoff, B.; Tang, K.; Yao, X. Characterizing environmental changes in robust optimization over time. In Proceedings of the 2012 IEEE Congress on Evolutionary Computation, Brisbane, QLD, Australia, 10–15 June 2012; pp. 1–8.

17. Fu, H.; Sendhoff, B.; Tang, K.; Yao, X. Finding robust solutions to dynamic optimization problems. In Proceedings of the Applications of Evolutionary Computation: 16th European Conference, EvoApplications 2013, Vienna, Austria, 3–5 April 2013; Proceedings 16. Springer: Berlin/Heidelberg, Germany, 2013; pp. 616–625.

18. Yazdani, D.; Branke, J.; Omidvar, M.N.; Nguyen, T.T.; Yao, X. Changing or keeping solutions in dynamic optimization problems with switching costs. In Proceedings of the Genetic and Evolutionary Computation Conference, Kyoto, Japan, 15–19 July 2018; pp. 1095–1102.

19. Novoa-Hernández, P.; Pelta, D.A.; Corona, C.C. Approximation models in robust optimization over time-an experimental study. In Proceedings of the 2018 IEEE Congress on Evolutionary Computation (CEC), Rio de Janeiro, Brazil, 8–13 July 2018; pp. 1–6.

20. Fox, M.; Yang, S.; Caraffini, F. An experimental study of prediction methods in robust optimization over time. In Proceedings of the 2020 IEEE Congress on Evolutionary Computation (CEC), Glasgow, UK, 19–24 July 2020; pp. 1–7.

21. Zhang, X.; Fang, Y.; Liu, Q. Finding Robust Pareto-Optimal Solutions Over Time for Dynamic Disassembly Sequence Planning. In Proceedings of the International Manufacturing Science and Engineering Conference, West Lafayette, IN, USA, 27 June–1 July 2022; American Society of Mechanical Engineers: New York, NY, USA, 2022; Volume 85819, p. V002T06A012.

22. Guzmán-Gaspar, J.-Y.; Mezura-Montes, E.; Domínguez-Isidro, S. Differential Evolution in Robust Optimization over Time Using a Survival Time Approach. *Math. Comput. Appl.* **2020**, *25*, 72. [CrossRef]

23. Yazdani, D.; Nguyen, T.T.; Branke, J.; Wang, J. A new multi-swarm particle swarm optimization for robust optimization over time. In Proceedings of the Applications of Evolutionary Computation: 20th European Conference, EvoApplications 2017, Amsterdam, The Netherlands, 19–21 April 2017; Part II 20; Springer International Publishing: Berlin/Heidelberg, Germany, 2017; pp. 99–109.

24. Chen, M.; Guo, Y.; Jin, Y.; Yang, S.; Gong, D.; Yu, Z. An environment-driven hybrid evolutionary algorithm for dynamic multi-objective optimization problems. *Complex Intell. Syst.* **2023**, *9*, 659–675. [CrossRef]

25. Zhang, Y.; Liu, Z.; Wu, Y.; Li, L. Research on Optimal Operation of Regional Integrated Energy Systems in View of Demand Response and Improved Carbon Trading. *Appl. Sci.* **2023**, *13*, 6561. [CrossRef]

26. Zhang, H.; Dang, W.; Jia, R.; Dang, J. Research on the Economic Optimization of an Electric–Gas Integrated Energy System Considering Energy Storage Life Attenuation. *Appl. Sci.* **2023**, *13*, 1080. [CrossRef]

27. Kalathil, D.; Wu, C.; Poolla, K.; Varaiya, P. The Sharing Economy for the Electricity Storage. *IEEE Trans. Smart Grid* **2019**, *10*, 556–567. [CrossRef]

28. Kang, C.; Liu, J.; Zhang, N. A new form of energy storage in future power system: Cloud energy storage. *Autom. Electr. Power Syst.* **2017**, *41*, 2–8.

29. Walker, A.; Kwon, S. Analysis on impact of shared energy storage in residential community: Individual versus shared energy storage. *Appl. Energy* **2021**, *282*, 116172. [CrossRef]

30. Zeng, A.; Xu, Q.; Ding, M.; Yukita, K.; Ichiyanagi, K. A classification control strategy for energy storage system in microgrid. *IEEJ Trans. Electr. Electron. Eng.* **2015**, *10*, 396–403. [CrossRef]

31. Huang, S.; Lu, H.; Chen, M.; Zhao, W. Integrated energy system scheduling considering the correlation of uncertainties. *Energy* **2023**, *283*, 129011. [CrossRef]

32. Zhang, N.; Kang, C.; Xia, Q.; Ding, Y.; Huang, Y.; Sun, R.; Huang, J.; Bai, J. A Convex Model of Risk-Based Unit Commitment for Day-Ahead Market Clearing Considering Wind Power Uncertainty. *IEEE Trans. Power Syst.* **2014**, *30*, 1582–1592. [CrossRef]

33. Gu, W.; Lu, S.; Wang, J.; Yin, X.; Zhang, C.L.; Wang, Z.H. Modeling of the heating network for multi-district integrated energy system and its operation optimization. *Proc. CSEE* **2017**, *37*, 1305–1315.

34. Chen, Q.; Zhang, S.; Cheng, H.; Yuan, K.; Song, Y.; Han, F. Multiple Energy Storage Planning of Multi-district Integrated Energy System Considering Heat Storage Characteristics of Heat Network. *Proc. CSEE* **2023**, *43*, 5890–5902.

RESEARCH ARTICLE

An Improved Dynamic Robust Optimization Algorithm and Its Application in Optimal Scheduling of Integrated Energy System Considering Carbon Emission Reduction

BO ZHOU[ID] **AND ERCHAO LI**[ID]

College of Electrical and Information Engineering, Lanzhou University of Technology, Lanzhou 730050, China

Corresponding author: Bo Zhou (zhoubo@lut.edu.cn)

ABSTRACT Under the background of low-carbon and efficient development of energy system, renewable energy will be vigorously developed and gradually become the main force of energy system. However, renewable energy has great uncertainty and randomness due to its own formation characteristics. In order to solve this problem and reduce the carbon emission of regional integrated energy system (RIES), this paper first introduces the optimal structure of RIES considering shared energy storage system (SESS) and power-to-gas (P2G). Secondly, a ladder type reward-punishment carbon trading mechanism model is proposed, which considers the reward and punishment interval of carbon emissions. At the meantime, an improved robust optimization over time (ROOT) method based on index contribution degree is proposed for dynamic problem considering uncertainty, based on the effect of each solution operator in the robust solution calculation process. Finally, a scheduling model with the lowest daily operation cost is established, and the effectiveness of the proposed low-carbon operation method is verified by comparison. Experimental results show that under the same dynamic test environment, the calculation accuracy of the improved ROOT method based on the contribution degree is increased by 3.56% on average, the calculation time is shortened by 2.93% on average. Meanwhile, the carbon emission can be reduced by 8.13% by adopting the carbon emission reduction measures, which ensures the system under low-carbon conditions.

NOMENCLATURE

RIES	Regional integrated energy system.
RES	Renewable energy source.
CCHP	Combined cooling heating and power.
CTM	Carbon reduction mechanism.
P2G	Power-to-gas.
SESS	Shared energy storage system.
NG	Natural gas.
SO	Stochastic optimization.
RO	Robust optimization.
ROOT	Robust optimization over time.
EPG	External power grid.
EL	Electrolyze.
MR	Methane reactor.
HFC	Hydrogen fuel cell.
mMPB	Modified moving peak benchmark.
AHP	Analytic hierarchy process.
CRITIC	Criteria importance through intercriteria correlation.
RA	Residential area.
CA	Commercial area.

The associate editor coordinating the review of this manuscript and approving it for publication was Wencong Su[ID].

IA	Industrial area.
OA	Office area.
t	Index of time periods.
i	Number of each CCHP.
η_A	Efficiency of equipment A.
E_t^{SESS}	Capacity of SESS.
$P_t^{SESS,abs}/P_t^{SESS,relea}$	Charge/Discharge power of SESS.
$\eta_{SESS}^{abs}/\eta_{SESS}^{loss}/\eta_{SESS}^{relea}$	Charge/Self-discharge/ Discharge efficiency of SESS.
$E_{\max}^{SESS}/E_{start}^{SESS}/E_{end}^{SESS}$	Maximum/Initial/Final capacity of SESS.
$\sigma_{SESS}^{\min}/\sigma_{SESS}^{\max}/\sigma_{SESS}^{init}$	Lower/Upper/Initial coefficient of SESS capacity.
$P_{\max}^{SESS}$	Maximum power of SESS.
$U_{t,abs}^{SESS}/U_{t,relea}^{SESS}$	Charging/Discharge state bits of SESS.
P_t^{EL}	Input electric energy of EL.
$G_{H_2,t}^{EL}$	Output hydrogen energy of EL.
$\Delta P_{\max}^{EL}/\Delta P_{\min}^{EL}$	Upper/Lower limit of EL ramp power.
$P_{\max}^{EL}/P_{\min}^{EL}$	Upper/Lower limit of input electric energy of EL.
$G_{H_2,t}^{MR}/G_{NG,t}^{MR}$	Input hydrogen energy/Output natural gas energy of MR.
$G_{H_2,\max}^{MR}/G_{H_2,\min}^{MR}$	Upper/Lower limits of input hydrogen energy of MR.
$\Delta G_{H_2,\max}^{MR}/\Delta G_{H_2,\min}^{MR}$	Upper/Lower limit of MR ramp power.
$G_{H_2,t}^{HFC}$	Input hydrogen energy of HFC.
P_t^{HFC}/H_t^{HFC}	Output electric/heat energy of HFC.
$G_{H_2,\max}^{HFC}/G_{H_2,\min}^{HFC}$	Upper/Lower limits of input hydrogen energy.
$\Delta P_{H_2,HFC}^{\max}/\Delta P_{H_2,HFC}^{\min}$	Upper/Lower limit of HFC ramp power.
$P_t^X/P_{i,t}^X$	Output electric power of equipment X.
$H_t^Y/H_{i,t}^Y$	Output heat power of equipment Y.
$C_t^Z/C_{i,t}^Z$	Output cold power of equipment Z.
$P_{\max}^X/P_{\min}^X$	Upper/Lower output electric power of equipment X.
$H_{\max}^Y/H_{\min}^Y$	Upper/Lower output heat power of equipment Y.
$C_{\max}^Z/C_{\min}^Z$	Upper/Lower output cold power of equipment Z.

I. INTRODUCTION

With the increasing demand of the society to use more clean and low-carbon electric energy and reduce the carbon emission of the whole society, RES has made great progress due to its low pollution characteristics [1], [2]. RIES, which consists of RES and CCHP, has become the basis of a new intelligent power system due to its efficient use of energy [3].

The research of RIES has changed from optimal economic benefits to the lowest carbon emissions. References [4], [5]. From the external market factors of RIES, CTM is the key factor to realize the carbon reduction of RIES [6], [7]. Reference [8] introduces traditional carbon trading model, based on electrical-gas coupling unit and carbon capture device, a low carbon scheduling model considering demand response is proposed. Reference [9] introduced economic scheduling model based on ladder type CTM. On this basis, reference [10] improved ladder type CTM and established reward-penalty CTM to strengthen the means to control carbon emissions from the power system. Increasing RES consumption rate is also an important measure to achieve carbon reduction. From the perspective of RIES's own factors, studies have proposed rational allocation of P2G [11], [12] converts surplus electric energy into natural gas, which enhances the stability of RES as a power source and maintains the carbon emission of the system at a low level due to the absorption of pollution sources such as carbon. In reference [13], P2G is introduced into RIES, and an economic scheduling model of multi-energy suppliers based on Nash game model is established. Reference [14] evaluated the economics of P2G and feasibility of producing natural gas to participate in energy market. Based on traditional P2G model, a bi-level economic dispatch model considering RES and CCHP is proposed in reference [15]. Many literatures only consider carbon emissions and do not consider the impact of RES uncertainty when dealing with RIES optimal scheduling problems. However, in the actual engineering environment, when the decision maker considers the RES power generation system, it is not only to consider the role of P2G and CTM, but also to consider the impact of other operating models on the low-carbon operation of the entire system. Based on this, reference [16] improved the sustainable development of the system by introducing the load probability emission model into RES. Considering the increasing popularity of electric vehicles, reference [17] introduced electric vehicles into the energy system as a charge and discharge load model and proposed an evolutionary algorithm and optimization strategy to optimize the scheme model, reducing the system operating cost and overall environmental pollution.

Among most uncertainty factors in modern power system, RES is the main cause of uncertainty on the power side due to the fluctuation of the natural environment [18]. At present, the main methods to solve the uncertainty mode are chance constraint method, scene generation method and robust optimization method. Based on the coupling relationship between chance constraints and constraint events, reference [19] refines and splits joint chance constraints to transform many and complex constraints into a single constraint that is intuitive and easy to solve and calculate. Based on support vector machine, reference [20] identifies zero-probability events in the event and optimizes the

distribution curve of cross probability through this method. Reference [21] considers that it is crucial to obtain reasonable wind power scenarios for optimal operation, so the gradient penalty method is introduced into Wasserstein Gan and a certain number of wind power output scenarios are obtained through calculation examples. Reference [22] proposes an improved generative adversarial network to solve RES modeling problem. Reference [23], [24] proposed a two-stage optimization model based on data-driven method and robust optimization method, aiming at the uncertainties of power system at source side and network side during operation.

At present, most of the research on carbon reduction measures only focuses on optimization measures and ignored the uncertainty in the actual optimal scheduling. Although most studies based on scenario analysis for RES uncertainty can obtain the output scenarios of RES, the robustness of the results in the actual engineering environment is questionable. Therefore, it has the important practical significance to further study the impacts of the carbon reduction mechanisms and uncertainty coordinated operations on RIES optimal scheduling and SESS capacity configuration. Aiming at these problems, we establish a RIES composed of multiple CCHPs. Through the establishment of SESS and multi-energy integrated P2G at the device level, combined with CTM at the external mechanism level, we propose carbon emission reduction measures that have mature cases and are in line with the actual environment. At the same time, based on the proposed algorithm, an improved ROOT algorithm based on index contribution (IROOT-IC) is proposed to solve the optimal scheduling problem of the established RIES model. The contributions are as follows:

(1) A multi-energy integrated P2G model is established by introducing HFC model, and a carbon emission reduction measure is formed by combining CTM.

(2) A ROOT considering the index contribution degree is proposed to improve the applicability of the robust optimization algorithm for the optimal scheduling problem considering uncertainty.

The rest of this paper is structured as follows. Section II introduces the basic structure of RIES and mathematical model of P2G model. Section III establishes a ladder type reward and punishment CTM. In section IV, the dynamic robust solution algorithm of RES uncertainty is introduced. Section V presents case studies, and Section VI gives the conclusions.

II. STRUCTURE MODELLING OF RIES INCLUDING MULTI-CCHPs BASED ON SESS AND P2G

A. OVERALL FRAMEWORK OF RIES

RIES structure with multiple CCHPs is shown in Fig 1. As shown in the Fig 1, the RIES consists of several independent sub-regions within the region, each of which is composed of a CCHP system and corresponding user load. Each sub-region is interlinked with the SESS through the transformer installed at the node, while each sub-area is interlinked with the EPG through the energy network. The
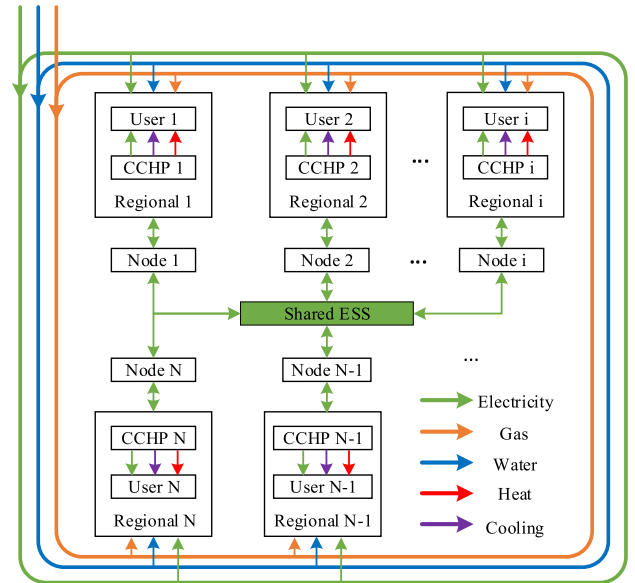
FIGURE 1. Structure of RIES.

purpose of setting SESS is to promote the consumption of RES in each sub-region and optimize the electric power, so there is no energy coupling relationship between SESS and EPG. Similarly, considering the island situation existing in the actual project, there is no energy coupling relationship between CCHPs.
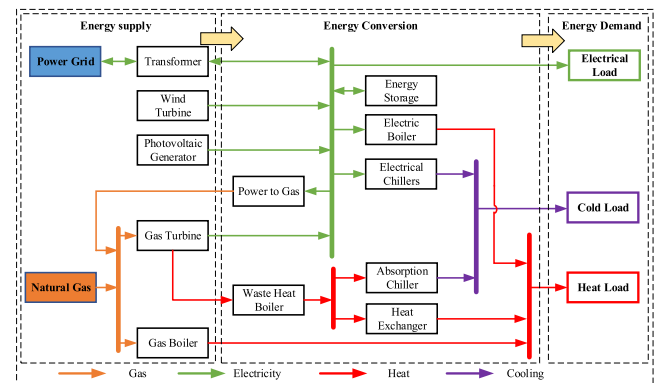
FIGURE 2. Structure of CCHP.

There are a variety of energy flows inside CCHP, and various forms of energy flows are coupled through coupling equipment. Generally speaking, according to the different functions of different energy flows in each part, CCHP can be divided into energy supply, energy conversion and energy demand. At present, common method to describe the energy conversion and coupling of different equipment is the energy bus model. According to the bus model, multi-energy flow generated by the coupling device inside the CCHP is shown in Fig 2. The energy supply consists of common energy generation equipment, including renewable energy generation equipment composed of photovoltaic (PV) and wind turbine (WT) and gas energy consumption equipment composed of gas turbine (GT) and

gas boiler (GB). The energy conversion includes the equipment that can complete the conversion of electric, heat and cold energy. The energy coupling devices included in this model composed of energy storage (ES), electrothermal coupling equipment electric boiler (EB), electric cooling coupling equipment electric chillers (EC); layered heat control equipment waste heat boiler (WHB); heat and cold coupling equipment absorption chiller (AC) and heat transfer equipment heat exchanger (HE). The mathematical model of each equipment and the constraints that should be obeyed during operation are described below. The operating mathematical model of WT and PV can be found in reference [25]. The rest of the equipment constraints are as follows [26], [27]:

1) GT

$$
\begin{cases}
P_t^{GT} = \eta_{GT}^e V_{gas}^{GT} H_{ng} \\
H_t^{GT} = \dfrac{1 - \eta_{GT}^e}{\eta_{GT}^e} \eta_{GT}^h P_t^{GT}
\end{cases} \tag{1}
$$

where η_{GT}^e is the generating efficiency; η_{GT}^h is the heating efficiency; V_{gas}^{GT} is the NG consumption of GT; H_{ng} is the calorific value of NG. When the GT is running, following constraints should be met:

$$
\begin{cases}
P_{\min}^{GT} \le P_t^{GT} \le P_{\max}^{GT} \\
P_{down}^{GT} \le P_t^{GT} - P_{t-1}^{GT} \le P_{up}^{GT}
\end{cases} \tag{2}
$$

2) GB

$$
H_t^{GB} = \eta_{GB} V_{gas}^{GB} H_{ng} \tag{3}
$$

where V_{gas}^{GB} is the NG consumption of GB. Meanwhile, GB must meet the following constraints:

$$
H_{\min}^{GB} \le H_t^{GB} \le H_{\max}^{GB} \tag{4}
$$

3) WHB

Due to the combustion of NG during GT operation, heat energy is also generated while generating electric energy. This part of heat energy is further absorbed and utilized by WHB.

$$
H_t^{WHB} = \eta_{WHB} H_t^{GT} \tag{5}
$$

4) EB

EB is part of the electrothermal conversion process in RIES, through which the system provides hot water to the user or for heating.

$$
H_t^{EB} = \eta_{EB} \left(1 - \eta_{EB}^{loss}\right) P_t^{EB} \tag{6}
$$

The following constraints should be met during operation:

$$
H_{\min}^{EB} \le H_t^{EB} \le H_{\max}^{EB} \tag{7}
$$

5) EC

EC compresses the piston of the compressor through the operation of the motor, so as to achieve the purpose of heat transfer.

$$
C_t^{EC} = COP_{EC} P_t^{EC} \tag{8}
$$

where COP_{EC} is the energy efficiency ratio of EC. The EC should meet the following constraints during operation:

$$
C_{\min}^{EC} \le C_t^{EC} \le C_{\max}^{EC} \tag{9}
$$

6) AC

AC use heat energy as input energy, through the process of heat absorption and condensation heat release, to achieve the production of cold energy.

$$
C_t^{AC} = COP_{AC} H_t^{AC} \tag{10}
$$

where COP_{AC} is the energy efficiency ratio of AC. The AC should meet the following constraints during operation:

$$
C_{\min}^{AC} \le C_t^{AC} \le C_{\max}^{AC} \tag{11}
$$

7) HE

HE is a heat energy conversion equipment of the RIES and the heat energy bus.

$$
H_t^{HE} = \eta_{HE} \left(H_t^{WHB} - H_t^{AC}\right) \tag{12}
$$

The HE should meet the following constraints during operation:

$$
H_{\min}^{HE} \le H_t^{HE} \le H_{\max}^{HE} \tag{13}
$$

In general, the mathematical model of ES and the constraints to be met during operation are similar to SESS. The SESS model and P2G model will be described in detail in the following.

B. MODELLING OF SESS

SESS refers to the behavior and corresponding mode of energy storage equipment owners renting equipment capacity/power to other energy participants [28], [29]. The sharing strategy of SESS equipment can improve the overall utilization rate of equipment, increase the absorption level of RES, and reduce the overall carbon emission of RIES [30], [31]. SESS should satisfy the following considerations.

1) POWER CONTINUITY CONSTRAINT

$$
\begin{aligned}
E_t^{SESS} = {} & \left(1 - \eta_{SESS}^{loss}\right) E_{t-1}^{SESS} \\
& + (\eta_{SESS}^{abs} P_t^{SESS,abs} - \frac{1}{\eta_{SESS}^{relea}} P_t^{SESS,relea}) \Delta t
\end{aligned} \tag{14}
$$

2) CAPACITY CONSTRAINTS

$$
\begin{cases}
\sigma_{SESS}^{\min} E_{\max}^{SESS} \le E_t^{SESS} \le \sigma_{SESS}^{\max} E_{\max}^{SESS} \\
E_{start}^{SESS} = \sigma_{SESS}^{init} E_{\max}^{SESS} = E_{end}^{SESS}
\end{cases} \tag{15}
$$

3) CHARGE AND DISCHARGE CONSTRAINTS

$$\begin{cases} 0 \le P_t^{SESS,abs} \le P_{\max}^{SESS} U_{t,abs}^{SESS} \\ 0 \le P_t^{SESS,relea} \le P_{\max}^{SESS} U_{t,relea}^{SESS} \\ U_{t,abs}^{SESS} + U_{t,relea}^{SESS} \le 1 \\ U_{t,abs}^{SESS} \in \{0,1\}\ U_{t,relea}^{SESS} \in \{0,1\} \end{cases} \tag{16}$$
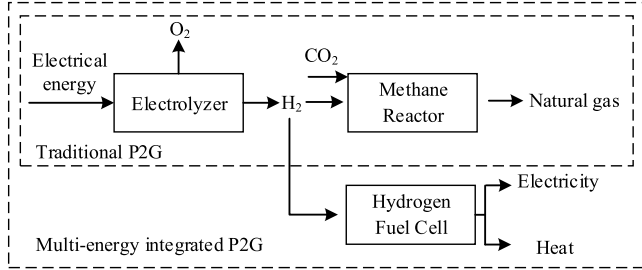

FIGURE 3. Structure of multi-energy integrated P2G.

C. MODELLING OF P2G

This paper proposes a multi-energy integrated P2G operation process based on the traditional P2G model by introducing HFC. The structure of P2G is shown in Fig.3. Each component should satisfy the following considerations.

1) EL

$$\begin{cases} G_{H_2,t}^{EL} = \eta_{EL} P_t^{EL} \\ P_{\min}^{EL} \le P_t^{EL} \le P_{\max}^{EL} \\ \Delta P_{\min}^{EL} \le P_{t+1}^{EL} - P_t^{EL} \le \Delta P_{\max}^{EL} \end{cases} \tag{17}$$

2) MR

$$\begin{cases} G_{NG,t}^{MR} = \eta_{MR} G_{H_2,t}^{MR} \\ G_{H_2,\min}^{MR} \le G_{H_2,t}^{MR} \le G_{H_2,\max}^{MR} \\ \Delta G_{H_2,\min}^{MR} \le G_{NG,t+1}^{MR} - G_{NG,t}^{MR} \le \Delta G_{H_2,\max}^{MR} \end{cases} \tag{18}$$

3) HFC

$$\begin{cases} P_t^{HFC} = \eta_{HFC}^e G_{H_2,t}^{HFC} \\ H_t^{HFC} = \eta_{HFC}^h G_{H_2,t}^{HFC} \\ G_{H_2,\min}^{HFC} \le G_{H_2,t}^{HFC} \le G_{H_2,\max}^{HFC} \\ \Delta G_{H_2,HFC}^{\min} \le G_{H_2,t+1}^{HFC} - G_{H_2,t}^{HFC} \le \Delta G_{H_2,HFC}^{\max} \end{cases} \tag{19}$$

III. LADDER TYPE REWARD-PENALTY CARBON TRADING MODEL

The operation of CTM is based on the individual's carbon emission as a commodity that can be bought and sold. The model of ladder type reward-penalty carbon trading model are as follows.

A. FREE CARBON EMISSION QUOTA MODEL

Each RIES is allocated a fixed amount of free carbon emission quota on each dispatch day based on its own established GT and GB.

$$\begin{cases} E_{free}^{CO_2} = E_{free}^{Grid,b} + E_{free}^{GT} + E_{free}^{GB} \\ E_{free}^{Grid,b} = \delta_{free}^{coal} \sum_{t=1}^{T} \sum_{i=1}^{N} P_{i,t}^{Grid,b} \\ E_{free}^{GT} = \delta_{free}^{gas} \left(\varphi \sum_{t=1}^{T} \sum_{i=1}^{N} P_{i,t}^{GT} + \sum_{t=1}^{T} \sum_{i=1}^{N} H_{i,t}^{GT} \right) \\ E_{free}^{GB} = \delta_{free}^{gas} \sum_{t=1}^{T} \sum_{i=1}^{N} H_{i,t}^{GB} \end{cases} \tag{20}$$

where $E_{free}^{CO_2}$ is total free carbon emissions quota of RIES; $E_{free}^{Grid,b}$, E_{free}^{GT} and E_{free}^{GB} are free carbon emissions quotas of EPG, GT and GB, respectively; δ_{free}^{coal} and δ_{free}^{gas} are carbon emission quota per unit of electricity issued by coal-fired units and heat issued by natural gas-fired units, respectively; φ is electric heat conversion coefficient.

B. ACTUAL CARBON EMISSION MODEL

Assuming that EPG purchases are derived from coal-fired unit.

$$\begin{cases} E_{actual}^{CO_2} = E_{actual}^{Grid,b} + E_{actual}^{GT} + E_{actual}^{GB} - E_{actual}^{MR} \\ E_{actual}^{Grid,b} = \sum_{t=1}^{T} \sum_{i=1}^{N} \left(a_1 + b_1 P_{i,t}^{Grid,b} + c_1 (P_{i,t}^{Grid,b})^2 \right) \\ E_{actual}^{GT} = \sum_{t=1}^{T} \sum_{i=1}^{N} \left(a_2 + b_2 P_{i,t}^{GT} + c_2 (P_{i,t}^{GT})^2 \right) \\ E_{actual}^{GB} = \sum_{t=1}^{T} \sum_{i=1}^{N} \left(a_2 + b_2 P_{i,t}^{GB} + c_2 (P_{i,t}^{GB})^2 \right) \\ E_{actual}^{MR} = \varpi \sum_{t=1}^{T} \sum_{i=1}^{N} G_{NG,t}^{MR} \end{cases} \tag{21}$$

where $E_{actual}^{CO_2}$ is total actual carbon emissions of RIES; $E_{actual}^{Grid,b}$, E_{actual}^{GT} and E_{actual}^{GB} are actual carbon emissions of EPG, GT and GB, respectively; E_{actual}^{MR} is actual carbon absorbed of MR; a_1, b_1, c_1 and a_2, b_2, c_2 are carbon emission calculation parameters; ϖ is parameters of carbon absorption in the process of MR.

C. LADDER TYPE REWARD-PENALTY CARBON TRADING MODEL

Through (20) and (21), the accurate carbon emissions of RIES are calculated, and the reasonable range of carbon emission rewards and punishments is divided. Based on this, a ladder-type reward and punishment CTM are established to further

reduce carbon emissions.

C_{carbon}

$$
= \begin{cases}
-\sigma(2 + 3y)d + \sigma(1 + 3y)(E_{actual}^{CO_2} - E_{free}^{CO_2} + 2d), \\
\quad E_{actual}^{CO_2} - E_{free}^{CO_2} \le -2d \\
-\sigma(1 + y)d + \sigma(1 + 2y)(E_{actual}^{CO_2} - E_{free}^{CO_2} + 2d) \\
\quad -2d < E_{actual}^{CO_2} - E_{free}^{CO_2} \le -d \\
-\sigma(1 + y)(E_{actual}^{CO_2} - E_{free}^{CO_2}), \\
\quad -d < E_{actual}^{CO_2} - E_{free}^{CO_2} \le 0 \\
\sigma(E_{actual}^{CO_2} - E_{free}^{CO_2}), \\
\quad 0 < E_{actual}^{CO_2} - E_{free}^{CO_2} \le d \\
\sigma d + \sigma(1 + x)\left(E_{actual}^{CO_2} - E_{free}^{CO_2} - d\right), \\
\quad d < E_{actual}^{CO_2} - E_{free}^{CO_2} \le 2d \\
\sigma(2 + x)d + \sigma(1 + 2x)(E_{actual}^{CO_2} - E_{free}^{CO_2} - 2d), \\
\quad 2d < E_{actual}^{CO_2} - E_{free}^{CO_2} \le 3d \\
\sigma(3 + x)d + \sigma(1 + 3x)(E_{actual}^{CO_2} - E_{free}^{CO_2} - 3d), \\
\quad 3d < E_{actual}^{CO_2} - E_{free}^{CO_2}
\end{cases}
$$
(22)

where C_{carbon} is carbon cost of RIES; σ is price of carbon emission rights per unit allowance; x is penalty factor; y is compensation factor; d is interval length of carbon emission.

IV. IMPROVED ROBUST OPTIMIZATION OVER TIME BASED ON INDEX CONTRIBUTION IN UNCERTAIN ENVIRONMENT

Although RO, SO and other approach with the meta-heuristic optimization are intuitive and easy to understand in solving uncertain optimization problems [32], [33], [34], the theoretical research has also made rich achievements. However, the above method requires algorithm can quickly find the current optimal solution after each environmental change, and can switch each optimal solution smoothly, which has many limitations in the actual engineering environment. For example, how to quickly find the optimal solution while ensuring smooth switching in practice. The dynamic robust optimization is expected to find a robust optimal solution with time-domain robustness in a certain period of time. That is, RO and SO and meta-heuristic optimization consider the influence of parameter uncertainty on system performance, while ROOT not only considers the parameter uncertainty, but also considers the cumulative effect of these uncertainties in the time domain.

A. THE CONTRIBUTION OF DIFFERENT INDICATORS
Based on the existing typical ROOT, reference [35] proposed three new robustness evaluation indexes: feasible direction (FD) R^{FD}, stability degree (SD) R^{SD} and sum of floating value (SFV) R^{SFV}. Based on these new indexes, an improved ROOT is proposed, and each index is defined as follows:

$$
R^{FD} = \frac{1}{p + q + 1} \sum_{i=t-p}^{t+q} |f(x, \alpha_{i+1}) - f(x, \alpha_i)| \quad (23)
$$

$$
R^{SD} = \frac{f(x, \alpha_j) - [\max f(x, \alpha_i) + \min f(x, \alpha_i)]}{\eta} \quad (24)
$$

$$
R^{SFV} = \sum_{i=t-p}^{i=t+q} (f(x, \alpha_{i+1}) - f(x, \alpha_i)) \quad (25)
$$

where p and q are the number of historical and future environments, respectively; η is the threshold set by the decision maker.

On the basis of the three new robustness evaluation indexes introduced, although the solution with better robustness can be obtained compared with the existing algorithms, the overall solution process of the algorithm is slow, which is not conducive to the requirement of obtaining the robust optimal solution that meets the requirements faster when facing the optimization problem of dynamic environment. In order to improve the solution speed of the algorithm, we first analyze the role of the three new robustness indexes mentioned above in the process of finding the dynamic robust optimal solution of the algorithm. For this purpose, this paper sets up the following seven comparison modes as shown in Table 1:

TABLE 1. List of factors to consider for different patterns.

Mode	Indicators to consider		
	R^{FD}	R^{SD}	R^{SFV}
Mode 1	√	×	×
Mode 2	×	√	×
Mode 3	×	×	√
Mode 4	√	√	×
Mode 5	×	√	√
Mode 6	√	×	√
Mode 7	√	√	√

The mMPB can well simulate the dynamic characteristics of the optimization problem over time because the change of each test peak is random [36], [37], that is, the height of each test peak and the center point position of the peak in the test interval will change with time. Therefore, all the experiments are carried out on the mMPB. mMPB can be described as follows:

$$
F_t\left(\vec{X}\right) = \max_{i=1}^{i=m} \left\{ H_t^i - W_t^i \times \left\| \vec{X} - \vec{C}_t^i \right\|_2 \right\} \quad (26)
$$

$$
H_{t+1}^i = H_t^i + height\_severity^i \times N(0, 1) \quad (27)
$$

$$
W_{t+1}^i = W_t^i + width\_severity^i \times N(0, 1) \quad (28)
$$

$$
\vec{C}_{t+1}^i = \vec{C}_t^i + \vec{v}_{t+1}^i \quad (29)
$$

$$
\vec{v}_{t+1}^i = \frac{s \times ((1 - \lambda) \times \vec{r} + \lambda \times \vec{v}_t^i)}{\left\| (1 - \lambda) \times \vec{r} + \lambda \times \vec{v}_t^i \right\|} \quad (30)
$$

The experimental simulation is tested under 150 mMPB with environmental changes. In each mode, the algorithm runs independently 15 times and obtained results are averaged, the robust results of average fitness and average survival time are shown in Table 2. It should be noted that the running time in the Table 2 is obtained by averaging the total time of running 15 times in the test environment.

Mode	Fitness thresholds = 40		Time window = 2	
	Average fitness	Running time	Survival time	Running time
Mode 1	3.83	62.7 s	63.03	76.4 s
Mode 2	3.80	61.9 s	61.56	75.3 s
Mode 3	3.79	61.7 s	61.13	74.7 s
Mode 4	3.91	67.6 s	67.02	79.9 s
Mode 5	3.87	64.2 s	66.46	77.5 s
Mode 6	3.89	66.7 s	64.43	78.6 s
Mode 7	3.97	71.3 s	68.71	83.8 s

It can be seen from the calculation results of Table 2 that R^{FD} is defined as the feasibility direction index, so it is used to judge whether the feasibility direction of the robust solution obtained by the prediction process is reasonable. As shown in mode 1, the addition of the direction judgment step determines that the operation time of the algorithm will be longer when the R^{FD} index is considered. R^{SD} judges the robustness of the predicted robust solution by introducing the stability index of the known robust solution and excludes the poor stability of the predicted solution. Similarly, R^{SFV} also determines the range of the next prediction solution by calculating the floating value of the prediction solution over a period of time. That is, R^{SD} uses the idea of average to judge the theoretical average range of future predictions, and R^{SFV} uses the idea of summation to judge the theoretical total value of future predictions. The theoretical background of R^{SD} and R^{SFV} is different, but the purpose of evaluation is the same. Therefore, it can be found from the results that the results of mode 2 and mode 3 are relatively close. Because R^{SD} has the concept of mean value, it is easier to judge the prediction solution, so the robustness of the solution is better than that of R^{SFV}.

By comparing the calculation results of mode 4, mode 5 and mode 6 with the previous analysis results, it can be seen that mode 4 has the best effect without considering all the robustness indexes. When the fitness threshold and time window are determined, the robustness indexes of the solution of mode 4 reach 98.49% and 97.54% of the improved algorithm, respectively. Because of the reduction of one evaluation index, the operation speed of mode 4 is better than that of the improved algorithm, but it is still higher than that of other modes.

Based on the above analysis, we can know that R^{FD} is mainly responsible for determining the robustness of short-term prediction. Although R^{FD} can improve the robustness of the results of dynamic optimization problems, it will also increase the running time of the algorithm, which is not conducive to obtaining the optimal robust solution of the optimization problem quickly. R^{SD} and R^{SFV} tend to be medium and long predicted, the operation time is short, but the robustness of the solution is low. Therefore, the above three robustness evaluation indexes are constructed according to their respective index contribution degrees, and an improved ROOT based on indicator contribution (IROOT-IC) is proposed. By constructing a new combined robustness evaluation index considering the weight coefficient, the algorithm can improve the robustness of the solution and reduce the running time when calculating the optimal robust solution. Since R^{SD} and R^{SFV} have similar functions, they are regarded as a whole and the following dynamic robust optimization algorithm based on indicator contribution is constructed.

B. THE WEIGHT COEFFICIENT OF DIFFERENT INDICATORS

Because the influence degree of different indexes is different, the weight coefficient is different. At present, the common and effective weight coefficient selection methods include AHP and CRITIC. AHP weights each index component based on the subjective number of layers of the index. CRITIC standardized the data of each group and calculated the objective weight coefficient of the index. The weight coefficient obtained by AHP is mainly based on the experience of decision makers. CRITIC mainly considers the objective information of sample data objectively. Therefore, on the basis of the above two methods to determine the weight coefficient, this paper combines the two methods. Considering the subjective and objective aspects, the sampling AHP-CRITIC mixed weighting is used to comprehensively weight the index components in IROOT-IC to ensure the comprehensiveness of the data indicators and the scientific rationality of the results. The formula for calculating the weight coefficient using AHP-CRITIC is as follows:

$$\omega^*_{AHP-CRITIC} = \frac{\omega^*_{AHP}\omega^*_{CRITIC}}{\sum \omega^*_{AHP}\omega^*_{CRITIC}} \tag{31}$$

where $* \in \{FD, SD, SFV\}$; ω^*_{AHP} refers to the weight coefficient of index $*$ obtained by AHP method; ω^*_{CRITIC} refers to the weight coefficient of index $*$ obtained by CRITIC method.

$$R^{IC} = \omega^{FD}_{AHP-CRITIC}R^{FD} + \omega^{SD}_{AHP-CRITIC}R^{SD}$$
$$+ \omega^{SFV}_{AHP-CRITIC}R^{SFV} \tag{32}$$

where ω_{FD}, ω_{SD} and ω_{SFV} are the weight coefficients of R^{FD}, R^{SD} and R^{SFV} respectively.

In summary, the IROOT-IC algorithm framework is constructed as shown in Fig 4.

V. MODELLING OF OPTIMAL SCHEDULING MODEL
A. OBJECTIVE FUNCTION

$$\min C_{IES} = C_{grid} + C_{gas} + C_{om} + C_{sess} + C_{carbon} \tag{33}$$

where C_{grid} is the electrical energy transaction cost with external electric grid; C_{gas} is the gas energy transaction cost with external gas grid; C_{om} is the operational and maintenance cost; C_{sess} is the transaction cost with SESS.

$$C_{grid} = \sum_{i=1}^{N}\sum_{t=1}^{T}\left(c^{gird}_{b,t}P^{Grid,buy}_{i,t} - c^{gird}_{s,t}P^{Grid,sell}_{i,t}\right)\Delta t \tag{34}$$

where N is the total number of CCHP; T is the length of the scheduling period; $c^{gird}_{b,t}$ is the price of purchasing electric
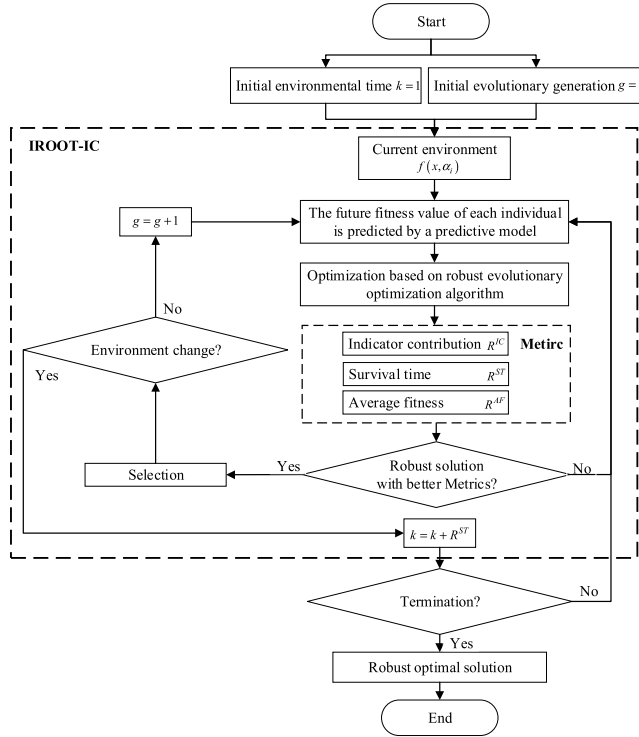
FIGURE 4. Framework of IROOT-IC.

energy from external grid; $c_{s,t}^{gird}$ is the price of selling electricity energy; Δt is scheduling time interval.

$$C_{gas} = \sum_{i=1}^{N} \sum_{t=1}^{T} c_{gas}$$
$$\left[\left(P_{i,t}^{GT,Total} - P_{i,t}^{GT,P2G} \right) \Big/ \left(\eta_i^{GT} H_{ng} \right) + \left(H_{i,t}^{GB,Total} - H_{i,t}^{GT,P2G} \right) \Big/ \left(\eta_i^{GB} H_{ng} \right) \right] \Delta t \quad (35)$$

where c_{gas} is the price of natural gas; $P_{i,t}^{GT,Total}$ and $P_{i,t}^{GT,P2G}$ are total electrical power of GT and electrical power of GT when using natural gas provided by P2G, respectively; $H_{i,t}^{GB,Total}$ and $H_{i,t}^{GT,P2G}$ are total heat power of GB and GT when using natural gas provided by P2G, respectively.

$$C_{om} = \sum_{i=1}^{N} \sum_{t=1}^{T} \left(K_{om}^{Elec} P_{i,t}^{Elec} + K_{om}^{Heat} H_{i,t}^{Heat} + K_{om}^{Cold} C_{i,t}^{Cold} \right) \Delta t \quad (36)$$

where K_{om}^{Elec}, K_{om}^{Heat} and K_{om}^{Cold} are operation and maintenance coefficient of equipment, respectively; $P_{i,t}^{Elec}$, $H_{i,t}^{Heat}$ and $C_{i,t}^{Cold}$ are respectively the electric energy, thermoelectric and cold electricity output by various energy equipment.

$$C_{sess} = \sum_{i=1}^{N} \sum_{t=1}^{T} \left(c_{b,t}^{sess} P_{i,t}^{SESS,cha} - c_{s,t}^{sess} P_{i,t}^{SESS,dis} \right) \Delta t \quad (37)$$

where $c_{b,t}^{sess}$ and $c_{s,t}^{sess}$ represent the electricity price interacting with SESS, respectively; $P_{i,t}^{SESS,cha}$ and $P_{i,t}^{SESS,dis}$ are charging and discharging power of CCHP.

B. OPTIMIZATION CONSTRAINT

The optimization operation of RIES is a complex optimization problem with multiple variables and constraints. In order to ensure that the results have practical engineering significance and meet the operating conditions of the various equipment included, RIES operation needs to meet the constraints of maintaining power balance on various energy busbars.

$$P_{i,t}^{WT} + P_{i,t}^{PV} + P_{i,t}^{GT} + P_{i,t}^{EPG} + P_{i,t}^{ES} + P_{i,t}^{HFC}$$
$$- P_{i,t}^{EB} - P_{i,t}^{EC} - P_{i,t}^{P2G} = P_{i,t}^{LOAD} \quad (38)$$

$$H_{i,t}^{GB} + H_{i,t}^{HE} + H_{i,t}^{HFC} + H_{i,t}^{EB} = H_{i,t}^{LOAD} \quad (39)$$

$$C_{i,t}^{EC} + C_{i,t}^{AC} = C_{i,t}^{LOAD} \quad (40)$$

The operating constraints of each device have been described in detail in Section II. Meanwhile, stipulate that the constraint of the energy interaction power between RIES and SESS should meet the equipment parameter specifications.

$$\sum_{i=1}^{N} \left(P_{i,t}^{SESS,dis} - P_{i,t}^{SESS,cha} \right) = P_t^{SESS,relea} - P_t^{SESS,abs} \quad (41)$$

Increase the heat energy output constraint of WHB, as shown below.

$$H_{i,t}^{HE} \Big/ \eta_{he} + C_{i,t}^{AC} \Big/ \eta_{ac} = H_{i,t}^{GT} \gamma_{gt} \eta_{whb} \quad (42)$$

where γ_{gt} is thermoelectric ratio of GT.

The hydrogen power balance constraint in P2G should be considered.

$$G_{H_2,t}^{EL} = G_{H_2,t}^{MR} + G_{H_2,t}^{HFC} \quad (43)$$

C. OPTIMIZATION METHOD

The uncertainty of RES is characterized by a class of time-varying parameters, so that the dynamic optimization problem considering uncertainty can be transformed into a dynamic optimization problem with time-varying parameters. Secondly, the IROOT-IC algorithm is used to optimize the above problems.

VI. CASE STUDY

A. SIMULATION SYSTEM

RIES as shown in Fig 5 was established to analyze the improved method and carbon management measure. As shown in the figure, the RIES consists of four sub-regions with separate CCHP systems and different scenarios. At the same time, each sub-region can interact with SESS and EPG for electrical energy, and the sub-region can obtain other domestic energy from EPG.

In order to better distinguish the difference of energy operation between different regions, in the experimental case, it is stipulated that the residential and office areas are no longer independently configured with ES due to their own operating costs, while the commercial and industrial areas need to be independently configured with ES due to the pursuit of economic operation. Similarly, since industrial area and office
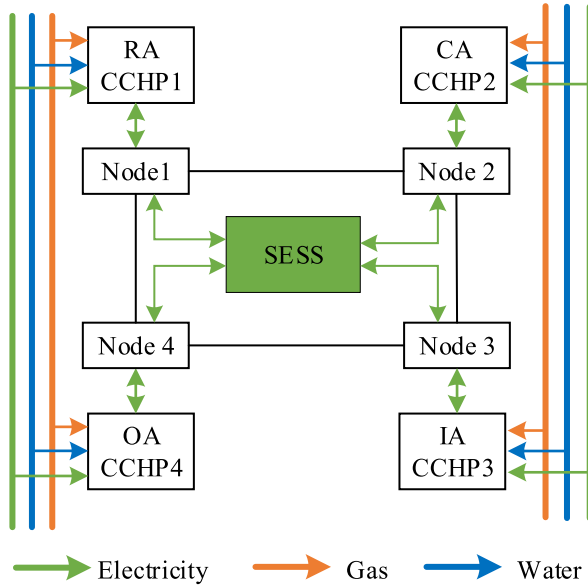
FIGURE 5. Structure diagram of the actual RIES.

area are regions with good renewable energy endowments, in order to further absorb renewable energy, P2G equipment mentioned in this paper is installed in the above two regions. The parameters of CCHP are shown in Appendix Table 7 and Table 8.
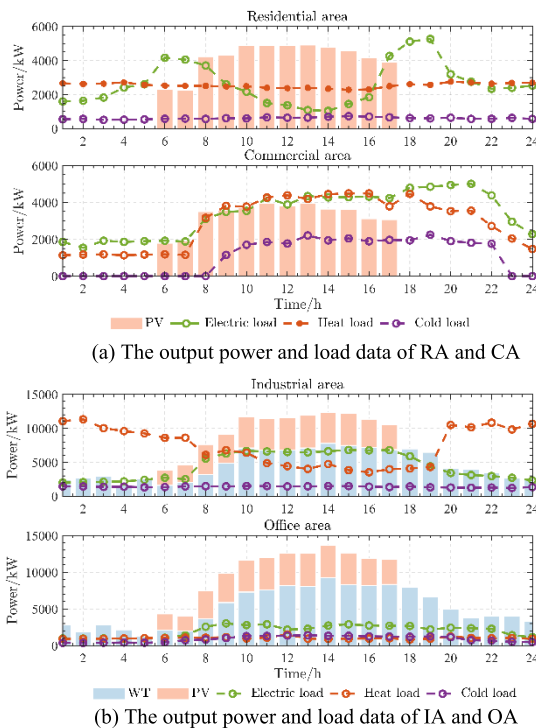

(a) The output power and load data of RA and CA

(b) The output power and load data of IA and OA

FIGURE 6. The RES output data and the load curve of each CCHP.

Carbon emission reduction measures include P2G and ladder reward-penalty carbon trading model. The parameters of

the SESS are shown in in Appendix Table 9, and the time-of-use price are shown in Appendix Table 10 and 11. the price of natural gas is 2.46 ¥/m^3, and H_{ng} is 9.78 kWh/m^3. The power data of RES and the load data of each CCHP are shown in Fig.6. δ_{free}^{coal} and δ_{free}^{gas} are 0.798 kg/(kWh) and 0.385 kg/(kWh) respectively, this paper stipulates 100% consumption of RES.
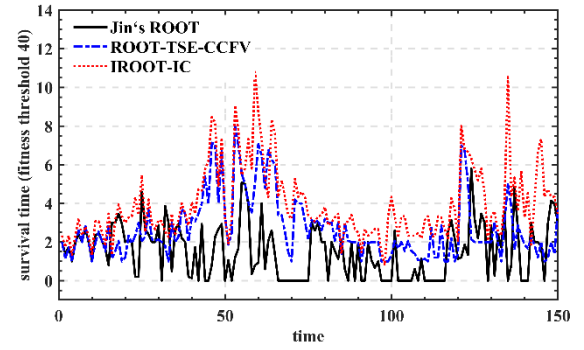
(a) fitness threshold = 40
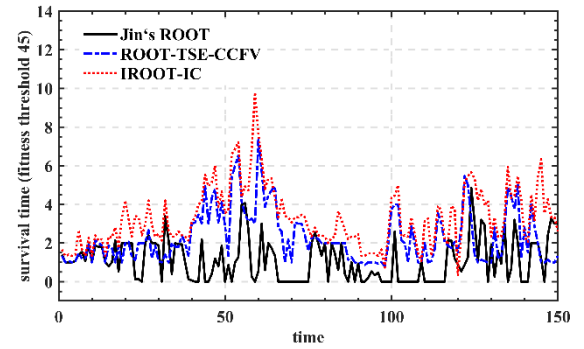
(b) fitness threshold = 45
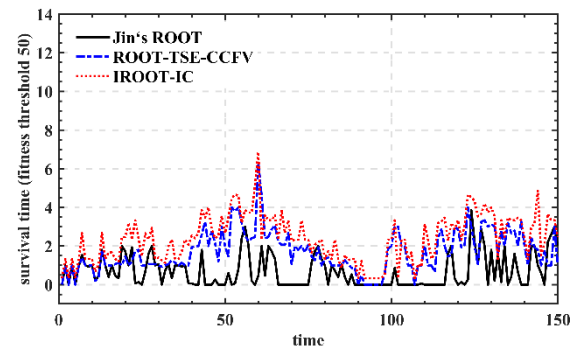
(c) fitness threshold = 50

FIGURE 7. The results of different ROOT in the mMPB test environment.

B. ANALYSIS THE EFFECTIVE OF IROOT-IC

The test environment for the validity verification of the algorithm in this paper is still based on the mMPB mentioned in Section IV. The effectiveness is illustrated by comparing and analyzing various algorithms in the same test environment. The comparative analysis test results of different algorithms in mMPB test environment are shown in Fig 7. Through the comparison diagram of the experimental results, it can be concluded that in the face of dynamic optimization

problems randomly generated by mMPB, IROOT-IC can control each solution factor by weight distribution method, so as to obtain a robust solution with longer survival time. Since the results cannot be quantified from the figure alone, the robustness results of different algorithms under the same test environment were averaged, and the results were shown in Table 3.

TABLE 3. Numerical results of different ROOT in mMPB test environment.

Mode	Fitness thresholds = 40		Time window = 2	
	Average fitness	Running time	Survival time	Running time
Jin' ROOT	1.54	81.7 s	25.95	92.6 s
ROOT-TSE-CCFV	3.97	71.3 s	68.71	83.8 s
IROOT-IC	4.12	67.8 s	70.13	81.6 s

From the calculation results in Table 3, compared with the ROOT-TSE-CCFV with better performance, the running time of the improved method decreases by 4.42% when the average fitness of the robust solution is increased by 3.78% in the test condition with the fitness threshold fixed at 40. Similarly, when the time window is 2, the robust solution of the proposed improved method decreases by 2.70% when the production time is increased by 2.07%. In summary, IROOT-IC can further reduce the running time of the algorithm while obtaining higher solution robustness.

C. ANALYSIS OF SESS CAPACITY CONFIGURATIONS

Aiming at the effectiveness of IROOT-IC in calculating SESS capacity configuration under uncertain conditions, the following four modes are established, and SO is introduced as a comparison algorithm.

Mode 1: SO is used for uncertainty calculation while without considering carbon reduction measures.

Mode 2: SO is used for uncertainty calculation while considering carbon reduction measure.

Mode 3: IROOT-IC is used for uncertainty calculation while without considering carbon reduction measure.

Mode 4: IROOT-IC is used for uncertainty calculation while considering carbon reduction measure.

In order to make the system run more closely to the actual engineering environment, from the perspective of SESS, it is stipulated that the energy injected into SESS by the system is positive, and the energy withdrawn from SESS is negative. Through calculation in different modes, the results are as follows in Table 4 and Fig 8.

TABLE 4. SESS capacity configuration results and RIES interaction costs.

Mode	Capacity configuration	RIES interaction cost
Mode 1	14,973.67 kWh	3,190.07 ¥
Mode 2	15,578.01 kWh	3,618.85 ¥
Mode 3	15,891.79 kWh	3,380.46 ¥
Mode 4	16,016.11 kWh	3,853.89 ¥

(a) Operating state of SESS under mode 1

(b) Operating state of SESS under mode 2

(c) Operating state of SESS under mode 3
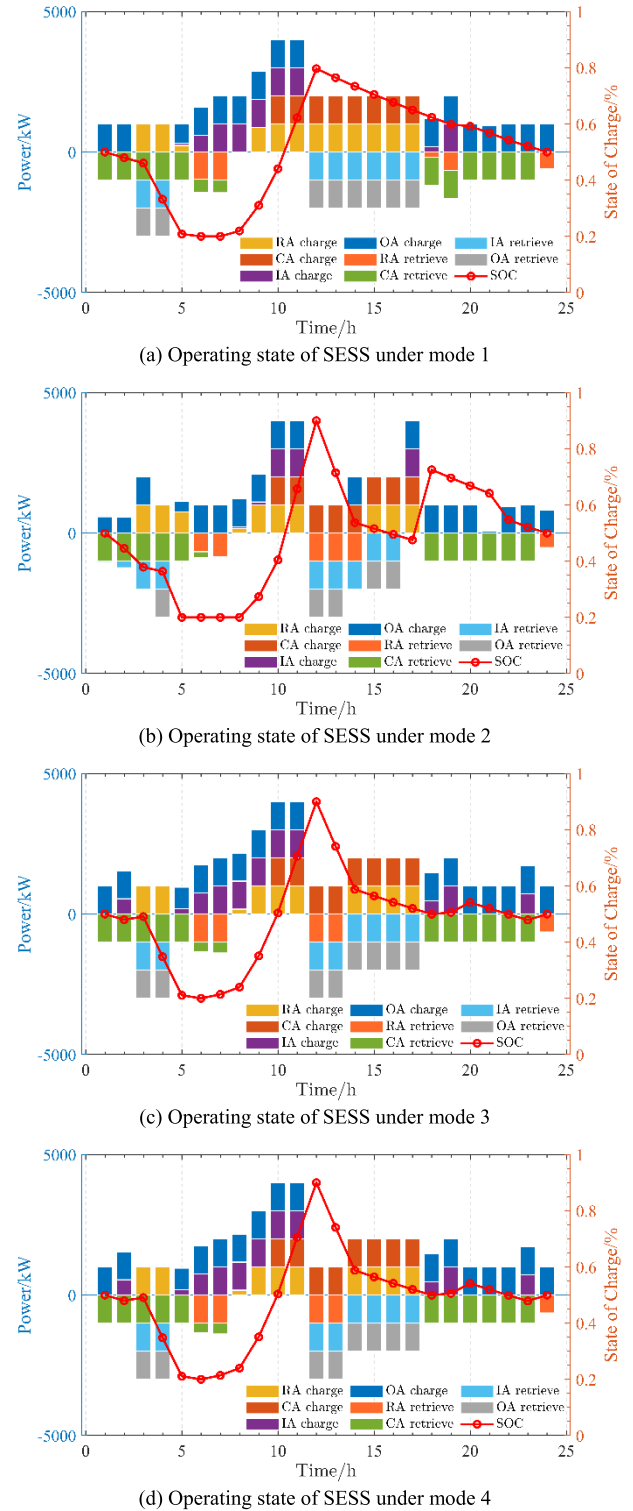
(d) Operating state of SESS under mode 4

FIGURE 8. SESS capacity configuration in different modes.

From Table 4 we know that the interaction cost is the highest under mode 4. Compared mode 4 with mode 2, RIES interaction cost is increased by 6.5% and SESS capacity configuration is increased by 2.8%. It also can be found

that when RIES consider carbon emissions measure which including P2G and CTM, the interaction cost between RIES and SESS is higher than that without considering carbon emissions measure.

To ensure the full utilization of RES in various regions, the interaction between RIES and SESS is more frequent, so the interaction cost with SESS increases. Comparing mode 1 and mode 3, we could obtain that after using IROOT-IC to dynamically optimize the renewable energy considering uncertainty in RIES, the robust solution of renewable energy is obtained, which improves the utilization efficiency of RIES for RES, thus increasing the interactive power between RIES and SESS. The capacity configuration of SESS and interaction cost of RIES are increased. Comparing mode 3 and mode 4, it can be seen that when carbon reduction measures are not adopted, RIES does not need to store excess renewable energy into SESS in order to absorb renewable energy, thus reducing the capacity of SESS and reducing the interaction between RIES and SESS. When carbon reduction measures equipment is added, it is necessary to consume excess renewable energy through P2G equipment and SESS, thereby increasing the capacity configuration of SESS and increasing the energy interaction cost between RIES and SESS. Comparing mode 2 and mode 4, it can be seen that SESS reaches full charge at 12:00 every day, OA area mainly charges inside SESS, and CA area mainly takes electricity from SESS, which is in line with the distribution law of load and renewable energy in each area mentioned in Fig 8. In the subsequent simulation verification of this paper, the SESS capacity is 16016.11 kWh.

D. ANALYSIS OF RIES OPERATING COST AND OPTIMAL SCHEDULING RESULTS

To verify the impact of different RES uncertainty calculation methods and carbon emission reduction measures on RIES optimal scheduling and carbon emissions, this section still takes the four modes mentioned above as examples to calculate the operating costs and carbon emissions of the system.

TABLE 5. (A) Operation cost of RIES under different model. (B) Operation cost of ries under different model.

(A)			
Cost	Electrical purchase	Gas purchase	Operation and Maintenance
Mode 1	11,185.39 ¥	64,045.36 ¥	5,922.09 ¥
Mode 2	18,007.45 ¥	56,564.43 ¥	5,736.29 ¥
Mode 3	10,964.22 ¥	61,383.79 ¥	5,808.86 ¥
Mode 4	17,469.73 ¥	54,044.74 ¥	5,677.43 ¥

(B)			
Cost	Carbon trading	Carbon emission weight	Total operating cost
Mode 1	/	86,532.37 kg	84342.91 ¥
Mode 2	7,532.59 ¥	78,869.75 kg	91459.61 ¥
Mode 3	/	84,953.43 kg	81537.33 ¥
Mode 4	7,281.93 ¥	78,130.35 kg	88,327.72 ¥

The operating costs and carbon emissions of RIES under the above four modes are shown in Table 5. From the above

data results, it can be seen that when dealing with the optimal scheduling problem of RIES considering renewable energy uncertainty, regardless of the CTM, the IROOT-IC can obtain more economical operating costs and lower carbon emissions than SO. The following is a detailed description of the influence of different CTM on the operating costs and carbon emissions of RIES, taking mode 3 and mode 4 as examples.

Mode 4 considers of the ladder-type CTM in the optimal scheduling of RIES, and the purchase price of carbon emission quotas shows a stepwise increase. Therefore, for the energy supply of RIES operators, it is cheaper to purchase natural gas to produce electricity than to purchase electricity directly from EPG. However, since RIES burning natural gas is in a state of high carbon emissions at this time, the cost of choosing gas purchase instead of electricity purchase has been lower than the cost of high carbon emission quotas generated by burning natural gas. The ladder-type CTM limits the carbon emissions of the RIES to a certain extent. Therefore, compared with mode 3, mode 4 increases the cost of electricity energy purchase by 37.24% while the cost of gas energy purchase decrease 11.68%, which make the RIES reach a new balance while meeting the load requirements and maintaining low-carbon operation. Compared with mode 3, mode 4 reduces its own operation and maintenance cost by increasing the energy interaction with EPG and reducing its own equipment output. From Table 4 we can see that the operation and maintenance cost is reduced by 2.26 %. Similarly, after the introduction of the ladder CTM, although the total operation cost of the RIES in model 4 increased by 6790.39 ¥compared with mode 3, the carbon emissions decreased by 5823.08 kg, that is an 7.02% reduction in emissions, reflecting that under ladder-type CTM the RIES can reduce emissions while ensuring lower operating costs. In summary, the ladder-type CTM has stronger constraints on carbon emissions compared with the traditional CTM, which can maximize carbon emissions and guide RIES to achieve carbon emission reduction. Model 4 is taken as an example to analyze the optimal scheduling results of each region of the system.

The optimal scheduling results of RIES electric load are shown in Fig 9. In the period when EPG's selling price is at a low point, since SESS is not directly connected with EPG, SESS attracts all sub-regions to purchase electricity from the external grid and store it into SESS by raising the higher purchasing price. This action loads the current energy storage system to arbitrage the peaking and valley price difference, for example, at 03:00 to 05:00 At this time, RA buys electric energy from EPG and stores it into SESS. At the same time, from 0:00 to 05:00, CA's electric load is low during this period, so it can purchase electric energy from SESS and EPG to meet its demand. At this time, the external electricity price is low, and there is no need to start carbon emission equipment, which reduces the operating cost of the overall system while maintaining low carbon emission. In the PV output period from 06:00 to 17:00, RA has a low power consumption, so the excess power will be sold to the external
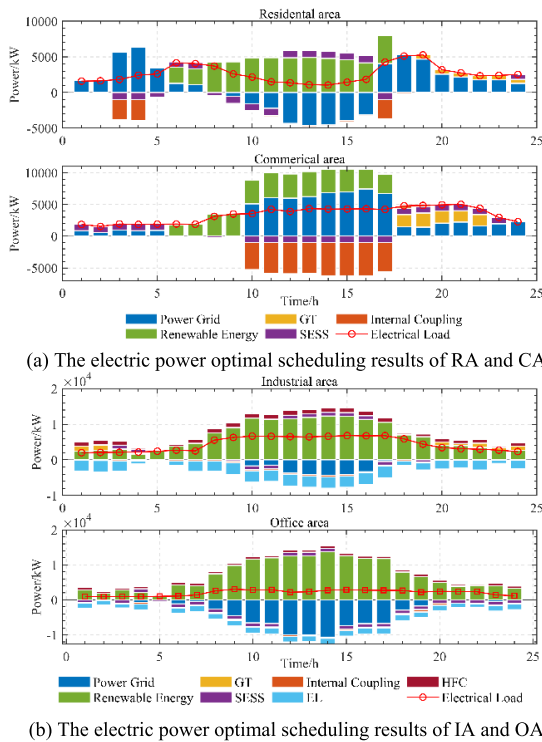
(a) The electric power optimal scheduling results of RA and CA.

(b) The electric power optimal scheduling results of IA and OA.

FIGURE 9. The optimal scheduling results of electric power in each region of RIES.

(a) The heat power optimal scheduling results of RA and CA.

(b) The heat power optimal scheduling results of IA and OA.

FIGURE 10. The optimal scheduling results of heat power in each region of RIES.

power grid, CA region's own PV cannot meet the requirements of the power load, so it needs to buy power from the external power grid, and through the internal energy coupling equipment to convert the power into other forms of energy supply to the user. From 18:00 to 22:00 at night, the CA power load is still high, so GT needs to be started to produce part of the electricity. It can be seen from the above that in order to meet the low-carbon requirements of the system, RA and CA basically do not use high-carbon emission equipment such as GT or GB, and at the same time, they reasonably interact with SESS to achieve their own low cost and low carbon emission operation requirements. Similarly, for IA and OA, due to their better renewable energy endowment, P2G equipment is reasonably installed. It can be seen that a large amount of renewable energy power generation is sold to P2G during peak electricity prices, while a certain amount of renewable energy is delivered to P2G. At the same time, in order to ensure the low-carbon and efficient operation of the system, IA and OA themselves do not use high-carbon emission equipment such as GT or GB.

The optimal scheduling results of RIES heat load are shown in Fig 10. On the whole, more than 88.5% of the heat load of the entire RIES is provided by the self-configured GB. The following is a detailed analysis of each region. Since no P2G equipment is installed in the RA and CA, the heat load in these two areas is mainly provided by GB heat generation. From 18:00 to 24:00, when the PV equipment no longer provides power, the system needs to start GT to provide power for RA and CA, and the heat generated by GT power generation can provide heat for itself through the
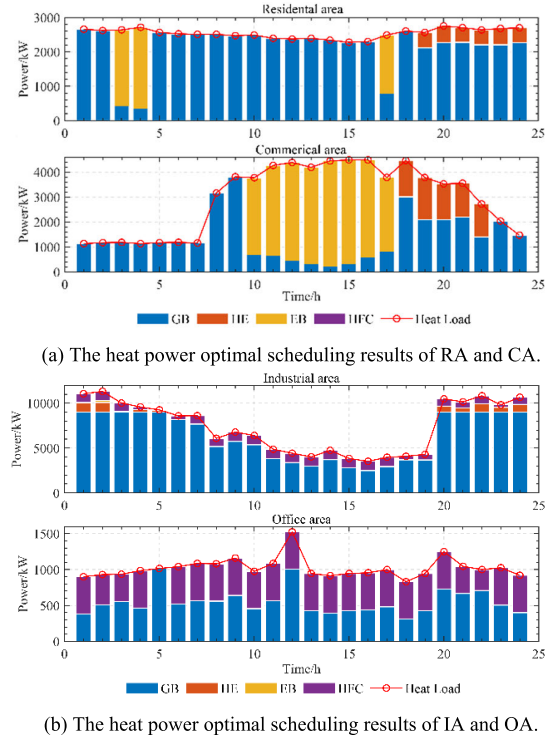
heat exchange device. Thus, it can be seen that RIES uses energy gradients efficiently. For IA and OA, by introducing the P2G model, HFC can provide heat energy through the absorption of renewable energy. It can be seen that HFC can provide objective heat energy supply for IA and OA with good renewable energy endowments. In addition to the heat energy provided by HFC and GB, a small amount of HE and EB is needed to provide a small part of the heat supply for areas with high heat load demand such as IA. In general, the introduction of P2G model can also reduce the carbon emissions of the system and provide more varieties of energy supply for the load side.

The optimal scheduling results of RIES cold load are shown in Fig 11. On the whole, due to the high use of GB in the heat load, the carbon emissions of the system are high, so in the cold load, more electric refrigeration equipment is used to provide cold energy for the load. It can also be seen that for RA and CA, during 18:00 to 24:00, when the GT equipment of the system runs power generation, the high-temperature waste heat generated is partially transferred to HE to produce heat energy through WHB, and the other part is transferred to AC to produce cold energy. In IA, when the renewable energy output is low from 0:00 to 05:00 and 20:00 to 24:00, GT power generation is also used to provide electric energy for the system, and AC is also started to generate cold energy by absorbing high-temperature exhaust gas to provide to load users. To sum up, in order to improve the cascade utilization rate of different energies and reduce the carbon emissions of the system, the system completes the coupling of electricity, cold and heat energy through coupling equipment,
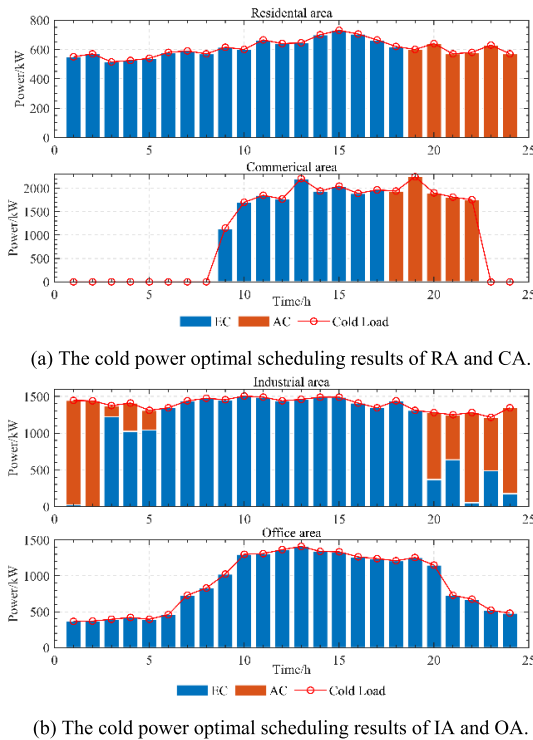
(a) The cold power optimal scheduling results of RA and CA.

(b) The cold power optimal scheduling results of IA and OA.

FIGURE 11. The optimal scheduling results of cold power in each region of RIES.

and meets the requirements of users for different energy sources at a lower cost.

E. ANALYSIS OF P2G REVENUE PROCESS

In order to verify the effectiveness of the P2G in RIES carbon emission reduction, the following three modes are set up.

Mode 5: Optimal scheduling under IROOT-IC and carbon trading model without considering P2G.

Mode 6: Optimal scheduling under IROOT-IC and carbon trading model considering traditional P2G.

Mode 7: Optimal scheduling under IROOT-IC and carbon trading model considering P2G.

TABLE 6. The optimal scheduling results of different modes of P2G.

Mode	Operating cost	Carbon emission	Carbon cost
Mode 5	90,897.36 ¥	78,129.58 kg	16,616.13 ¥
Mode 6	90,176.56 ¥	77,637.27 kg	15,993.79 ¥
Mode 7	88,327.72 ¥	77,130.35 kg	15,117.51 ¥

The operation results of each mode are shown in Table 6. mode 1 does not include P2G devices, so excess renewable energy can only be stored in SESS or consumed and supplied by electric heating and cooling coupling equipment. In mode 2, P2G equipment is added, which can convert excess electric energy into natural gas during the surplus period of renewable power and provide to GT and GB, which reduces the cost of purchasing electricity and gas from external power grid and the dependence on SESS. The operation cost of RIES is further optimized. In mode 3, RIES first inputs abundant

renewable energy into EL equipment to produce hydrogen Part of the hydrogen energy is transported to HFC for thermoelectric production, and the other part is transported to MR synthetic natural gas. The thermoelectric production efficiency of hydrogen energy in HFC is high, and at the same time, an intermediate energy conversion link is reduced. At the same time, natural gas is synthesized by MR and then transmitted to GB and GT for energy supply, which reduces the energy cascade loss and reduces its own carbon emission. At this time, the system operating cost is optimal.

VII. CONCLUSION

As the foundation of the future energy system, how to reduce the carbon emissions of RIES is crucial for the low-carbon operation of the whole society. Based on the above considerations, on the basis of the establishment of RIES model, this paper proposes a comprehensive P2G model with multi-energy output and a SESS model considering shared characteristics and establishes a ladder type reward-punishment CTM model considering carbon emission intervals. Aiming at the uncertainty caused by RES, an improved dynamic robust optimization algorithm considering the index contribution degree is proposed. The effectiveness of the proposed dynamic optimization algorithm and carbon reduction measures was verified through scenario comparative analysis experiments, and the conclusions were as follows:

(1) An improved ROOT based on index contribution is proposed. Under the mMPB dynamic problem testing environment, the average computational robustness of the proposed algorithm is improved by 3.56%, and the computation time is shortened by 2.93%. The improved ROOT can better obtain the optimal robust solution when considering the uncertain factors.

(2) This paper considers the SESS and P2G models in the RIES equipment part, and the ladder type reward and punishment CTM in the mechanism part. When the uncertainty of RES is considered, the proposed improved ROOT is used to optimize of RIES. The experimental results show that the carbon emission reduction measures in this paper can reduce the carbon emission of the whole system by 8.13%, thus ensuring the low-carbon and efficient operation of RIES.

(3) The P2G model can better rationally plan and utilize the internal energy of RIES, enrich the internal energy coupling relationship of RIES on the basis of reducing the energy loss of RIES, and provide more types of energy for the load side.

The carbon emission reduction measures and improved optimization algorithms have certain engineering practical significance for solving optimization scheduling problems under uncertain engineering environments in the future. However, at present, the method is still only suitable for solving single-objective optimization problems, and for solving any multi-objective dynamic optimization problems, it is the next problem to be solved.

APPENDIX A
See Tables 7–11.

TABLE 7. Units for magnetic properties.

Equipment	RA	CA	IA	OA
PV	5000	5000	5000	5000
WT	/	/	10000	10000
ES	/	1000	/	2000
GT	5000	5000	8000	3000
WHB	5000	5000	8000	5000
GB	5000	5000	9000	5000
EB	5000	5000	8000	5000
EC	5000	5000	8000	5000
AC	5000	5000	8000	5000
HE	4000	4000	4000	4000
EL	/	/	4000	2000
MR	/	/	2000	1000
HFC	/	/	2000	1000

TABLE 8. Units for magnetic properties.

Parameter	RA	CA	IA	OA
η_{GT}	0.35	0.35	0.35	0.35
η_{WHB}	0.73	0.73	0.73	0.73
η_{GB}	0.85	0.85	0.85	0.85
η_{EH}	0.98	0.98	0.98	0.98
η_{EC}	4	4	4	4
η_{AC}	1.2	1.2	1.2	1.2
η_{HE}	0.9	0.9	0.9	0.9
$P^{ES}_{\max}$	/	200 kW	400 kW	/
η^{cha}_{ES}	/	0.95	0.95	/
η^{dis}_{ES}	/	0.95	0.95	/
η^{loss}_{ES}	/	0.04	0.04	/
$E^{ES}_{\min}$	/	200 kWh	400 kWh	/
$E^{ES}_{\max}$	/	900 kWh	1800 kWh	/

TABLE 9. Units for magnetic properties.

Parameter	Value
η^{abs}_{SEES}	0.95
η^{relea}_{SEES}	0.95
η^{loss}_{SEES}	0.04
σ^{init}_{SEES}	0.50
σ^{max}_{SEES}	0.90
σ^{min}_{SEES}	0.20
$P^{SESS}_{\max}$	1000 kW

TABLE 10. Units for magnetic properties.

Price type	Time interval	Purchase price	Sell price
Peak time	08:00-11:00 18:00-23:00	0.759	0.415
Normal time	00:00-02:00 05:00-07:00 12:00-14:00 23:00-00:00	0.510	0.415
Valley time	00:00-04:00 15:00-17:00	0.261	0.415

TABLE 11. Units for magnetic properties.

Price type	Time interval	Purchase price	Sell price
Peak time	08:00-11:00 18:00-23:00	0.725	0.435
Normal time	00:00-02:00 05:00-07:00 12:00-14:00 23:00-00:00	0.475	0.435
Valley time	00:00-04:00 15:00-17:00	0.271	0.435

REFERENCES

[1] R. M. Elavarasan, G. M. Shafiullah, S. Padmanaban, N. M. Kumar, A. Annam, A. M. Vetrichelvan, L. Mihet-Popa, and J. B. Holm-Nielsen, "A comprehensive review on renewable energy development, challenges, and policies of leading Indian states with an international perspective," *IEEE Access*, vol. 8, pp. 74432–74457, 2020, doi: 10.1109/ACCESS.2020.2988011.

[2] S. Zhou, Y. Han, K. Mahmoud, M. M. F. Darwish, M. Lehtonen, P. Yang, and A. S. Zalhaf, "A novel unified planning model for distributed generation and electric vehicle charging station considering multi-uncertainties and battery degradation," *Appl. Energy*, vol. 348, Oct. 2023, Art. no. 121566.

[3] L. Liu, X. Yao, X. Qi, and Y. Han, "Low-carbon economy configuration strategy of electro-thermal hybrid shared energy storage in multiple multi-energy microgrids considering power to gas and carbon capture system," *J. Cleaner Prod.*, vol. 428, Nov. 2023, Art. no. 139366.

[4] J. Fan, J. Wang, M. Liu, W. Sun, and Z. Lan, "Scenario simulations of China's natural gas consumption under the dual-carbon target," *Energy*, vol. 252, Aug. 2022, Art. no. 124106.

[5] M. Wu, J. Xu, and Z. Shi, "Low carbon economic dispatch of integrated energy system considering extended electric heating demand response," *Energy*, vol. 278, 2023, Art. no. 127902.

[6] G. Liu, Z. Qin, T. Diao, X. Wang, P. Wang, and X. Bai, "Low carbon economic dispatch of biogas-wind-solar renewable energy system based on robust stochastic optimization," *Int. J. Electr. Power Energy Syst.*, vol. 139, Jul. 2022, Art. no. 108069.

[7] L. Wang, H. Dong, J. Lin, and M. Zeng, "Multi-objective optimal scheduling model with IGDT method of integrated energy system considering ladder-type carbon trading mechanism," *Int. J. Electr. Power Energy Syst.*, vol. 143, Dec. 2022, Art. no. 108386.

[8] M. Chen, H. Lu, X. Chang, and H. Liao, "An optimization on an integrated energy system of combined heat and power, carbon capture system and power to gas by considering flexible load," *Energy*, vol. 273, Jun. 2023, Art. no. 127203.

[9] Y. Li, F. Bu, J. Gao, and G. Li, "Optimal dispatch of low-carbon integrated energy system considering nuclear heating and carbon trading," *J. Cleaner Prod.*, vol. 378, Dec. 2022, Art. no. 134540.

[10] R. Wang, X. Wen, X. Wang, Y. Fu, and Y. Zhang, "Low carbon optimal operation of integrated energy system based on carbon capture technology, LCA carbon emissions and ladder-type carbon trading," *Appl. Energy*, vol. 311, Apr. 2022, Art. no. 118664.

[11] G. Guandalini, S. Campanari, and M. C. Romano, "Power-to-gas plants and gas turbines for improved wind energy dispatchability: Energy and economic assessment," *Applied Energy*, vol. 147, Jul. 2015, Art. no. 11730.

[12] Y. He, M. Yan, M. Shahidehpour, Z. Li, C. Guo, L. Wu, and Y. Ding, "Decentralized optimization of multi-area electricity-natural gas flows based on cone reformulation," *IEEE Trans. Power Syst.*, vol. 33, no. 4, pp. 4531–4542, Jul. 2018.

[13] X. Zhang, K. W. Chan, H. Wang, J. Hu, B. Zhou, Y. Zhang, and J. Qiu, "Game-theoretic planning for integrated energy system with independent participants considering ancillary services of power-to-gas stations," *Energy*, vol. 176, pp. 249–264, Jun. 2019.

[14] S. Clegg and P. Mancarella, "Integrated modeling and assessment of the operational impact of power-to-gas (P2G) on electrical and gas transmission networks," *IEEE Trans. Sustain. Energy*, vol. 6, no. 1, Jul. 2015, Art. no. 123444.

[15] G. Li, R. Zhang, T. Jiang, H. Chen, L. Bai, and X. Li, "Security-constrained bi-level eco nomic dispatch model for integrated natural gas and electricity systems considering wind power and power-to-gas process," *Applied Energy*, vol. 194, May 2017, Art. no. 696704.

[16] I. Ahmed, M. Rehan, A. Basit, and K.-S. Hong, "Greenhouse gases emission reduction for electric power generation sector by efficient dispatching of thermal plants integrated with renewable systems," *Sci. Rep.*, vol. 12, no. 1, p. 12380, Jul. 2022.

[17] I. Ahmed, M. Rehan, A. Basit, M. Tufail, and K.-S. Hong, "A dynamic optimal scheduling strategy for multi-charging scenarios of plug-in-electric vehicles over a smart grid," *IEEE Access*, vol. 11, pp. 28992–29008, 2023.

[18] W. Yi, Y. Zhang, Z. Zhao, and Y. Huang, "Multiobjective robust scheduling for smart distribution grids: Considering renewable energy and demand response uncertainty," *IEEE Access*, vol. 6, pp. 45715–45724, 2018, doi: 10.1109/ACCESS.2018.2865598.

[19] Y. Huang, L. Wang, W. Guo, Q. Kang, and Q. Wu, "Chance constrained optimization in a home energy management system," *IEEE Trans. Smart Grid*, vol. 9, no. 1, pp. 252–260, Jan. 2018.

[20] K. Baker and A. Bernstein, "Joint chance constraints in AC optimal power flow: Improving bounds through learning," *IEEE Trans. Smart Grid*, vol. 10, no. 6, pp. 6376–6385, Nov. 2019.

[21] Y. Zhang, Q. Ai, F. Xiao, R. Hao, and T. Lu, "Typical wind power scenario generation for multiple wind farms using conditional improved Wasserstein generative adversarial network," *Int. J. Electr. Power Energy Syst.*, vol. 114, Jan. 2020, Art. no. 105388.

[22] Y. Li, B. Wang, Z. Yang, J. Li, and C. Chen, "Hierarchical stochastic scheduling of multi-community integrated energy systems in uncertain environments via Stackelberg game," *Appl. Energy*, vol. 308, Feb. 2022, Art. no. 118392.

[23] Y. Li, M. Han, M. Shahidehpour, J. Li, and C. Long, "Data-driven distributionally robust scheduling of community integrated energy systems with uncertain renewable generations considering integrated demand response," *Appl. Energy*, vol. 335, Apr. 2023, Art. no. 120749.

[24] J. Yang and C. Su, "Robust optimization of microgrid based on renewable distributed power generation and load demand uncertainty," *Energy*, vol. 223, May 2021, Art. no. 120043.

[25] S. Huang, H. Lu, M. Chen, and W. Zhao, "Integrated energy system scheduling considering the correlation of uncertainties," *Energy*, vol. 283, Nov. 2023, Art. no. 129011.

[26] B. Miao, J. Lin, H. Li, C. Liu, B. Li, X. Zhu, and J. Yang, "Day-ahead energy trading strategy of regional integrated energy system considering energy cascade utilization," *IEEE Access*, vol. 8, pp. 138021–138035, 2020.

[27] H. Qiu, W. Gu, W. Sheng, L. Wang, Q. Sun, and Z. Wu, "Resilience-oriented multistage scheduling for power grids considering nonanticipativity under tropical cyclones," *IEEE Trans. Power Syst.*, vol. 38, no. 4, pp. 1–14, May 2022.

[28] M. Faisal, M. A. Hannan, P. J. Ker, A. Hussain, M. B. Mansor, and F. Blaabjerg, "Review of energy storage system technologies in microgrid applications: Issues and challenges," *IEEE Access*, vol. 6, pp. 35143–35164, 2018, doi: 10.1109/ACCESS.2018.2841407.

[29] E. Oh and S.-Y. Son, "Shared electrical energy storage service model and strategy for apartment-type factory buildings," *IEEE Access*, vol. 7, pp. 130340–130351, 2019, doi: 10.1109/ACCESS.2019.2939406.

[30] C. Kang, J. Liu, and N. Zhang, "A new form of energy storage in future power system: Cloud energ," *Automat. Electr. Power Syst.*, vol. 41, no. 21, pp. 2–8, 2017.

[31] A. Walker and S. Kwon, "Analysis on impact of shared energy storage in residential community: Individual versus shared energy storage," *Appl. Energy*, vol. 282, Jan. 2021, Art. no. 116172.

[32] I. Ahmed, M. Rehan, A. Basit, S. H. Malik, W. Ahmed, and K.-S. Hong, "Adaptive salp swarm algorithm for sustainable economic and environmental dispatch under renewable energy sources," *Renew. Energy*, vol. 223, Mar. 2024, Art. no. 119944.

[33] I. Ahmed, M. Rehan, A. Basit, M. Tufail, and K. S. Hong, "Neuro-fuzzy and networks-based data driven model for multi-charging scenarios of plug-in-electric vehicless," *IEEE Access*, vol. 11, pp. 87150–87165, 2023.

[34] P. Li, Z. Wang, N. Wang, W. Yang, M. Li, X. Zhou, Y. Yin, J. Wang, and T. Guo, "Stochastic robust optimal operation of community integrated energy system based on integrated demand response," *Int. J. Electr. Power Energy Syst.*, vol. 128, Jun. 2021, Art. no. 106735.

[35] B. Zhou and E. Li, "Multi-regional integrated energy economic dispatch considering renewable energy uncertainty and electric vehicle charging demand based on dynamic robust optimization," *Energies*, vol. 17, p. 2453, Aug. 2024.

[36] H. Fu, B. Sendhoff, K. Tang, and X. Yao, "Finding robust solutions to dynamic optimization problems," in *Proc. 16th Eur. Conf.*, 2013, pp. 616–625.

[37] Y. Jin, K. Tang, X. Yu, B. Sendhoff, and X. Yao, "A framework for finding robust optimal solutions over time," *Memetic Comput.*, vol. 5, pp. 3–18, Jun. 2013.

BO ZHOU received the M.S. degree from Lanzhou University of Technology, Lanzhou, China, in 2017, where he is currently pursuing the Ph.D. degree. His research interests include integrated energy optimization scheduling and robust optimization.

ERCHAO LI received the M.S. degree from Yanshan University, Qinhuangdao, China, in 2005, and the Ph.D. degree from Lanzhou University of Technology, Lanzhou, China, in 2011. He is currently working as a Professor and the Ph.D. Supervisor with the College of Electrical and Information Engineering, Lanzhou University of Technology. His current research interests include dynamic optimization and robust optimization.
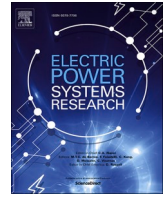
● ● ●

Research on robust optimal operation strategy of regional integrated energy system considering heating network transmission model

Bo Zhou [*], Erchao Li

College of Electrical and Information Engineering, Lanzhou University of Technology, Lanzhou 730050, China

ABSTRACT

Regional integrated energy system (RIES) is an effective way to achieve the goal of energy conservation and emission reduction of the whole energy system, and regional heating network (HN) is an important energy transmission way in the RIES. This paper focuses on the RIES optimal scheduling problem considering HN. Firstly, the RIES structure model with multiple combined cooling heating and power (CCHP) subsystems is established. Secondly, according to the basic principle of energy transmission through pipelines, a general simplified model of HN considering node flow balance and heat flow constraints is established. At the same time, considering the excellent distribution of solutions in the population method and the operability of the robust optimization over time (ROOT) in solving dynamic optimization problems, an improved ROOT based on particle swarm optimization (PSO) is proposed. Finally, an optimal scheduling model with the goal of minimum daily operating cost is established. The simulation results show that the improved ROOT can reduce the RIES operation cost by 4.58 %, and the operating cost of RIES can be reduced by 6.34 % after the HN is configured. Considering the above two measures, the total operating cost of RIES can be reduced by 10.93 %.

Abbreviation

RIES,	Regional integrated energy system;
CCHP,	Combine cooling heating and power;
HN,	Heating network;
PSO,	Particle swarm optimization;
ROOT,	Robust optimization over time;
DOP,	Dynamic optimization problem;
EPG,	External energy grid;
SOC,	State of charge;
mMPB,	Modified moving peak benchmark;
N,	Total number of CCHP;
T,	Length of scheduling period;
i,	Serial number of CCHP;
t,	Time period;
Δt,	Scheduling interval;
$P_{i,t}^{X}$,	The electrical power output of the equipment X in the $i-th$ CCHP at time t;
$H_{i,t}^{Y}$,	The heat power output of the equipment Y in the $i-th$ CCHP at time t;
$C_{i,t}^{Z}$,	The cold power output of the equipment Z in the $i-th$ CCHP at

time t

1. Introduction

Recent years, RIES based on CCHP can carry out unified planning and coordinated optimization operation [1,2], which has attracted the attention of academia and industry [3,4].

With the gradual increase of various scales of CCHP in the same area, various CCHPs form RIES through the interconnection of power grid and HN [5]. However, compared with the power grid transmission model, the HN transmission model is more complex. As an important energy channel connecting the CCHP, the simulation modeling of the energy transmission model of the HN can further analyze the coupling adjustment ability between the units in the whole region and improve the stability of the system operation. On this basis, the operation characteristics of the overall operation process can also be grasped to improve the efficiency of optimal scheduling. In the aspect of HN modeling. Ref [6] established a linear model of the district HN by referring to the equivalent infinitesimal replacement theorem under the assumption that the temperature of the load nodes is approximately equal. Ref [7] proposed a density-based topology optimization to establish a nonlinear
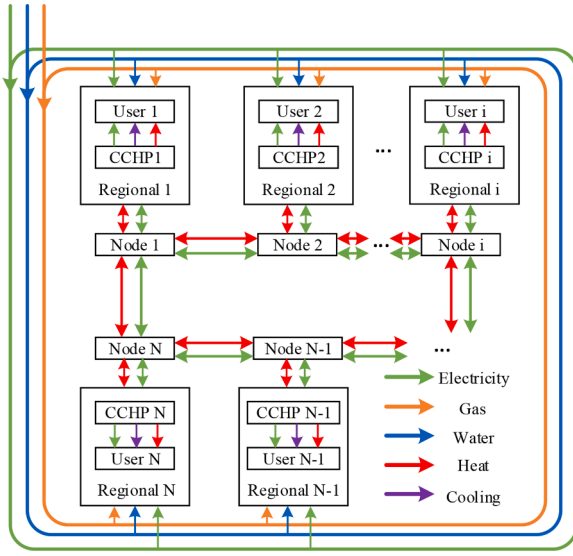
Fig. 1. The structure of RIES.

HN transmission model. According to the characteristics of thermodynamic constraints, Ref [8] introduced the equivalent pipeline model and the analytical heat source load function into the HN modeling and proposed a new dynamic model of thermal network. In Ref [9,10], a mixed integer quadratic constraint programming model is proposed for a new generation of district HN integrated with waste heat sources, considering the temperature constraints within the HN. In Ref [11], considering the problem of nonlinear discretization in heat energy transmission, a method based on the combination of double-labeled characteristic line method and full analytical method is proposed to describe the HN model, which enhances the accuracy of state estimation. The above method describes the HN energy transmission model by applying other complex formula models to achieve the accurate establishment of the model, but this is not conducive to the rapid solution of the entire multi-constrained multi-coupled CCHP scheduling problem. Therefore, under the condition of ensuring the accuracy of the model in the acceptable range, the power transmission model of the HN is optimized by Taylor series expansion, and a simplified heat network model close to the practical application of the project is proposed.

At present, there are many methods for RIES optimal scheduling, but in actual operation, the optimization problem of RIES is a kind of dynamic optimization problem, which can usually be solved by robust

optimization (RO) or population-based stochastic optimization (SO). However, the above two methods do not consider the dynamic influencing factors in the problem. In order to solve this problem, ROOT is a new method to solve this kind of dynamic optimization problem because it can combine the advantages of the above two methods [12]. Due to the adaptability to DOPs, ROOT has achieved rapid development. Ref [13] analyzed the solution behavior of ROOT based on the approximate model combined with the radial basis network model. Ref [14] introduced the multi-population framework into the original framework and used the advantages of multi-population to search for useful information faster. Adam proposed a combined ROOT solution method [15], which significantly improved the robustness of ROOT results. Other scholars have carried out research on the predictive robust solution method of ROOT [16,17], including replacing the prediction method and enhancing the accuracy of the prediction results by online mode. Ref [18] proposed a ROOT based on random sampling method to calculate the DOPs. Ref [19] proposed two parts of ROOT, one is used for robustness estimation, and the other is responsible for calculating resource allocation. Based on the advantages of ROOT in different environments, a hybrid dynamic optimization algorithm driven by environment is proposed in Ref [20]. At present, the main problem faced by ROOT is that the solution speed is slow, and the distribution of potential solutions is not sufficient. Therefore, this paper combines the advantages of particle swarm optimization in particle distribution and iterative convergence and proposes ROOT-CPSPSO based on the improvement of PSO. The main contributions of are as follows:

(1) The heat energy flow model between CCHPs in multi-area RIES is established, and the flow characteristics and power characteristics of HN nodes and pipelines are analyzed. At the same time, a power-flow-temperature model of the HN is proposed under the condition of satisfying the engineering error.
(2) For the optimal scheduling problem, considering the convergence and distribution of the population algorithm, combined with the advantages of ROOT for solving DOPs, a combined optimization method is proposed.

2. Modeling of RIES considering multi-energy flow

The structure of RIES discussed is shown in Fig 1. From the inside, the area contains multiple CCHP, each CCHP is connected to each other through the node transformer. From the outside, EPG provides electricity, water and natural gas for the entire region. The internal structure of $i-th$ CCHP is shown in Fig. 2. Energy supply side mainly includes
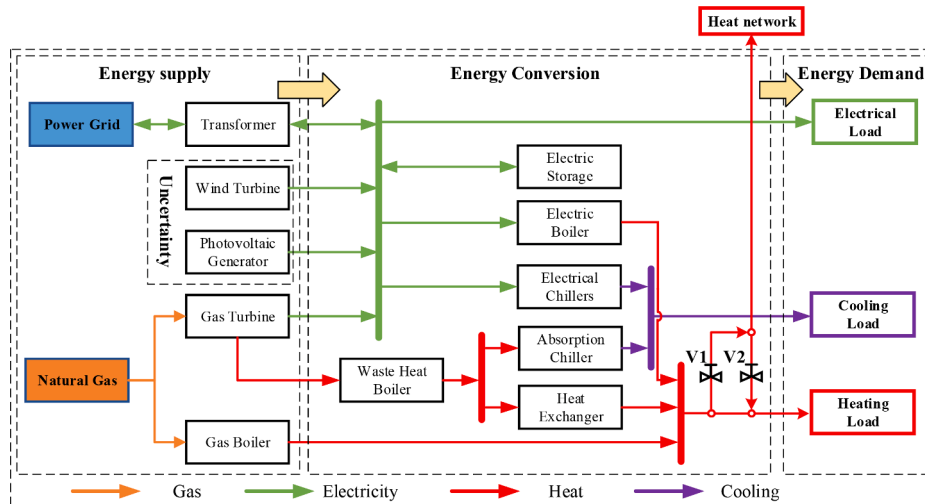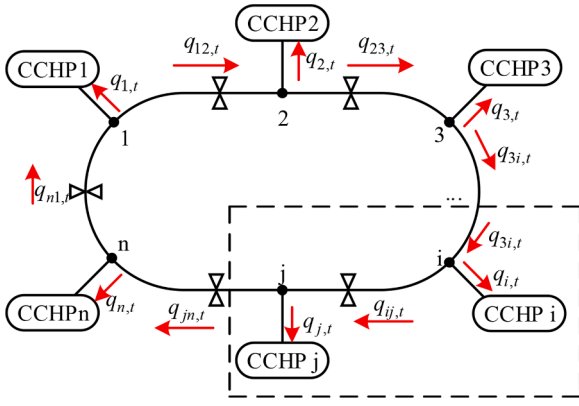

Fig. 2. The structure of CCHP.

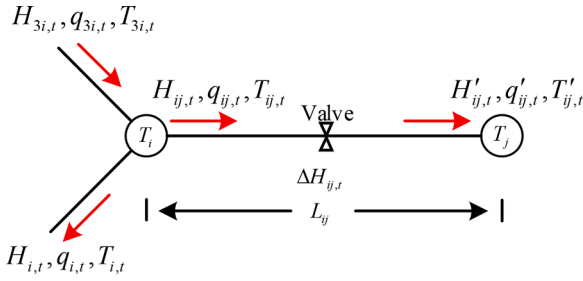**Fig. 3.** The model of RIES internal heating network.

Fig. 4. Piping parameter model of heating network.

energy generation equipment, which is composed of wind turbine (WT), photovoltaic (PV), gas turbine (GT) and gas boiler (GB). Energy conversion part is mainly composed of electric heating and cooling coupling equipment, which is composed of waste heat boiler (WHB), electric boiler (EB), electric chiller (EC), absorption chiller (AC) and heat exchanger (HE). The energy demand side is mainly composed of the user 's electricity, heat and cold load. The HN is connected to the heat bus and the heat load through valves V1 and V2, respectively. When CCHP injects heat into the HN, the valve V1 opens, V2 closes, and the HN is directly connected to the heat bus. When the HN absorbs heat from the CCHP, the valve V1 closes and V2 opens, and the HN is directly connected to the heat load. At present, the modeling of CCHP system has been more unified, so detailed modelling work of the equipment in CCHP can be found in Ref. [21–22].

3. Modelling of heating network

This paper studies the HN that provides heat energy interaction for each CCHP in RIES, which belongs to the 'source-source' network. Generally speaking, RIES has higher requirements for heat energy transmission. Therefore, this paper designs the use of ring HN layout to enhance the safety and reliability of heat energy supply. In the actual engineering environment, if the HN between any two CCHPs is damaged, the available shut-off valve will disconnect the pipeline to be repaired from the rest of the pipeline. The internal HN model of RIES is shown in Fig 3, and the heat energy distribution of the annular HN are shown in Fig. 4. In these figures, black indicates the pipe, and red indicates the direction of heat medium flow. The HN between the $i - th$ CCHP access network node i and the $j - th$ CCHP access network node j is selected as an example to explain the variables in the HN. It is specified that the heat medium temperature at node i and node j is T_i and T_j, respectively. The heat power contained in the heat medium flowing out of node i is $H_{ij,t}$, the flow rate of the heat medium is $q_{ij,t}$, and the initial temperature of the heat medium is $T_{ij,t}$. The heat medium flows through the HN with a length of L_{ij}. When it flows into node j, the heat power

contained in the heat medium is $H'_{ij,t}$, the flow rate of the heat medium is $q'_{ij,t}$, and the initial temperature of the heat medium is $T'_{ij,t}$. In view of the fact that CCHP is the supply side and the receiving side of heat energy, the heat medium does not transfer after flowing into CCHP. Therefore, when the heat medium flows from node i to the $i - th$ CCHP, the heat power contained is $H_{i,t}$, the heat medium flow rate is $q_{i,t}$, and the heat medium temperature is $T_{i,t}$. Due to the long-distance flow and transmission of the heat medium, there is a heat loss ΔH, so the heat medium parameters of the pipe flowing into the node i are different from those of the pipe flowing out of the node j.

Similar to the power grid, the HN is essentially an energy network containing heat medium flowing through. Its parameters can reflect the changes of energy parameters of each pipeline and node. At the same time, HN is also the main network system connecting the heat source and heat load, which undertakes the transmission and exchange of heat energy. In this paper, the hot water network of the scene is taken as the research object. According to Kirchhoff 's law and Sukhov 's pipeline temperature drop formula, the coupling relationship between the parameters of the HN is modeled. At the same time, it is stipulated that the energy is negative when the heat energy flows out and positive when it flows in.

3.1. Equilibrium equation of HN nodes

According to Kirchhoff 's law and the first law of thermodynamics, any HN needs to satisfy the node energy balance constraint. Therefore, for any node in the HN, the total flow of heat medium flowing into the node and the heat power contained in the heat medium should be equal to the total flow of heat medium flowing out of the node and the heat power contained in the heat medium.

$$q_{i,t} + \sum_{j\in\Omega} q_{ij,t} = 0 \tag{1}$$

$$H_{i,t} + \sum_{j\in\Omega} H_{ij,t} = 0 \tag{2}$$

where Ω is the set of nodes connected to node i.

3.2. Temperature-flow equation of HN pipeline

According to Sukhov 's temperature drop formula, The heat medium with temperature of $T_{ij,t}$ starts from the node i, flows through the pipe $i - j$, and the temperature $T'_{ij,t}$ when it flows out of the node j should meet the following conditions:

$$T'_{ij,t} = \left(T_{ij,t} - T_e\right)e^{-\frac{\lambda L_{ij}}{C_p\rho q_{ij,t}}} + T_e \tag{3}$$

where λ is the total heat resistance per kilometer; T_e is the ambient temperature; C_p is the specific heat capacity of heat medium; ρ is the density of the heat medium.

The nonlinear term $e^{-\frac{\lambda L_{ij}}{C_p\rho q_{ij,t}}}$ in the (6) is not conducive to the optimization calculation. Therefore, we regard the pipe length L_{ij} between $i - j$ as an independent variable, and use the Taylor series to expand the nonlinear term $e^{-\frac{\lambda L_{ij}}{C_p\rho q_{ij,t}}}$ at $L_{ij} = 0$ The first-order Taylor series expansion results of the nonlinear term $e^{-\frac{\lambda L_{ij}}{C_p\rho q_{ij,t}}}$ here are as follows:

$$e^{-\frac{\lambda L_{ij}}{C_p\rho q_{ij,t}}} \approx 1 - \frac{\lambda L_{ij}}{C_p\rho q_{ij,t}} \tag{4}$$

Considering (6) and (7), the temperature drops after the heat medium flows through the HN pipeline with a length of L_{ij} can be obtained as follows:

Table 1
Linearization results and relative error of ΔH.

Temperature	$H_{ij,t}$=500 kW $L_{ij,t}$=1.5 km			$H_{ij,t}$=500 kW $L_{ij,t}$=2.0 km		
	$T_{ij,t}$=80 °C	$T_{ij,t}$=85 °C	$T_{ij,t}$=90 °C	$T_{ij,t}$=80 °C	$T_{ij,t}$=85 °C	$T_{ij,t}$=90 °C
Exact	37.5202	39.7727	42.0115	49.9484	52.9015	55.8383
Approximate	37.6991	40.0553	42.4115	50.2655	53.4071	56.5487
Relative error %	0.48	0.73	0.91	0.65	0.95	1.27

$$T'_{ij,t} = T_{ij,t} - \frac{\lambda \left(T_{ij,t} - T_e\right) L_{ij}}{C_p \rho q_{ij,t}} \tag{5}$$

3.3. Heat power equation of HN pipeline

According to Sukhov 's temperature drop formula of the HN, the heat loss Δh per unit length of the pipeline is expressed as follows:

$$\Delta h = \lambda \left(T_{pipe} - T_e\right) \tag{6}$$

where T_{pipe} is the temperature of ambient. For a stable HN, it is assumed that the conduction coefficient of the network is constant with the ambient temperature. Therefore, while the heat medium flows through a pipe $i - j$ of length L_{ij}, the total heat loss $\Delta H_{ij,t}$ is as follows

$$\Delta H_{ij,t} = \int_0^{L_{ij}} \Delta h dx = \int_0^{L_{ij}} \lambda \left[T_{ij}(x) - T_e(x)\right] dx \tag{7}$$

Substituting (8) into (10), the calculation of $\Delta H_{ij,t}$ can be obtained as follows:

$$\Delta H_{ij,t} = \left(H_{ij,t} - C_p \rho q_{ij,t} T_e\right) \left(1 - e^{-\frac{\lambda L_{ij}}{C_p \rho q_{ij,t}}}\right) \tag{8}$$

In a stable environment, the physical characteristic parameters of the heat medium and the ambient temperature can be regarded as constants, so the pipeline thermal power loss $\Delta H_{ij,t}$ can be regarded as a function of the ambient temperature, pipeline length and initial heat power. According to the previous results, the Taylor expansion (4) of the nonlinear term is substituted into (8), and the linear simplified expression of the heat loss power is obtained as follows:

$$\Delta H_{i,j} \approx \lambda \left(T_{i,j} - T_e\right) L_{i,j} \tag{9}$$

Due to the use of linear expressions instead of nonlinear expressions, errors will occur. In order to check whether the error meets the requirements of calculation accuracy and verify the feasibility of substitution, the exact value of $\Delta H_{ij,t}$ is calculated by (8), and the approximate value of $\Delta H_{ij,t}$ is calculated by (9). The heat power loss and relative error calculated by different formulas are shown in Table 1. From the results of the Table 1 we can know that when the initial temperature $T_{ij,t}$= 90 °C and the pipeline length $L_{ij,t}$=2.0 km, the relative error between the estimated value and the actual value is the largest, which is 1.27 %. However, the relative error is still lower than the error requirement of ± 5 % stipulated by the national HN power measurement. Therefore, the estimated value calculated by (9) can be applied to practical engineering. Therefore, to improve the timeliness of RIES optimal scheduling results, the simplified formula shown in (9) is used to optimize the RIES scheduling calculation composed of HN and cogeneration.

The heat energy transported by the HN is related to the physical characteristics such as pipeline specifications, so the following constraints on the energy transmission of the HN should be satisfied:

$$H_{i,j}^{\min} \le H_{i,j} \le H_{i,j}^{\max} \tag{10}$$

$$\begin{cases} H_{i,j}^{\min} = \lambda \left(T_{i,j} - T_e\right) L_{i,j} \\ H_{i,j}^{\max} = C_p \rho v_{i,j}^{\max} \left(T_{i,j} - T_e\right) S_{i,j} \end{cases} \tag{11}$$

where $v_{i,j}^{\max}$ is the maximum flow velocity of the pipe $i - j$, m s^{-1}; $S_{i,j}$ is the cross-sectional area of the pipe $i - j$.

4. Optimal scheduling algorithm

At present, for the solution of optimization problems considering multi-coupling constraints, according to the complexity of problem constraints, RO or SO based on population strategies can be used. RO comprehensively considers the influence of each coupling constraint condition, and the expected robust optimal solution is still applicable when the constraint fluctuation is large. The population based SO utilizes the distribution and optimization characteristics of the population in the constraint space of the problem solution and expects to obtain the optimal solution quickly when the external environment changes. However, both of the above methods have disadvantages. The optimal robust solution obtained by the former in solving practical problems is more conservative and cannot meet the requirements of economic operation of the system. The latter requires the algorithm to obtain higher accuracy while reducing the complexity of the algorithm itself, and to obtain and switch to a new optimal solution in time. In engineering practice, the change of equipment parameters is often very fast, and the required calculation accuracy and performance cannot be achieved.

Therefore, combining the characteristics of the above two optimization methods, Yu et al. proposed ROOT [12]. The core idea of this method is to apply the optimal solution obtained in a certain environment as a better solution with certain satisfaction to one or more continuous dynamic environments in the future. The robustness of the solution is defined by the survival time R^{st} and the average fitness R^{af} of each robust solution proposed in Ref [12]. The mathematical expression is:

$$R^{st}(x, t, \delta) = \begin{cases} 0, if f(x, \alpha_i) < \delta \\ \max\{l | t \le i \le t + l : f(x, \alpha_i) \ge \delta\}, otherwise \end{cases} \tag{12}$$

$$R^{af}(x, t, T) = \frac{1}{T} \sum_{i=t}^{t+T-1} f(x, \alpha_i) \tag{13}$$

where T is time window, δ is the robustness threshold, l is the time duration. R^{st} represents the length of time that the robust solution maintains in the time domain under the condition that the predetermined robust threshold is satisfied, and R^{af} represents the average fitness of the robust solution in the time domain within the predetermined time window. At present, ROOT performs poorly in global search and convergence speed. In view of the above problems, considering that the population algorithm has strong global search ability and fast convergence speed to the optimal solution, this paper replaces the improved PSO as the optimizer into the ROOT framework, and proposes a ROOT based on PSO with combined parameter strategy (ROOT-CPSPSO).

4.1. PSO combination parameter strategy

4.1.1. Activating factor strategy

In PSO, the potential solution of the optimization problem can be regarded as a particle. All particles have a fitness value determined by the objective function and a velocity parameter that determines the position and flight direction of each particle. Each particle follows the current optimal particle at this rate $v_{id}(t)$ to search in the solution space. The optimal solution found by a single particle is called the individual optimal solution s_{io}, and the optimal solution obtained by the entire population search is called the global optimal solution s_{go}. To ensure that the particles in the solution space of the problem can jump out of the point in time when they fall into the local optimal solution, maintain the continuous search action and finally find the global optimal point. Compared with the global optimal solution s_{go}, the role of the individual optimal solution s_{io} only provides the direction vector guidance for the particle to converge to the optimal target solution and does not affect the overall consciousness of the particle to approach the global optimal point, so the individual optimal solution s_{io} is modified. The specific correction method is to increase the vitality coefficient A before item s_{io}, to ensure that the individual cognitive information $(s_{io} - u_{id})$ still has certain vitality when the particle searches for the current global optimal point. The PSO after adding the activation factor A, the improved particle swarm optimization algorithm updates the velocity and position of the particles in the iteration through the individual optimal solution and the group optimal solution. The iterative formula for the velocity and position is shown below.

$$v_{id}(t+1) = \omega_{adap}v_{id}(t) + \eta_1 rand()A(s_{io} - u_{id}(t)) + \eta_2 rand()(s_{go} - u_{id}(t)) \tag{14}$$

$$u_{id}(t+1) = u_{id}(t) + v_{id}(t+1) \tag{15}$$

where $u_{id}(t)$ is the current position of the particle; $v_{id}(t)$ represents the particle moving speed; η_1 and η_2 are cognitive learning factor and social learning factor respectively, and ω is inertia weight.

4.1.2. Adaptive inertial particle strategy

Considering that the evolutionary speed factor and the aggregation factor are the main factors affecting the optimization of particle swarm optimization, the above two factors are optimized, and a new evolutionary speed factor P_{spe} and an aggregation factor P_{tog} are proposed.

$$P_{spe} = \frac{1}{\exp\left(\min\left(\left(P_{best}^{now} - P_{best}^{before}\right), \left(P_{best}^{before} - P_{best}^{now}\right)\right)\right) + 1} \tag{16}$$

$$P_{tog} = \frac{1}{\exp\left(\min\left(\left(s_{go} \times pop - \sum_1^{pop} s_{io}\right), \left(\sum_1^{pop} s_{io} - s_{go} \times pop\right)\right)\right) + 1} \tag{17}$$

where P_{best}^{now} and P_{best}^{before} are the optimal fitness values of the current algebraic and previous algebraic algorithms, respectively, pop is the number of populations set. The updated inertia weight is expressed as follows

$$\omega_{adap} = 1.0 - P_{spe} \times \omega_{sep} + P_{tog} \times \omega_{tog} \tag{18}$$

where ω_{sep} is a random number within $0.4 \sim 0.6$; ω_{tog} is a random number in the range of 0.05–0.20.

4.2. ROOT-CPSPSO

The improved PSO through the above optimization strategy is substituted into the ROOT framework to obtain ROOT-CPSPSO. The historical data in the database is the saved operating data, the current data is the optimal data at the current moment, and the forecast data is
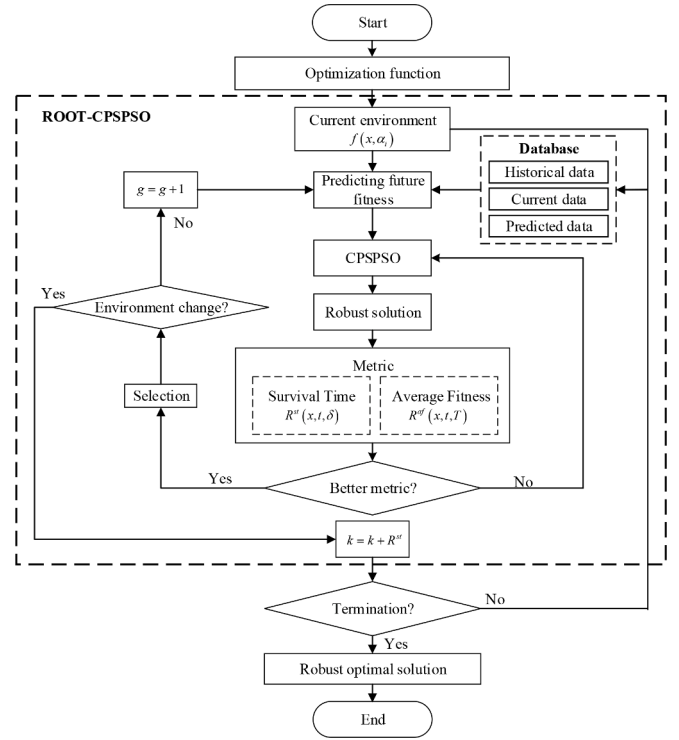

Fig. 5. Process of ROOT-CPSPSO.

the data calculated by the forecaster. The detailed introduction of the module is visible reference [23]. The algorithm flow is shown in Fig 5. In ROOT-CPSPSO, the current environmental fitness value is first calculated, and the future fitness value is predicted by the database data in the ROOT module, and then the initial robust solution is calculated by the CPSPSO. The obtained robust solution is judged and optimized by the survival time index and the average fitness index in the ROOT module, and finally the optimal dynamic robust solution in the current target environment is obtained.

5. Optimal scheduling model

5.1. Optimization objective

$$\min C_{RIES} = C_{grid} + C_{gas} + C_{om} \tag{19}$$

where C_{grid} is the electrical energy transaction cost with EPG; C_{gas} is the gas energy transaction cost with EPG; C_{om} is the maintenance and operation cost of RIES.

$$C_{grid} = \sum_{i=1}^{N} \sum_{t=1}^{T} \left(c_{b,t}^{gird} P_{i,t}^{Grid,buy} - c_{s,t}^{gird} P_{i,t}^{Grid,sell}\right) \Delta t \tag{20}$$

where $c_{b,t}^{gird}$ is the purchase price of electric energy; $P_{i,t}^{Grid,buy}$ is the amount of electricity purchased; $c_{s,t}^{gird}$ is the sale price of electric energy; $P_{i,t}^{Grid,sell}$ is the amount of electricity sold.

$$C_{gas} = \sum_{i=1}^{N} \sum_{t=1}^{T} c_{gas} \left[P_{i,t}^{GT} \Big/ \left(\eta_i^{GT} H_{ng}\right) + H_{i,t}^{GB} \Big/ \left(\eta_i^{GB} H_{ng}\right)\right] \Delta t \tag{21}$$

where c_{gas} is the price of natural gas; η_i^{GT} and η_i^{GB} are the efficiencies of GT and GB, respectively; H_{ng} is the heating value of natural gas.

$$C_{om} = \sum_{i=1}^{N} \sum_{t=1}^{T} \left(K_{om}^{Elec} P_{i,t}^{Elec} + K_{om}^{Heat} H_{i,t}^{Heat} + K_{om}^{Cold} C_{i,t}^{Cold}\right) \Delta t \tag{22}$$
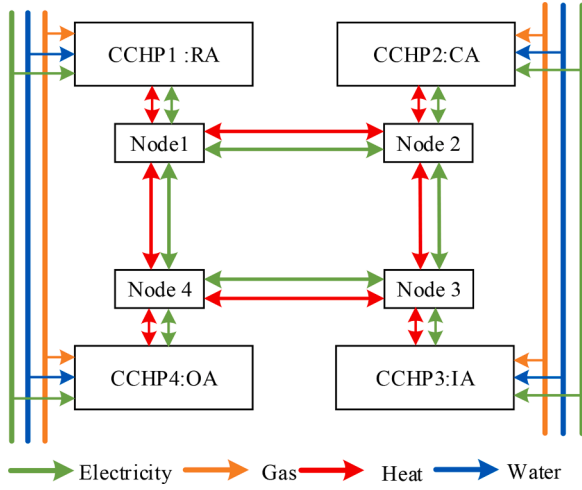
Fig. 6. The schematic diagram of RIES structure.

where K_{om}^{Elec}, K_{om}^{Heat}, K_{om}^{Cold} are the operating and maintenance cost of electric, heat and cold energy equipment, respectively; $P_{i,t}^{Elec}$, $H_{i,t}^{Heat}$ and $C_{i,t}^{Cold}$ are the output of electric, heat and cold power of various types of energy equipment, respectively.

5.2. Operational constraints

5.2.1. Power balance constraint

$$\begin{cases} P_{i,t}^{WT} + P_{i,t}^{PV} + P_{i,t}^{GT} + P_{i,t}^{EPG} + P_{i,t}^{ES} - P_{i,t}^{EB} - P_{i,t}^{EC} = P_{i,t}^{LOAD} \\ H_{i,t}^{GB} + H_{i,t}^{HE} + H_{i,t}^{EB} + H_{i,t}^{NH} = H_{i,t}^{LOAD} \\ C_{i,t}^{EC} + C_{i,t}^{AC} = C_{i,t}^{LOAD} \end{cases} \tag{23}$$

where $P_{i,t}^{LOAD}$, $H_{i,t}^{LOAD}$ and $C_{i,t}^{LOAD}$ are the user's electricity, heat and cold load, respectively.

5.2.2. Equipment output constraint

$$\begin{cases} P_{i,t}^{X,\min} \leq P_{i,t}^{X} \leq P_{i,t}^{X,\max} \\ H_{i,t}^{Y,\min} \leq H_{i,t}^{Y} \leq H_{i,t}^{Y,\max} \\ C_{i,t}^{Z,\min} \leq C_{i,t}^{Z} \leq C_{i,t}^{Z,\max} \end{cases} \tag{24}$$

where $P_{i,t}^{X,\min}$ and $P_{i,t}^{X,\max}$ are the lower and upper limits of electric equipment X output, respectively; $H_{i,t}^{Y,\min}$ and $H_{i,t}^{Y,\max}$ are the lower and upper limits of heat equipment Y output, respectively; $C_{i,t}^{Z,\min}$ and $C_{i,t}^{Z,\max}$ are the lower and upper limits of cold equipment Z output.

5.2.3. Heat power transfer balance constraint

$$H_{i,t}^{HE} \Big/ \eta_{he} + C_{i,t}^{AC} \Big/ \eta_{ac} = H_{i,t}^{GT} \gamma_{gt} \eta_{whb} \tag{25}$$

where η_{he}, η_{ac} and η_{whb} are the efficiency of HE, AC and WHB, respectively; γ_{gt} is the thermoelectric ratio of GT. Due to the limited space, the remaining constraints can be referred to [24,25], which will not be described in detail here.

6. Simulation and analysis

6.1. Simulation data

A RIES composed of four sub-regions, including residential area (RA), commercial area (CA), industrial area (IA) and office area (OA), shown in Fig 6, is established as an example model to analyze and verify the HN model and ROOT-CPSPSO. As mentioned above, each sub-region configures its own CCHP, and each subsystem interacts with EPG through the pipe network. The curves of PV and WT output power and various loads on typical days in each sub-region are shown in Fig 7. Fig 7a) and Fig 7b) represent the curves of the corresponding data of RA and CA, IA and OA, respectively. Equipment and pipeline setting parameters References [26,27].

6.2. Algorithm comparison test

In this paper, mMPB is used as a test function to compare and analyze the robustness of ROOT-CPSPSO and other ROOT in solving DOP. The parameter setting of mMPB is described in [28]. Comparison methods References [13,14,23,28]. The average survival time and average fitness results of robust solutions under different ROOT are shown in Fig 8 and Table 2. Fig 8a) and Fig 8b) show the change curve of the robustness of the solution of each algorithm corresponding to the mMPB test environment under the set fitness threshold parameters. Fig 8c) and Fig 8d) show the change curve of the robustness of the solution of each algorithm corresponding to the mMPB test environment under the set time window parameters. From Fig. 8 and Table 2 we know that the robustness of the solution obtained by ROOT-CPSPSO is better than that of the other ROOT when dealing with dynamic optimization problems under different fitness thresholds. Similarly, with the improvement of the robustness index set by the decision maker, the robustness of the solutions obtained by each algorithm decreases, but ROOT-CPSPSO can always filter out the solution with the best robustness due to the wide distribution of its own particles in the solution space. Under the fitness threshold equal to 40, the average fitness and solution generation time of the solution calculated by ROOT-CPSPSO are 58.48 % and 63.07 %
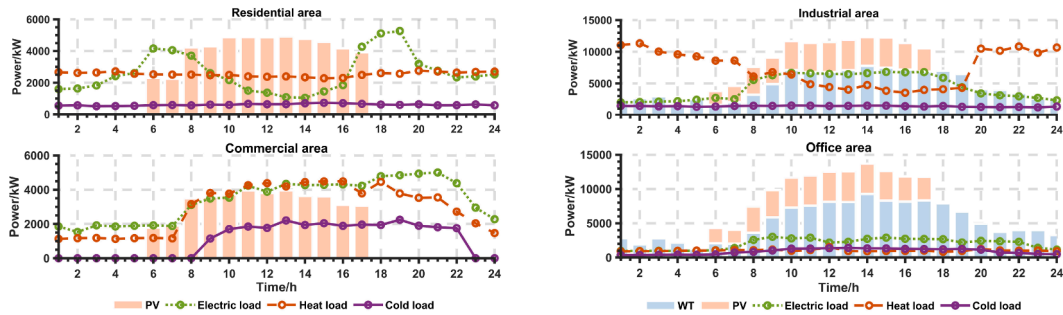
a) Load and PV/WT data of RA and CA   **b) Load and PV/WT data of IA and OA**

Fig. 7. The PV/WT output and the load curve of each region.

a) fitness threshold = 40

b) fitness threshold = 50

c) time window = 2

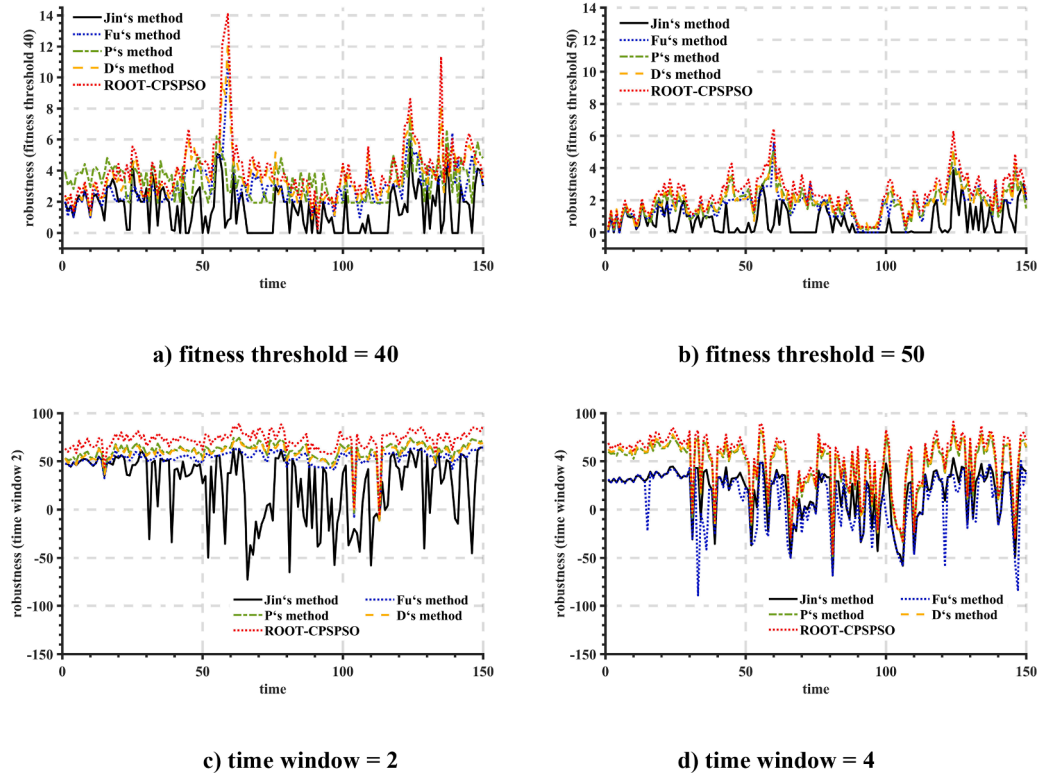**d) time window = 4**

Fig. 8. The robustness of different ROOT under mMPB.

Table 2
Different ROOT experimental results under mMPB environment.

Algorithm	Fitness threshold		Time window	
	40	50	2	4
Jin's ROOT [28]	1.53	0.71	25.32	22.20
Fu's ROOT [23]	3.03	1.69	53.48	26.99
P's ROOT [13]	3.35	1.82	61.88	45.31
Y's ROOT [14]	3.62	1.95	59.35	47.62
ROOT-CPSPSO	4.07	2.13	72.39	51.79

Table 3
Operation cost composition of RIES and SESS configuration under different models.

Cost details	Mode 1	Mode 2	Mode 3	Mode 4
Electrical energy purchasing cost	15,118.82 ¥	18,008.17 ¥	14,220.23 ¥	16,706.16 ¥
Gas energy purchasing cost	71,075.07 ¥	65,551.29 ¥	66,693.63 ¥	61,618.52 ¥
Operation and maintenance cost	6007.59 ¥	4825.63 ¥	6010.79 ¥	4788.51 ¥
Total operating cost	92,201.48 ¥	88,385.09 ¥	86,924.65 ¥	83,113.19 ¥

higher than those of the existing ROOT, respectively. In summary, on the basis of combining the advantages of population theory and ROOT framework, the proposed algorithm improves the robustness to DOP solutions.

6.3. Analysis of optimal scheduling results under different models

To verify the influence of the HN and proposed methods on the optimal scheduling results of RIES, the following four modes are established.

Mode 1: PSO is used for optimization without considering the HN connection.

Mode 2: PSO is used for optimization while considering the HN connection.

Mode 3: ROOT-CPSPSO is used for optimization without considering the HN connection.

Mode 4: ROOT-CPSPSO is used for optimization while considering the HN connection.

The result of RIES operating costs and SESS capacity configuration under the above four modes are shown in Table 3. Comparing mode 2 and mode 4, it can be seen that compared with PSO, the total cost of the system is reduced when ROOT-CPSPSO is used to solve the RES uncertainty problem. Compared with mode 2, the total operating cost of mode 4 is reduced by 6.34 %. At the same time, the capacity configuration of SESS is increased. Results shows that ROOT-CPSPSO can obtain a more robust solution and make RIES run under better conditions. Comparing mode 3 and mode 4, it can be seen that when RIES considers the use of heat network connection between CCHPs, due to the increase of heat energy interaction channels, areas with abundant renewable energy can generate heat energy through electric heating to supply other areas, thus reducing the cost of RIES gas purchase, so the cost of RIES gas purchase from EPG is reduced by 8.24 %. The decrease of gas purchase cost leads to the decrease of operation times and output power of its own gas-electric coupling equipment. Therefore, it is necessary to purchase some electric energy from EPG, and the purchase cost of the system increases by 17.48 %. Due to the interconnection of the equipment, the peak and valley heat energy has supplemented each other, which reduces the operating pressure and further reduces the operation and maintenance cost of the whole system by 25.53 %. In summary, when the thermal energy interaction between CCHPs in RIES is considered through HN, the operating cost of RIES can be reduced by 4.59 %.

6.4. Analysis of heating network condition

The results of the flow rate and heat power of the heat medium in the

a) Result of heat medium velocity and heat power   b) Result of heat energy exchange
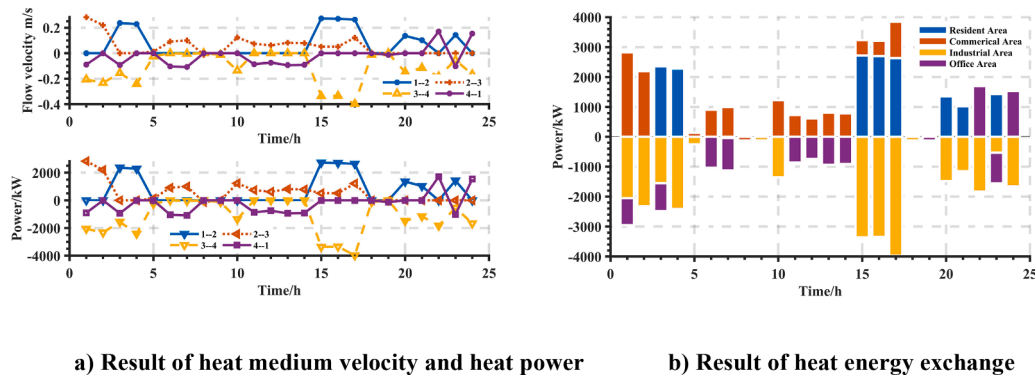
Fig. 9. Result of heat medium flow velocity and heat power of each regional.

HN are shown in Fig. 9, where it is assumed that the heat medium flows clockwise in Fig. 6 is positive, and vice versa. Fig 9a) shows the flow velocity of the heat medium in the HN connected to each CCHP; Fig. 9b) represents the thermal power of each region interacting from the HN. From the results, we can find that the heat medium flow rate curve is basically consistent with the heat transfer power curve of the pipe section. At the same time, at least one section of the pipeline has no hot water at any time, which is determined by the ring network structure. Combined with Fig. 6, we can find that the area with low heat load mainly wants to heat the HN, while the area with high heat load absorbs heat energy from the HN. It is worth noting that although both 04:00–05:00 and 15:00–18:00 are heat energy transported from RA to IA, the paths are slightly different, which is mainly due to the randomness of heat energy transmission.

7. Conclusion

Based on the establishment of a multi-regional RIES model, this paper establishes the topology of the HN in RIES and models the flow energy model of the heat network nodes and the energy flow rate model of the HN pipeline through the Taylor expansion method. At the same time, considering the excellent distribution of the solution of the population algorithm and the operability of the ROOT in solving DOP, an improved ROOT based on PSO is proposed, which provides a certain theoretical and algorithm basis for promoting the application of HN in actual RIES and improving the economy of RIES operation. Finally, the following conclusions are obtained through the example verification.

1) The ROOT-CPSPSO proposed can solve the DOP problem well. In the same test environment, compared with the existing ROOT, the survival time of the robust solution obtained by the improved ROOT is increased by 63.07 % on average, and the average fitness is increased by 58.48 % on average. Using ROOT-CPSPSO can reduce the operating cost of RIES by 4.58 %.
2) The proposed HN model fully considers the heat balance constraints of the HN nodes, and the transportation constraints of the HN pipelines, and better simulates the actual operation of the HN. Through the example verification, it can be seen that when the CCHPs are connected through the HN, the redistribution and transfer of the heat power inside the RIES can be realized, and the economy of the system can be further improved. In the case of a district HN, the operating cost of RIES can be reduced by 6.34 %.

The HN model proposed in this paper only considers the ideal operating state of the HN and does not consider the complex environment faced by the actual operation of the HN. At the same time, the proposed algorithm is mainly used to solve the single-objective optimization problem. Therefore, the future work is to study the HN model under complex operating environment and the application of ROOT in multi-objective dynamic optimization problem.

CRediT authorship contribution statement

Bo Zhou: Writing – review & editing, Writing – original draft, Validation, Methodology. **Erchao Li:** Writing – review & editing, Supervision, Methodology.

Declaration of competing interest

The authors declare that they have no known competing financial interests or personal relationships that could have appeared to influence the work reported in this paper.

Data availability

Data will be made available on request.

Acknowledgements

References

[1] H. Feng, Y.J. Hu, C. Li, H. Wang, Rolling horizon optimisation strategy and initial carbon allowance allocation model to reduce carbon emissions in the power industry: case of China, Energy 277 (2023) 127659.
[2] C. Wang, C. Lv, P. Li, G. Song, S. Li, X. Xu, J. Wu, Modeling and optimal operation of community integrated energy systems: A case study from China, Appl. Energy 230 (2018) 1242–1254.
[3] H. Liu, Z. Geng, Y. Gu, Z. Mo, Z. Yu, X. He, S. Lu, A regional integrated energy system with a coal-fired CHP plant, screw turbine and solar thermal utilization: Scenarios for China, Energy Convers. Manage 212 (2020) 112812.
[4] M. Wang, H. Yu, R. Jing, H. Liu, P. Chen, C Li, Combined multi-objective optimization and robustness analysis framework for building integrated energy system under uncertainty, Energy Convers. Manage 208 (2020) 112589.
[5] F. Xu, L. Hao, L. Chen, et al., Integrated heat and power optimal dispatch method considering the district heating networks flow rate regulation for wind power accommodation, Energy 263 (2023) 125656.
[6] H. Tan, W. Yan, Z. Ren, et al., A robust dispatch model for integrated electricity and heat networks considering price-based integrated demand response, Energy, 239 (2022) 121875.
[7] Y. Wack, M. Baelmans, R. Salenbien, et al., Economic topology optimization of District Heating Networks using a pipe penalization approach, Energy 264 (2023) 126161.
[8] S. Zhang, W. Gu, S. Lu, et al., Dynamic security control in heat and electricity integrated energy system with an equivalent heating network model, IEEe Trans. Smart. Grid. 12 (6) (2021) 4788–4798.
[9] D. Hering, A. Xhonneux, D. Müller, Design optimization of a heating network with multiple heat pumps using mixed integer quadratically constrained programming, Energy, 226 (2021) 120384.
[10] D. Hering, M.E. Cansev, E. Tamassia, et al., Temperature control of a low-temperature district heating network with model predictive control and mixed-integer quadratically constrained programming, Energy, 224 (2021) 120140.

[11] S. Zhang, W. Gu, X. Zhang, et al., Fully analytical model of heating networks for integrated energy systems, Appl. Energy 327 (2022) 120081.

[12] X. Yu, Y. Jin, K. Tang, et al., Robust optimization over time—A new perspective on dynamic optimization problems//IEEE Congress on evolutionary computation, IEEE (2010) 1–6.

[13] P. Novoa-Hernández, D.A. Pelta, C.C. Corona, Approximation models in robust optimization over time-an experimental study//2018 IEEE Congress on Evolutionary Computation (CEC), IEEE (2018) 1–6.

[14] D. Yazdani, T.T. Nguyen, J. Branke, Robust optimization over time by learning problem space characteristics, IEEE Trans. Evol. Comput. 23 (1) (2018) 143–155.

[15] L. Adam, X. Yao, A simple yet effective approach to robust optimization over time//2019, in: IEEE Symposium Series on Computational Intelligence (SSCI), IEEE, 2019, pp. 680–688.

[16] M. Fox, S. Yang, F. Caraffini, An experimental study of prediction methods in robust optimization over time//2020, in: IEEE Congress on Evolutionary Computation (CEC), IEEE, 2020, pp. 1–7.

[17] X. Zhang, Y. Fang, Q. Liu, Finding robust pareto-optimal solutions over time for dynamic disassembly sequence planning//international manufacturing science and engineering conference, Am. Soc. Mech. Eng. (2022) 85819. V002T06A012.

[18] J.Y. Guzmán-Gaspar, E. Mezura-Montes, Domínguez-Isidro S. Differential evolution in robust optimization over time using a survival time approach, Math. comput. appl. 25 (4) (2020) 72.

[19] D. Yazdani, D. Yazdani, J. Branke, et al., Robust optimization over time by estimating robustness of promising regions, IEEE Trans. Evol. Comput. 27 (3) (2022) 657–670.

[20] M. Chen, Y. Guo, Y. Jin, et al., An environment-driven hybrid evolutionary algorithm for dynamic multi-objective optimization problems, Complex. Intell. Systems. 9 (1) (2023) 659–675.

[21] S. Huang, H. Lu, M. Chen, W Zhao, Integrated energy system scheduling considering the correlation of uncertainties, Energy 283 (2023) 129011.

[22] C. Wang, C. Liu, P. Yang, et al., Data-driven flexibility evaluation methodology for community integrated energy system in uncertain environments[J], Electr. Power Syst. Res. 231 (2024) 110347.

[23] Y. Jin, K. Tang, X. Yu, B. Sendhoff, X Yao, A framework for finding robust optimal solutions over time, Memet. Comput. 5 (2013) 3–18.

[24] X. Luo, Y. Liu, P. Feng, et al., Optimization of a solar-based integrated energy system considering interaction between generation, network, and demand side, Appl. Energy 294 (2021) 116931.

[25] M. Yan, Y. He, M. Shahidehpour, et al., Coordinated regional-district operation of integrated energy systems for resilience enhancement in natural disastersS, IEEe Trans. Smart. Grid. 10 (5) (2018) 4881–4892.

[26] B. Zhou, E. Li, Multi-Regional Integrated Energy Economic Dispatch Considering Renewable Energy Uncertainty and Electric Vehicle Charging Demand Based on Dynamic Robust Optimization[J], Energies. (Basel) 17 (11) (2024) 2453.

[27] W. Gu, S. Lu, J. Wang, et al., Modeling of the heating network for multi-district integrated energy system and its operation optimization, Proceedings of the CSEE 37 (5) (2017) 1305–1315.

[28] H. Fu, B. Sendhoff, K. Tang, X. Yao, Finding Robust Solutions to Dynamic Optimization Problems, in: the 16th European Conference on Applications of Evolutionary Computation, 2013, pp. 616–625.

甘肃省优秀博士生项目结题材料

项目名称：计及共享储能的微能源网多目标优化运行研究

项目编号：　　　　　22JR5RA241　　　　　

承担单位：　　　　　兰州理工大学　　　　　

研究起止年限：　2022.10.01　至　2023.09.30　

结题验收时间：　　　　2023.11.23

目　　录

‖‖‖‖‖‖‖‖‖‖‖‖‖‖‖‖‖‖‖‖
21012655803 6

甘肃省科技计划项目任务书

（自然科学基金）

（2022年度）

项目名称： 计及共享储能的微能源网多目标优化运行研究

项目负责人： 周勃

主管处室： 基础研究处

组织部门： （甲方）甘肃省科学技术厅

承担单位： （乙方）兰州理工大学 （盖章）

推荐单位： （丙方）兰州理工大学 （盖章）

起止年限： 2022年10月01日 至 2023年09月30日

（乙方丙方为同一单位的，只在承担单位一栏盖章）

甘肃省科学技术厅 制

一、项目基本信息表

项目承担单位	兰州理工大学				
组织机构代码/统一社会信用代码	12620000438002561J				
单位通讯地址	兰工坪287号		邮编	730050	
单位性质	全额事业单位（如高等院校等）				
推荐部门	兰州理工大学				
其他主要参加单位	序号	单位名称		组织机构代码/统一社会信用代码	
参加单位总数（个）	0				

项目负责人	姓名	周勃		性别	男
	学位	硕士		专业	控制理论与控制工程
	职称	工程师		职务	无
	联系电话	0931-2976079		手机	18291497127
	证件类型	身份证		证件号码	620102198911135310
	年龄	33		政治面貌	中共党员
	传真			E-mail	446712595@qq.com
	所在单位	兰州理工大学			

参加项目总人数（人）	1	其中	高级	0	中级	1	初级	0	其他	0
			博士	0	硕士	1	学士	0	其他	0

所属技术领域	能源
创新类型	□原始创新 ■集成创新 □引进消化吸收再创新
项目概要	中国"30·60"双碳目标的背景下，以提高可再生能源的渗透率，促进可再生能源的合理消纳，达到降低整个社会碳排放为目的，本项目拟对含有共享储能的综合能源系统进行研究。以含共享储能的微能源网系统为基础，分析含有共享储能的系统运行特性、建立微能源网内部各元件的数学模型及共享储能的数学模型，研究系统中各个元件之间的运行耦合关系，提出系统优化目标及约束条件，并通过多目标优化算法，得到系统优化调度结果。
项目完成考核指标简述	1、理论研究报告、数字仿真报告； 2、发表高水平研究论文2篇以上；其中SCI、EI收录论文不低于1篇、权威期刊论文不低于1篇；
课题设置（无课题设置的项目无需填写）	无
预期成果	□专利　　□技术标准　□新产品（或农业新品种）　□新工艺 □新装置　□新材料　　□计算机软件　　■论文 □论著　研究报告　□科普　　□其他

一、项目基本信息表

项目承担单位	兰州理工大学						
组织机构代码/统一社会信用代码	12620000438002561J			邮编	730050		
单位通讯地址	兰工坪287号						
单位性质	全额事业单位（如高等院校等）						
推荐部门	兰州理工大学						
其他主要参加单位（个）	序号	单位名称		组织机构代码/统一社会信用码			
	0						
参加单位总数（个）	0						
项目负责人	姓名	周勃		性别	男		
	学位	硕士		专业	控制理论与控制工程		
	职称	工程师		职务	无		
	联系电话	0931-2976079		手机	18291497127		
	证件类型	身份证		证件号码	620102198911135310		
	年龄	33		政治面貌	中共党员		
	传真			E-mail	446712595@qq.com		
	所在单位	兰州理工大学					
	其中	高级 0	中级 0	初级 1	其他 0		
		博士 0	硕士 1	学士 1	其他 0		
参加项目总人数（人）	1						
所属技术领域	能源						
创新类型	□原始创新 ■集成创新 □引进消化吸收再创新						
项目概要	中国"30·60"双碳目标的背景下，以提高可再生能源的合理消纳，达到降低整个社会碳排放为目的，本项目拟对含有共享储能的微能源网系统为基础，分析含有共享储能的系统运行特性，建立微能源网内部各元件的运行耦合关系，提出有共享储能的数学模型及共享储能约束条件，研究系统优化目标及多目标优化中各个元件之间的运行耦合关系，得到兼顾系统优化调度算法，得到兼顾多目标协同最优的数学模型，并通过对多目标进行优化，得到最终系统优化结果。						
项目完成考核指标简述	1、理论研究报告、数字仿真报告；2、发表高水平研究论文2篇以上：其中SCI、EI收录论文不低于1篇，权威期刊论文不低于1篇；						
课题设置（无课题设置的项目无需填写）	无						
预期成果	□专利 □技术标准 □新产品（或农业新品种） □新工艺						
	□新装置 □新材料 □计算机软件 ■论文						
	□论著 □研究报告 □科普 □其他						

成果转移转化的方式目标	■自我转化 □向他人转让 □许可他人使用 □合作转让 □作价投资 □其他				
科技报告	本项目共提交科技报告1份。				
预期知识产权	国外发明专利（项）	0	国内发明专利（项）	0	其他（项） 1
预期技术标准制定	国际标准 □国家标准 □行业标准 □地方标准 □企业标准 ■无标准制定			1	0
高校院所、企业等创新主体计划外开发科研辅助岗位（个）	1	计划吸纳的应届毕业生（人）			1

二、目标与任务

（①立项意义；②研究目标；③课题研究内容及任务分解；④要解决的主要技术难点和问题；⑤技术方案；⑥创新点等。）

一、立项意义

目前，我国社会能源结构仍主要以化石能源为主，这种能源消费结构使得环境污染问题日益严重，以传统化石能源发电为基础的能源结构难以适应日益严苛的碳排放要求，也不符合国家可持续发展的目标，可再生能源发电愈发得到重视。根据国家能源局最新数据显示，截止到2022年第一季度，我国风电、光伏发电累计装机量位居世界第一。然而可再生能源发电出力的波动性以及用户侧需求响应导致的用电在时空上的随机性，加剧了电网能量的非线性及不可控性，使得电网运行调度控制及电力系统管理的难度增大，造成传统电网对大规模可再生能源发电并网的接纳能力不足。

作为现代电力系统消纳可再生能源及提高供电系统可靠性的重要手段，微能源网(Micro-Energy Grid, MEG)已经在传统电力系统中广泛存在。而储能系统（Energy Storage System, ESS）作为微能源网的重要组成部分和关键支撑技术，能够完成电力系统发电及用电在时间层面上的解耦，使得传统意义上的"刚性"系统转变为可灵活控制的"柔性"系统，极大的提高了电力系统安全性、稳定性及可靠性。随着"十四五"阶段可再生能源的更大规模的开发和利用，可以预见未来的电力系统是一个包含传统发电系统、可再生能源发电系统及能源存储系统的复杂非线性系统。这其中储能发挥着重要的支撑作用，储能的支撑功能将贯穿发电、输电、配电、用电等各个环节。因此，储能系统是我国未来实现能源互联网的必要组成部分，是我国推动电力系统体制改革的基础，是促进能源新业态发展的前提。

在中国"30•60"双碳目标的要求下，全社会对储能及其在电网中发挥的关键作用愈加重视，国家近几年发布的若干重要指导文件也说明对于发展储能产业的信心与决心。然而除抽水蓄能，其余储能技术尚处于发展初期，对于投资者来说，缺乏合理的回报机制且缺乏可复制的成熟商业模式，导致储能技术发展缓慢。因此，在全球范围内掀起的"共享经济模式"成为许多国内外专家学者的关注重点。综上，在中国"30•60"双碳目标的要求下，社会对于构建包含"共享储能"的更清洁、更灵活的微能源网提出了更高要求。利用"共享储能"来提升社会对可再生能源的接纳程度并完成电力用户的削峰填谷已成为当前研究的重点内容。

二、研究目标

基于"30•60"双碳目标，以改变能源结构，提高可再生能源的渗透率，促进电力系统对于可再生能源的合理消纳，通过调整能源结构使整个社会达到低碳排放为目的，本项目拟对含有共享储能的微能源网系统进行研究。以所建立含共享储能的微能源网系统为基础，分析含有共享储能的微能源网系统的运行特性，建立微能源网内部各元件的数学模型及共享储能的数学模型，揭示整个系统中各个元件之间的运行耦合关系，提出系统优化目标及约束条件，最终通过启发式多目标优化算法，得到该系统的优化调度结果，为今后电力规划人员合理布置共享储能电站提出建议。

三、课题研究内容及内容分解

（1）建立共享储能电站数学模型
根据已有储能电站运行实际对共享储能电站进行数学建模，并确定共享储能电站的运行指标、运行约束条件。
（2）建立共享储能电站的盈利机制
针对共享储能电站服务模式界定不清、收益模式不完善的问题，提出符合市场交易规则的共享储能电站收益机制。
（3）提出共享储能的运行方式及容量配置
提出微能源网共享储能电站的综合运行方式，研究多微电网情况下共享储能电站容量规划配置问题。
（4）建立含共享储能的微能源网模型及其多目标优
化调度模型根据当地风电、光伏等可再生能源出力的历史数据，得到风电与光伏典型出力特性，并考虑运行成本、碳排放、环境影响、能效消纳等多考核指标建立优化目标函数，同时对微能源网进行数学建模，并进行多目标优化调度研究。

四、要解决的主要难点和问题

（1）共享储能电站模型建立在总结国内外已有共享储能研究及已有储能电站运行实际的基础上，建立共享储能电站优化模型；
（2）共享储能电站运行方式及盈利机制建立针对目前共享储能电站运行模式缺乏可复制性及盈利机制不确定的问题，设计一种稳定的共享储能盈利策略，提升共享储能电站运营稳定性，提高社会层面的投资热度；
（3）建立含共享储能电站的微能源网模型，采用启发式算法对其多目标优化调度问题进行研究，验证模型及方法的准确性，使项目所提的优化调度方法为电力参与者合理配置共享储能提供有力的研究分析工具。

五、技术方案

（1）使用Matlab软件对共享储能电站、微能源网进行数学建模；
（2）使用Matlab软件编写启发式算法，验证算法在求解多目标问题时的收敛性及有效性；
（3）在Matlab中调用商业求解器CPLEX/GUROBI和YALMIP工具箱，结合启发算法，对规划调度问题进行求解分析。

六、创新点

（1）目前国内外尚未对共享储能电站进行统一建模，项目将对共享储能电站进行详细建模，成为后来学者的参考；
（2）储能电站建设成本较高、市场盈利模式尚未确定，各地对共享储能电站政策不统一，项目将结合实际对共享储能运行、盈利模式进行验证；
（3）对共享储能电站及微能源网协同运行问题进行深入研究，深入挖掘共享储能电站潜能。

三、预期成果及验收考核指标

（①主要技术指标：如形成的知识产权、技术标准、新技术、新产品、新方法、新装置、新模式等数量等。指标及其水平等；②主要经济指标：生产线及其规模等；④人才队伍建设；⑤科研条件建设；⑥其他应考核的指标。项目实施期形成的发表发表论文专注形成的示范基地。中试线等。然而用户端需求响应形成的示范基地，加剧了电网对大规模消纳可再生能源及电力系统的难度时应计较机量显居世界第一。随着可再生能源发电及不可控性，使电力系统消纳可再生能源及提高供电质量的难度不足。

①主要技术指标：
（1）理论研究报告、数字仿真报告；
（2）发表高水平研究论文2篇以上；共中SCI，EI收录论文不低于1篇；权威期刊论文不低于1篇；
②人才队伍（任进状）
（1）培养博士生名，硕士生1名；
（2）建立可再生能源项目研究团队1个；

项目负责人栏注"甘肃省科技计划资助"字样及项目编号）

四、项目的承担单位、参加单位及主要研究人员

项目负责人	姓名	周勃	性别	男	民族	汉族	出生年月	1989-11-13
	证件类型	身份证	证件号码	6201021989111 35310				
	政治面貌	中共党员						
	职称	工程师	从事专业	控制理论与控制工程	职务	无	项目分工	项目负责人
	学位	硕士						
	手机	18291497127	联系电话	0931-2976079	传真		E-mail	446712559@qq.com

项目联系人	姓名	李二超	性别	男	民族	汉族	出生年月	1979-06-05
	证件类型	身份证	证件号码	130682197906050097				
	职称	教授	从事专业	自动化	职务	副院长	项目分工	理论与算法研究
	学位	博士						
	手机	13919409360	联系电话	0931-2973506	传真		E-mail	lecstarr@163.com

项目组主要研究人员

姓名	证件号码	性别	出生年月	职称	学位	从事专业	累计为项目工作时（月）	项目任务分工	所在单位	职务
周勃	62010219891113 5310	男	1989-11-13	高级	中级	控制理论与控制工程	12	项目负责人	兰州理工大学	无
				工程师 0	硕士 1	初级 1	0		其他	0

项目组总人数（人）

注：项目成员排列表仅限于填写本项目任务书时使用，用以保证完成项目内容。不作他用，外籍人士可填写护照信息作为证件号码。

五、年度计划进度

时间区间	计划进度及完成的主要研究工作

一、立项意义

目前，我国社会能源结构仍主要以石化能源为主。这种能源结构带得环境污染问题严重，以传统化石能源发电为基础的能源结构难以适应国家可持续发展的要求。截止到2022年第一季度，我国风电、光伏发电累计装机量位居世界第一。然而可再生能源发电及不可控性，加剧了电网对大规模消纳可再生能源及电力系统的难度增大，造成传统电力系统消纳可再生能源的必要……

（其余正文内容因旋转及分辨率原因难以完整辨识）

2022年10月01日 到 2022年11月30日	课题调研、可行性分析和前期理论研究
2022年12月01日 到 2023年01月31日	含共享储能的微能源网相关内容进行理论研究
2023年02月01日 到 2023年04月30日	进一步对含共享储能的微能源网优化运行调度模型进行研究
2023年05月01日 到 2023年07月31日	对模型求解得到的结果进行对比研究，完善理论结果
2023年08月01日 到 2023年09月30日	项目结题

2022年10月01日 到 2022年11月30日	课题调研、可行性分析和前期理论研究
2022年12月01日 到 2023年01月31日	含共享储能的微能源网相关内容进行理论研究
2023年02月01日 到 2023年04月30日	进一步对含共享储能的微能源网优化运行调度模型进行研究
2023年05月01日 到 2023年07月31日	对模型求解得到的结果进行对比研究，完善理论结果
2023年08月01日 到 2023年09月30日	项目结题

六、项目经费（投资计划）

单位：万元

序号	年度	拟下达省级科技计划经费	自筹资金				合计	备注
			银行贷款	风险投资	自有资金	其他		
1	2022	4.00	0.00	0.00	0.00	0.00	4.00	包括元器件采购/劳务费/差旅费/论文出版费
合计		4.00	0.00	0.00	0.00	0.00	4.00	/

七、项目绩效目标

一级指标	二级指标	三级指标	单位	目标值
产出指标	知识产权	1.专利申请数	件	1
		（1）国外专利	件	0
		（2）发明专利	件	0
		（3）实用新型	件	1
		（4）外观设计	件	0
		2.专利授权数	件	0
		（1）国外专利	件	0
		（2）发明专利	件	0
		（3）实用新型	件	0
		（4）外观设计	件	0
		3.制定技术标准	项	0
		（1）国际标准	项	0
		（2）国家标准	项	0
		（3）行业标准	项	0
		（4）地方标准	项	0
		（5）企业标准	项	0
		4.软件著作权	项	3
		5.发表论文数	篇	1
		（1）国内发表	篇	1
		（2）国际发表	篇	1
		（3）SCI、EI、ISTP收录论文数	篇	1
	论文著作	6.出版著作	部	0
		（1）外文专著	部	0
		（2）中文专著	部	0
		（3）译著	部	0

	7. 工业新产品	个	0
	8. 植物新品种	个	0
	9. 新技术	项	0
	10. 新材料	种	0
	11. 新装置（装备）	套	0
	12. 生产线	条	0
	13. 中试线	条	0
	14. 实验基地/孵化基地	个	0.00
	15. 新建农业新品种/农技推广示范基地面积	亩	0
	16. 科技信息服务平台	个	0
成果产出	17. 提供技术咨询/技术服务次数	次数	0
	18. 研究/评估/调研报告	篇	0
	19. 研究成果被省部级政府部门采纳	次	0
	20. 研究成果被地厅级行业部门采纳	次	0.00
	21. 专利融资	亿元	0
	22. 新药证书	项	0
	23. 药物临床试验批件	个	0
	24. 科技成果奖励	项	0
	（1）国家级奖励	项	0
	（2）省部级奖励	项	0
	（3）地厅级奖励	项	0
	（4）其它	项	0
	25. 主办国际会议	次	0
	26. 主办国际会议参加人数	人	0
合作交流	27. 主办国内会议	次	0
	28. 主办国内会议参加人数	人	0
	29. 参加国际会议	人次	1
	30. 参加国内会议	人次	1
	31. 已登记的成果数	项	0
	32. 转化应用成果数	项	0
	33. 产业化的成果数	项	0
	34. 成果转让合同数	项	0.00
	35. 成果转让合同总金额	万元	0.00
	36. 成果转让合同技术交易金额	万元	0
	37. 认定登记的技术合同数	项	0.00
	38. 认定登记的技术合同总金额	万元	0.00

成果应用

分类	序号 指标名称	单位	值
成果应用	39. 认定登记的技术合同技术交易金额	万元	0.00
效益指标 · 经济效益	40. 扶持企业税收贡献增长率	万元	0.00
	41. 新产品产值	万元	0.00
	42. 新增工业增加值	万元	0.00
	43. 新增产值	万元	0.00
	44. 新增销售收入	万元	0.00
	45. 新增利润	万元	0.00
	46. 新增税收	万元	0
	47. 新增出口创汇	万美元	0
	48. 培养高新技术企业	家	0
科研仪器设备	49. 新增5万元以上仪器设备数量	台/套	0.00
	50. 新增20万元以上仪器设备数量	台/套	0
	51. 新增5万元以上仪器设备原值	万元	0.00
	52. 新增20万元以上仪器设备原值	万元	0
	53. 开放共享仪器设备数	台/套	0.00
	54. 科研仪器设备对外服务率	%	0
社会效益	55. 服务企业数	家	0
	56. 带动就业人数	人	0
	57. 新增就业	人	0
	58. 新增入选省级及以上人才计划专家	名	0
	59. 培养团队	个	0
	60. 培养博士后	名	0
	61. 培养博士	名	1
	62. 培养硕士	名	1
满意度指标 · 满意度	63. 被服务企业满意度	%	0.00
	64. 被服务民众满意度	%	0.00
	65. 从事相关工作科研人员满意度	%	90.00

分类	序号 指标名称	单位	值
成果产出	7. 工业新产品	个	0
	8. 植物新品种	个	0
	9. 新技术	项	0
	10. 新材料	种	0
	11. 新装置（装备）	套	0
	12. 生产线	条	0
	13. 中试线	条	0
	14. 实验基地/孵化基地	个	0.00
	15. 新建农业新品种/农技推广示范基地面积	亩	0
	16. 科技信息服务平台	个	0
	17. 提供技术咨询/技术服务次数	次数	0
	18. 研究/评估/调研报告	篇	0
	19. 研究成果被省部级政府部门采纳	次	0
	20. 研究成果被地市级行业部门采纳	次	0.00
	21. 专利融资	亿元	0
	22. 药证证书	项	0
	23. 药物临床试验批件	个	0
	24. 科技成果奖励	项	0
	(1) 国家级奖励	项	0
	(2) 省部级奖励	项	0
	(3) 地厅级奖励	项	0
	(4) 其它	项	0
合作交流	25. 主办国际会议	次	0
	26. 主办国际会议参加人数	人	0
	27. 主办国内会议	次	0
	28. 主办国内会议参加人数	人	0
	29. 参加国际会议	人次	1
	30. 参加国内会议	人次	1
	31. 已登记的成果数	项	0
	32. 转化应用成果数	项	0
	33. 产业化的成果数	项	0
	34. 成果转让合同数	项	0.00
	35. 成果转让合同总金额	万元	0.00
	36. 成果转让合同技术交易金额	万元	0
	37. 认定登记的技术合同数	项	0.00
	38. 认定登记的技术合同总金额	万元	0.00

八、共同条款

第一条 甘肃省科学技术厅（以下简称甲方）与兰州理工大学（以下简称乙方）、兰州理工大学（以下简称丙方），根据《中华人民共和国技术合同法》和国家有关规定，为顺利完成甲方下达的甘肃省甘肃省优秀博士生项目中的《计及共享储能的微能源网多目标优化运行研究》项目，特订立本任务书，作为甲乙丙三方在任务书执行中共同遵守的依据。

第二条 双方均应严格遵守任务书各项条款。甲方应严格按任务书进行经费核拨与工作协调，监督、检查任务书的执行情况；乙方应按本任务书签订内容完成项目任务。

第三条 甲方在本任务书签字生效后应及时将任务书规定之经费拨给乙方，并逐年按任务书规定核拨经费。乙方应按任务书规定的开支范围，实行专款专用，不得挪用，并接受甘肃省科技厅审计。如果乙方违反上述规定或经甲方检查确认计划进度不符合任务书规定和省级财政科技计划项目经费开支规定，甲方有权负责提出调整意见，有权要求乙方支付违约金，直至赔偿经济损失。情节严重者甲方可终止任务书执行，并追究乙方责任。

第四条 在项目执行期内，乙方必须按甲方要求编报年度计划执行情况、下一年度经费预算和有关统计报表，及时上报甲方，逾期不报，甲方有权视同乙方未完成年度工作计划并暂缓或暂停拨款；乙方每年年初将项目开展工作情况通过甘肃省科技计划管理信息平台填报相关数据，并以书面形式报告甲方（一份）。执行期在当年度不足三个月的项目乙方可在下一年度一并上报项目开展工作情况。

第五条 任何一方提出变更任务书内容或解除任务书的要求，需与对方协商，签订变更条款或协议。任务执行过程中，甲方无故中止任务时，所拨经费、物资不得追回，并承担善后处理所发生的费用。乙方在任务书执行过程因某种原因（如：技术措施或某些条件不落实、关键技术方案变更、项目负责人变更、挪用经费、不可抗力因素）致使任务书签订内容发生变化或无法执行，应及时通报甲方，甲方审核批准后方可执行；如乙方没有提出中止任务的要求或说明，甲方可根据调查情况有权提出中止任务的处理建议，并有权要求乙方退还部分或全部所拨财政经费。

第六条 项目执行过程中或完成后直接取得科技成果要按照《科技成果登记办法》等有关规定进行登记和管理。涉及国家秘密的，执行《科学技术保密规定》。项目、课题形成的知识产权，其归属和管理按照有关知识产权的法律法规和政策规范性文件的规定执行。乙方应加强知识产权的产生、管理和保护工作。

第七条 乙方若要公开发表与本项目有关的各类保密资料，必须由保密审查部门根据我国保密有关规定审查后，确定准否发表。擅自发表者承担失密责任，直接依法对当事人追究刑事责任。

第八条 乙方在实际执行项目期间形成的论文、专著、产品和技术的宣传推广必须标注"甘肃省科技计划资助"字样及项目编号，不做标注的成果，评估或验收时不予认可。

第九条 乙方在项目实施中，要按照中共中央办公厅国务院办公厅印发《关于进一步加强科研诚信建设的若干意见》要求，诚实守信、追求真理、崇尚创新、鼓励探索、勇攀高峰，保障项目取得预期成效。

第十条 丙方的职责是：

1. 督促、检查项目任务书执行情况，定期提交项目进展和财务决算情况；

2. 协助甲方处理项目任务书执行中的问题；

3. 协助或接受甲方委托组织项目论证、验收及其他有关工作。

第十一条 凡根据项目具体情况，经协商订立的附加条款作为本任务书的正式内容的一部分。

第十二条 本任务书一式四份，甲方存两份，乙方存一份，丙方存一份。

九、其他附加条款

八、共同条款

第一条 甘肃省科学技术厅（以下简称甲方）与兰州理工大学（以下简称乙方）、兰州理工大学（以下简称丙方），根据《中华人民共和国技术合同法》和国家有关规定，为顺利完成甲方下达的甘肃省优秀博士生项目中的《计及共享储能的微能源网多目标优化运行研究》项目，特订立本任务书，作为甲乙丙三方在任务书执行中共同遵守的依据。

第二条 双方均应严格遵守任务书各项条款。甲方应按任务书进行经费核拨与工作协调、监督，检查任务书的执行情况；乙方应按本任务书签订内容完成项目任务。

第三条 甲方应在本任务书签字生效后应及时将任务书规定之经费拨给乙方，并逐年按任务书规定核拨经费。乙方应按任务书规定的开支范围，实行专款专用，不得挪用、不得挪作他用。并接受甘肃省科技厅审计。如果乙方违反上述规定经甲方检查确认计划进度不符合任务书规定和省级财政计划项目经费开支规定，甲方有权负责提出调整意见，有权要求乙方支付违约金，直至赔偿经济损失。情节严重者甲方可终止任务书执行，并追究乙方责任。

第四条 在项目执行期内，乙方必须按甲方要求编报年度计划执行情况、下一年度经费预算和有关统计报表。及时上报甲方，逾期上报，甲方有权视同乙方未完成年度工作计划并暂缓或暂不拨款；乙方每年年初将项目开展工作情况通过甘肃省科技计划管理信息平台填报相关数据，并以书面工作情况报告甲方（一份）。执行期在当年年度总结不足三个月的项目乙方可于下一年度一并上报项目开展工作情况。

第五条 任何一方提出变更任务书内容或解除任务书的要求。需与对方协商，签订变更条款成协议。任务执行过程中，甲方无故中止任务时，所拨经费，物资不得追回，并承担善后处理所发生的费用。乙方在任务书执行过程因某种原因（如：技术措施或某些条件不落实，关键技术方案变更，项目负责人变更，挪用经费，不可抗力因素）致使任务书签订内容发生变化或无法执行，应及时通报甲方，甲方审核批准后方可执行；如乙方没有提出中止任务的要求或成的要求，甲方可根据调查情况有权提出中止任务的处理建议。并有权要求乙方退还部分或成全部所拨财政经费。

第六条 项目执行过程中或对完成成果后直接取得科技成果要按照《科技成果登记办法》等有关规定进行登记管理。涉及国家秘密的，执行《科学技术保密规定》。项目、课题形成的知识产权，其归属和管理按照有关知识产权的法律法规和政策规范性文件的规定执行。乙方应加强知识产权的产生、管理和保护工作。

第七条 乙方若要公开发表与本项目有关的各类保密资料，必须由保密审查部门根据我国国家密有关规定审查后。确定准予发表，擅自发表者承担相失密责任，直接依法对当事人追究刑事责任。

第八条 乙方在实际执行项目及期间形成的论文、专著、产品和技术的宣传推广必须标注"甘肃省科技计划资助"字样及项目编号，不做标注的成果、评估或验收时不予认可。

第九条 乙方在项目实施中，要按照中共中央办公厅国务院办公厅印发《关于进一步加强科研诚信建设的若干意见》要求、诚实守信，追求真理，崇尚创新，勇攀高峰，保障项目取得预期预期成效。

第十条 丙方的职责是：
1、督促、检查项目任务书执行情况；
2、协助甲方处理项目任务书执行中的问题；

十、本任务书签约各方
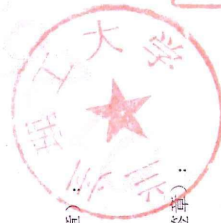
甲方：甘肃省科学技术厅（盖章）：

单位负责人（签章）：

主管处室负责人（签章）：

年 月 日

乙方：项目承担单位（盖章）：

单位负责人（签章）：

年 月 日

项目负责人（签章）：周劲

2022年10月20日

丙方：推荐单位（盖章）：

单位负责人（签章）：

主管部门负责人（签章）：

年 月 日

甘肃省科技计划项目研究人员科研诚信承诺书

1. 本人在甘肃省科技计划项目实施（包括项目申请、评估评审、检查、项目执行、验收等过程）中，对提交的有关材料真实性负责。

2. 本人严格遵守中共中央办公厅、国务院办公厅印发的《关于进一步加强科研诚信建设的若干意见》中科研诚信和科研道德的有关要求。

3. 本人严格执行《甘肃省科技计划项目管理办法》中的管理规定和《甘肃省科技计划项目任务书》中的相关约定，负责开展和完成本项目的研究任务。

4. 本人遵守《中华人民共和国保守国家秘密法》和《科学技术保密规定》等相关法律法规，所填报信息不涉及涉密内容。

如有不符，愿意承担相关后果并接受相应的处理。

项目负责人（签字）： 闫玮办

项目参与人（签字）：

2022年10月20日

十、本任务书签约各方

甲方：甘肃省科学技术厅（盖章）：

单位负责人（签字）：

主管处室负责人（签章）：

年 月 日

乙方：项目承担单位（盖章）：

单位负责人（签字）：

项目负责人（签字）： 闫玮办

2022年10月20日

丙方：推荐单位（盖章）：

单位负责人（签章）：

主管部门负责人（签章）：

年 月 日

项目编号：22JR5RA241

甘肃省科技计划项目
验收申请表

（2022年度）

项目名称：计及共享储能的微能源网多目标优化运行研究

项目负责人：周勃

主管处室：基础研究处

组织部门：甘肃省科学技术厅

承担单位：兰州理工大学 　　　　　　　　　　　（盖章）

推荐单位：兰州理工大学

起止时间：2022-10-01至2023-09-30

提交时间：2023-11-14

甘肃省科学技术厅

一、项目基本信息表

项目名称	计及共享储能的微能源网多目标优化运行研究			
项目类别	甘肃省优秀博士生项目			
项目编号	22JR5RA241			
承担单位	兰州理工大学			
起止时间	2022-10-01 至 2023-09-30			
推荐单位	兰州理工大学			
主管处室	基础研究处			
验收形式	结题			
项目负责人	姓名	周勃	联系电话	0931-2976079
	手机	18291497127	E-mail	446712595@qq.com
项目联系人	姓名	李二超	联系电话	0931-2973506
	手机	13919409360	E-mail	lecstarr@163.com
	通讯地址	甘肃省兰州市七里河区兰工坪路36号兰州理工大学		

项目完成考核指标情况简述及取得成果和应用情况

考核指标简述
（1）建立共享储能电站数学模型；
（2）建立共享储能电站运行方式及盈利机制
（3）提出启发式算法对含共享储能的冷热电联供系统优化调度问题进行求解；
（4）发表高水平论文不少于2篇。

取得的成果和应用
（1）项目根据综合能源系统包含冷、热、电、气不同能源特性，建立了异质能源网络耦合分析的统一模型，即能源集线器模型。能源集线器建模的主要思路是先形成描述输入能源和输出负荷端口的耦合矩阵，用来表示冷、热、电、气等不同能源之间的转化、存储以及传输之间的关系，在此基础上与各能源系统的稳态模型或暂态模型组合形成能源集线器模型。
（2）项目以国内外已经存在的共享储能试点项目为基础，探讨了共享储能电站的服务模式。由于目前国内大部分微能源网由于电能质量等问题，所产生电能不满足向电网倒送电相关技术要求及相关政策限制，因此若微能源网用户存在剩余电能，共享储能电站以充电的形式吸收用户剩余电能。
（3）项目以国内外已经存在的共享储能试点项目为基础，探讨了共享储能电站的运行模式及盈利机制。在共享储能电站模型中，规定其应设置储能电站调控中心，储能电站调控中心根据用户的历史信息如从电网购电电价、冷热电负荷曲线、可再生能源出力曲线等，通过合理的优化调度模型计算出用户所需的储能容量和最大充放电功率，用户根据计算结果与储能电站运营商签订储能电站服务协议，约定用户所需的最大充放电功率、储能容量、充放电功率计划等，并向用户收取储能电站服务费。
（4）项目建立了以共享储能电站运营成本最优为决策目标的目标函数，以储能容量倍率、荷电状态以及充放电功率条件为约束条件的数学模型。并在已有共享电储能的基础上，将共享储的概念推广至热/电混合共享储能系统，建立了热/电混合共享储能系统数学模型，并将其应用在区域综合能源系统优化调度方案之中。
（5）考虑到综合能源系统内可再生能源发电以及负荷用电的不确定性，项目将其看作是一类存在时变参数的鲁棒优化问题，以此为基础，提出了一种基于问题特征变化引导的时域鲁棒优化算法。
（6）项目通过算例验证了所提鲁棒优化算法的有效性及可行性，同时也验证了在综合能源系统中引入共享储能系统可以不仅提高可再生能源的消纳率，同时也可以降低系统运行成本，提高用户用能的满意度。

本项目存在的技术问题或不足

（1）模型建立不够全面。

在项目建立冷热电综合能源系统异质能源网络耦合分析的统一模型时，系统内部存在的设备模型尚未考虑周全，例如P2G模型未加入项目所建立的综合能源系统模型，P2G作为一项消纳可再生能源的优秀技术，将在后续研究中纳入冷热电综合能源系统。

（2）引入热储能后并未对热能的特性进行分析说明

在热储能建立时，由于热能传输速度慢且存在较长延时，同时热力系统基于传输延时、热损耗方程以及管道导热、节点温度混合方程的偏微分方程描述热网动态特性，忽略热网传输特性而将其用电储能数学方程进行描述容易引起较大计算误差，求得的实际调度结果较难应用至实际调度场景中，将在后续研究在热能方面加入热网管道的分析及考虑。

（3）共享储能运营模式及盈利机制不够成熟

项目所探讨的共享储能的运营模式仅为理论推断，而实际共享储能项目面临更多机遇与挑战，因此在将来共享储能究竟以何种方式运营盈利尚未可知，本项目起到抛砖引玉之作用。

（4）算法有待提高

本项目所提基于问题特征变化引导的时域鲁棒优化算法尚有改进空间，同时其他启发式算法应用在考虑源荷不确定性情况下效果如何也将在后续研究中进行对比分析。

二、项目主要完成人员名单

序号	姓名	性别	出生年月	身份证号	文化程度	工作单位	本项目主要负责工作
1	周劼	男	1989-11-13	620102198911135310	硕士	兰州理工大学	项目负责人

三、甘肃省省级科技计划项目执行情况自评估报告

主 要 内 容

一、任务书规定的研究任务、考核目标及主要技术经济指标。

1. 研究任务

（1）建立共享储能电站数学模型

根据已有储能电站运行实际对共享储能电站进行数学建模，并确定共享储能电站的运行指标、运行约束条件。

（2）建立共享储能电站的盈利机制

针对共享储能电站服务模式界定不清、收益模式不完善的问题，提出符合市场交易规则的共享储能电站收益机制。

（3）提出共享储能的运行方式及容量配置

提出微能源网共享储能电站的综合运行方式，研究多微电网情况下共享储能电站容量规划配置问题。

（4）建立含共享储能的冷热电联供微能源网模型及其多目标优化调度模型

根据当地风电、光伏等可再生能源出力的历史数据，得到风电与光伏典型出力特性，并考虑运行成本、碳排放、环境影响、能效消纳等多角度建立优化目标函数，同时对冷热电联供微能源网进行数学建模，并进行多目标优化调度研究。

2. 考核目标及主要技术经济指标

预期成果

（1）共享储能电站模型建立

在总结国内外已有共享储能研究及已有储能电站运行实际

的基础上，详细建立共享储能电站优化模型；

（2）共享储能电站运行方式及盈利机制建立

针对目前共享储能电站运行模式缺乏可复制性及盈利机制混乱的问题，设计一种稳定的共享储能盈利策略，提升共享储能电站运营稳定性，提高社会层面的投资热度；

（3）建立含共享储能电站的冷热电联供微能源网模型，采用启发式算法对其多目标优化调度问题进行研究，验证模型及方法的准确性，使项目所提的优化调度方法为今后电网工作人员而言具有一定的参考价值。

（4）在被 SCI 或 EI 等检索的高水平学术期刊上发表 1 篇以上学术论文，在中文核心期刊上发表 1 篇以上学术论文。

（5）培养博士研究生 1 名，硕士研究生 1 名

二、项目执行情况评价（包括目标、任务完成情况、解决的关键技术、取得的重大科技成果、专利情况、获得的各种奖励情况、整体水平及配套性以及项目完成后建成的试验基地、中试线、生产线，人才培养等情况）。

针对项目合同书规定的研究内容，已开展如下研究：

（1）项目根据综合能源系统包含冷、热、电、气不同能源特性，建立了异质能源网络耦合分析的统一模型，即能源集线器模型。能源集线器建模的主要思路是先形成描述输入能源和输出负荷端口的耦合矩阵，用来表示冷、热、电、气等不同能源之间的转化、存储以及传输之间的关系，在此基础上与各能源系统的稳态模型或暂态模型组合形成能源集线器模型。

（2）项目以国内外已经存在的共享储能试点项目为基础，探讨了共享储能电站的服务模式。由于目前国内大部分微能源网由于电能质量等问题，所产生电能不满足向电网倒送电相关技术

要求及相关政策限制，因此若微能源网用户存在剩余电能，共享储能电站以充电的形式吸收用户剩余电能。

（3）项目以国内外已经存在的共享储能试点项目为基础，探讨了共享储能电站的运行模式及盈利机制。在共享储能电站模型中，规定其应设置储能电站调控中心，储能电站调控中心根据用户的历史信息如从电网购电电价、冷热电负荷曲线、可再生能源出力曲线等，通过合理的优化调度模型计算出用户所需的储能容量和最大充放电功率，用户根据计算结果与储能电站运营商签订储能电站服务协议，约定用户所需的最大充放电功率、储能容量、充放电功率计划等，并向用户收取储能电站服务费。

（4）项目建立了以共享储能电站运营成本最优为决策目标的目标函数，以储能容量倍率、荷电状态以及充放电功率条件为约束条件的数学模型。并在已有共享电储能的基础上，将共享储的概念推广至热/电混合共享储能系统，建立了热/电混合共享储能系统数学模型，并将其应用在区域综合能源系统优化调度方案之中。

（5）考虑到综合能源系统内可再生能源发电以及负荷用电的不确定性，项目将其看作是一类存在时变参数的鲁棒优化问题，以此为基础，提出了一种基于问题特征变化引导的时域鲁棒优化算法。

（6）项目通过算例验证了所提鲁棒优化算法的有效性及可行性，同时也验证了在综合能源系统中引入共享储能系统可以不仅提高可再生能源的消纳率，同时也可以降低系统运行成本，提高用户用能的满意度。

2. 项目技术指标完成情况

通过一年的研究工作，以完成项目计划的技术指标，

具体：

（1）建立了共享储能的数学模型，同时探讨了共享储能的服务模式、运行方式及盈利机制，为共享储能的进一步研究发展打下基础。

（2）建立了考虑冷热电能特性的异质能源网络耦合分析的统一模型，即能源集线器模型。

（3）提出了求解含共享储能及风光不确定性的综合能源系统优化调度的基于问题特征变化引导的时域鲁棒优化算法。

（4）在被 SCI 或 EI 等检索的国际国内学术期刊上投稿论文 3 篇；在中文核心期刊上发表论文 3 篇。

（5）培养博士研究生 1 名（周勃），硕士研究生 3 名（张生辉、赵凤凯、李双）。

3．解决的关键问题

项目建立了冷热电联供系统的能源集线器模型以及共享储能系统的数学模型，同时创新的提出了基于问题特征引导的时域鲁棒优化算法，研究成果不仅对共享储能系统已有的理论基础具有一定补充效果，同时新提出的算法在解决考虑源荷不确定性的含共享储能的综合能源系统优化调度问题具有一定的有效性。

4．取得成果的整体水平

在"碳达峰、碳中和"目标的前提下，对共享储能系统的研究是目前的热点以及难点，如何更好的利用共享储能系统消纳可再生能源，提高可再生能源渗透率以及降低碳排放已经成为各高校研究所的重点研究对象。在此背景下，本项目为国内相关研究起到抛砖引玉的效果，为将来跟多关于共享储能的研究提供一定的思考与建议。

三、成果转化、产业化情况以及所取得的直接效益和间接效益（经济、社会和环境效益），成果推广应用前景的评价。

本项目是自动化、电气工程以及控制理论等学科有机交叉、新颖且富有挑战的研究方向，具有非常明确的社会需求。本项目可以促进共享储能系统在综合能源系统的应用，拓展共享储能系统的理论研究方向，提高共享储能系统的实际应用价值。

四、经费决算和经费使用评价。

经费使用主要包括：科研业务费（含参加国内外学术会议、论文版面费、文献检索、网络及技术咨询、邮寄费、交通等费用）、实验材料费（含计算机耗材、移动存储器等）、学校管理费等。科研经费按照科学合理的规划进行使用，有效避免了经费浪费以及管理不当的问题出现。

五、组织管理经验(侧重评价科技工作面向经济、社会发展、成果转化及产业化的经验)。

1. 课题的理论成果直接成为含共享储能的综合能源系统优化调度依据，为将来实际工程应用及考虑更多耦合关系的综合能源系统奠定了理论基础。

2. 由于项目是针对含共享储能的综合能源系统优化调度实际问题所提出的，因而其结果为今后电力规划人员合理布置共享储能电站具有一定的参考意义。

六、存在的问题。

（1）模型建立不够全面。

在项目建立冷热电综合能源系统异质能源网络耦合分析的统一模型时，系统内部存在的设备模型尚未考虑周全，例如电转气模型未加入项目所建立的综合能源系统模型，电转气作为一项消纳可再生能源的优秀技术，将在后续研究中纳入冷热电综合能源系统。

（2）引入热储能后并未对热能的特性进行分析说明

在热储能建立时，由于热能传输速度慢且存在较长延时，同时热力系统基于传输延时、热损耗方程以及管道导热、节点温度混合方程的偏微分方程描述热网动态特性，忽略热网传输特性而将其用电储能数学方程进行描述容易引起较大计算误差，求得的实际调度结果较难应用至实际调度场景中，将在后续研究在热能方面加入热网管道的分析及考虑。

（3）共享储能运营模式及盈利机制不够成熟

项目所探讨的共享储能的运营模式仅为理论推断，而实际共享储能项目面临更多机遇与挑战，因此在将来共享储能究竟以何种方式运营盈利尚未可知，本项目起到抛砖引玉之作用。

四、项目验收信息表

项目名称	计及共享储能的微能源网多目标优化运行研究
项目编号	22JR5RA241
承担单位	兰州理工大学
完成情况	达到预期指标

实际参加研究人员（人）

总计	1				
其中	高级职称	0	中级职称	1	初级职称	0
	博士	0	硕士	1		

主要成果

新产品（项）	0	新技术、新工艺（项）	0	新材料（种）	0
获专利（项）	0	其中：国外发明专利（项）	0	国内发明专利（项）	0
研究报告、论文(篇)	3	其中：国内发表(篇)	3	在国际上发表(篇)	0
示范点（个）	0	中试线（条）	0	生产线（种）	0
培养博士后（名）	0	培养博士（名）	1	培养硕士（名）	1
获奖（项）	0	其中：部级（项）	0	国家级（项）	0

应用情况

成果转化合同数	0项
成果转让合同额	0.00万元
已商品化成果数	0项
实际应用成果数	0项
已获综合经济效益	0.00万元

直接经济效益

新增产值	0.00万元
新增利税	0.00万元
出口创汇	0.00万美元

五、项目经费决算表

项目名称	计及共享储能的微能源网多目标优化运行研究	
项目编号	22JR5RA241	
承担单位	兰州理工大学	
收入	**实际金额（万元）**	
合计	4.00	
省级科技计划拨款	4.00	
部门拨款	0.00	
单位自筹	0.00	
其 他	0.00	
支出	**总金额（万元）**	**其中：省级科技计划拨款（万元）**
合计	4.00	4.00
（一）直接费用	3.76	3.76
1、设备费	0.00	0.00
2、业务费	3.12	3.12
3、劳务费	0.64	0.64
（二）间接费用	0.24	0.24
1、绩效支出	0.00	0.00
2、间接成本	0.24	0.24

以上填报数据属实。

承担单位负责人（签字）：

财务负责人（签字）：

（财务章）　　　　　（单位公章）

年　　月　　日

注：1.部门拨款指本项目获得国家科技计划或其他部门财政资金资助；2.单位自筹包括单位自有资金用于本项目的投入，用于本项目的银行贷款等资金；3.设备费包括购置设备费、试制设备费、设备改造与租赁费。

六、附件清单

序号	附件名称	是否必传
1	项目任务书	是
2	项目执行期间取得的成果（基金标示的论文、专利等）	是
3	工作报告（杰出青年基金、基础研究创新群体、自然科学基金和省青年科技基金计划项目无需填写）	否
4	技术报告	否
5	项目财务审计报告	否
6	其他	否

七、审核意见

承担单位意见	以上申请材料属实，同意验收申请。 盖　章 年　　月　　日
省科技厅主管处室意见	同意验收申请。 盖　章 年　　月　　日
省科技厅发展规划处意见	同意验收申请。 盖　章 年　　月　　日

甘肃省科技计划项目

准予总结结题表

项目名称：计及共享储能的微能源网多目标优化运行研究

项目编号：22JR5RA241

项目负责人：周勃

完成单位：兰州理工大学 （盖章）

推荐单位：兰州理工大学

组织单位：甘肃省科学技术厅

甘肃省科学技术厅

一、项目基本信息表

项目名称	计及共享储能的微能源网多目标优化运行研究			
项目类别	甘肃省优秀博士生项目			
项目编号	22JR5RA241			
承担单位	兰州理工大学			
起止时间	2022-10-01 至 2023-09-30			
推荐单位	兰州理工大学			
主管处室	基础研究处			
项目负责人	姓名	周勃	联系电话	0931-2976079
	手机	18291497127	E-mail	446712595@qq.com
项目联系人	姓名	李二超	联系电话	0931-2973506
	手机	13919409360	E-mail	lecstarr@163.com

二、项目主要完成人员名单

序号	姓名	性别	出生年月	身份证号	文化程度	工作单位	本项目主要负责工作
1	周勃	男	1989-11-13	620102198911135310	硕士研究生	兰州理工大学	项目负责人

三、 目标与任务、考核指标完成情况

一、立项意义

目前，我国社会能源结构仍主要以化石能源为主，这种能源消费结构使得环境污染问题日益严重，以传统化石能源发电为基础的能源结构难以适应日益严苛的碳排放要求，也不符合国家可持续发展的目标，可再生能源发电愈发得到重视。根据国家能源局最新数据显示，截止到2022年第一季度，我国风电、光伏发电累计装机量位居世界第一。然而可再生能源发电出力的波动性以及用户侧需求响应导致的用电在时空上的随机性，加剧了电网能量的非线性及不可控性，使得电网运行调度控制及电力系统管理的难度增大，造成传统电网对大规模可再生能源发电并网的接纳能力不足。

作为现代电力系统消纳可再生能源及提高供电系统可靠性的重要手段，微能源网(Micro-Energy Grid, MEG)已经在传统电力系统中广泛存在。而储能系统（Energy Storage System, ESS）作为微能源网的重要组成部分和关键支撑技术，能够完成电力系统发电及用电在时间层面上的解耦，使得传统意义上的"刚性"系统转变为可灵活控制的"柔性"系统，极大的提高了电力系统安全性、稳定性及可靠性。随着"十四五"阶段可再生能源的更大规模的开发和利用，可以预见未来的电力系统是一个包含传统发电系统、可再生能源发电系统及能源存储系统的复杂非线性系统。这其中储能发挥着重要的支撑作用，储能的支撑功能将贯穿发电、输电、配电、用电等各个环节。因此，储能系统是我国未来实现能源互联网的必要组成部分，是我国推动电力系统体制改革的基础，是促进能源新业态发展的前提。

在中国"30·60"双碳目标的要求下，全社会对储能及其在电网中发挥的关键作用愈加重视，国家近几年发布的若干重要指导文件也说明对于发展储能产业的信心与决心。然而除抽水蓄能，其余储能技术尚处于发展初期，对于投资者来说，缺乏合理的回报机制且缺乏可复制的成熟商业模式，导致储能技术发展缓慢。因此，在全球范围内掀起的"共享经济模式"成为许多国内外专家学者的关注重点。综上，在中国"30·60"双碳目标的要求下，社会对于构建包含"共享储能"的更清洁、更灵活的微能源网提出了更高要求。利用"共享储能"来提升社会对可再生能源的接纳程度并完成电力用户的削峰填谷已成为当前研究的重点内容。

二、研究目标

基于"30·60"双碳目标，以改变能源结构，提高可再生能源的渗透率，促进电力系统对于可再生能源的合理消纳，通过调整能源结构使整个社会达到低碳排放为目的，本项目拟对含有共享储能的微能源网系统进行研究。以所建立含共享储能的微能源网系统为基础，分析含有共享储能的微能源网系统的运行特性，建立微能源网内部各元件的数学模型及共享储能的数学模型，揭示整个系统中各个元件之间的运行耦合关系，提出系统优化目标及约束条件，最终通过启发式多目标优化算法，得到该系统的优化调度结果，为今后电力规划人员合理布置共享储能电站提出建议。

三、课题研究内容及内容分解

（1）建立共享储能电站数学模型

根据已有储能电站运行实际对共享储能电站进行数学建模，并确定共享储能电站的运行指标、运行约束条件。

（2）建立共享储能电站的盈利机制

针对共享储能电站服务模式界定不清、收益模式不完善的问题，提出符合市场交易规则的共享储能电站收益机制。

（3）提出共享储能的运行方式及容量配置

提出微能源网共享储能电站的综合运行方式，研究多微电网情况下共享储能电站容量规划配置问题。

（4）建立含共享储能的微能源网模型及其多目标优化调度模型根据当地风电、光伏等可再生能源出力的历史数据，得到风电与光伏典型出力特性，并考虑运行成本、碳排放、环境影响、能效消纳等多考核指标建立优化目标函数，同时对微能源网进行数学建模，并进行多目标优化调度研究。

四、要解决的主要难点和问题

（1）共享储能电站模型建立在总结国内外已有共享储能研究及已有储能电站运行实际的基础上，建立共享储能电站优化模型；

（2）共享储能电站运行方式及盈利机制建立针对目前共享储能电站运行模式缺乏可复制性及盈利机制不确定的问题，设计一种稳定的共享储能盈利策略，提升共享储能电站运营稳定性，提高社会层面的投资热度；

（3）建立含共享储能电站的微能源网模型，采用启发式算法对其多目标优化调度问题进行研究，验证模型及方法的准确性，使项目所提的优化调度方法为电力参与者合理配置共享储能提供有力的研究分析工具。

五、技术方案

（1）使用Matlab软件对共享储能电站、微能源网进行数学建模；

（2）使用Matlab软件编写启发式算法，验证算法在求解多目标问题时的收敛性及有效性；

（3）在Matlab中调用商业求解器CPLEX/GUROBI和YALMIP工具箱，结合启发算法，对规划调度问题进行求解分析。

六、创新点

（1）目前国内外尚未对共享储能电站进行统一建模，项目将对共享储能电站进行详细建模，成为后来学者的参考；

（2）储能电站建设成本较高、市场盈利模式尚未确定，各地对共享储能电站政策不统一，项目将结合实际对共享储能运行、盈利模式进行验证。

（3）对共享储能电站及微能源网协同运行问题进行深入研究，深入挖掘共享储能电站潜能。

计划任务书签订的预期成果及验收考核指标

①主要技术指标
　（1）理论研究报告、数字仿真报告；
　（2）发表高水平研究论文2篇以上；其中SCI、EI收录论文不低于1篇、权威期刊论文不低于1篇；
②人才队伍建设
　（1）培养博士生1名、硕士生1名；
　（2）建立可再生能源项目研究团队1个；

计划任务书签订的预期成果及验收考核指标

考核指标简述
　（1）建立共享储能电站数学模型；
　（2）建立共享储能电站运行方式及盈利机制
　（3）提出启发式算法对含共享储能的冷热电联供系统优化调度问题进行求解；
　（4）发表高水平论文不少于2篇。
取得的成果和应用
　（1）项目根据综合能源系统包含冷、热、电、气不同能源特性，建立了异质能源网络耦合分析的统一模型，即能源集线器模型。能源集线器建模的主要思路是先形成描述输入能源和输出负荷端口的耦合矩阵，用来表示冷、热、电、气等不同能源之间的转化、存储以及传输之间的关系，在此基础上与各能源系统的稳态模型或暂态模型组合形成能源集线器模型。
　（2）项目以国内外已经存在的共享储能试点项目为基础，探讨了共享储能电站的服务模式。由于目前国内大部分微能源网由于电能质量等问题，所产生电能不满足向电网倒送电相关技术要求及相关政策限制，因此若微能源网用户存在剩余电能，共享储能电站以充电的形式吸收用户剩余电能。
　（3）项目以国内外已经存在的共享储能试点项目为基础，探讨了共享储能电站的运行模式及盈利机制。在共享储能电站模型中，规定其应设置储能电站调控中心，储能电站调控中心根据用户的历史信息如从电网购电电价、冷热电负荷曲线、可再生能源出力曲线等，通过合理的优化调度模型计算出用户所需的储能容量和最大充放电功率，用户根据计算结果与储能电站运营商签订储能电站服务协议，约定用户所需的最大充放电功率、储能容量、充放电功率计划等，并向用户收取储能电站服务费。
　（4）项目建立了以共享储能电站运营成本最优为决策目标的目标函数，以储能容量倍率、荷电状态以及充放电功率条件为约束条件的数学模型。并在已有共享电储能的基础上，将共享储的概念推广至热/电混合共享储能系统，建立了热/电混合共享储能系统数学模型，并将其应用在区域综合能源系统优化调度方案之中。
　（5）考虑到综合能源系统内可再生能源发电以及负荷用电的不确定性，项目将其看作是一类存在时变参数的鲁棒优化问题，以此为基础，提出了一种基于问题特征变化引导的时域鲁棒优化算法。
　（6）项目通过算例验证了所提鲁棒优化算法的有效性及可行性，同时也验证了在综合能源系统中引入共享储能系统可以不仅提高可再生能源的消纳率，同时也可以降低系统运行成本，提高用户用能的满意度。

四、审核意见

承担单位意见	同意结题 盖　章 年　月　日
省科技厅主管处室意见	该项目已完成任务书规定目标任务，资料齐全，同意结题。 处室负责人签章：郭涛 盖　章 2023年 11月 29日
省科技厅发展规划处意见	同意结题 处室负责人签章：许瑞泉印 盖　章 年　月　日

甘肃省优秀研究生"创新之星"项目结题报告

项目编号：　　<u>2023CXZX-465</u>

项目名称：　<u>考虑系统不确定性的含共享储能</u>

　　　　　　<u>的综合能源系统优化控制</u>

项目负责人：　　<u>周　勃</u>

项目导师：　　　<u>李二超</u>

项目起止年限：　2023 年 1 月至 2023 年 12 月

兰州理工大学研究生院

二〇二三年制

一、受资助期间完成的主要工作（简述已完成的主要工作，并提供图片、典型数据等）

1 改进的时域鲁棒优化算法

本课题首先基于时域鲁棒优化算法（robust optimization over time, ROOT）提出以问题特征变化引导的动态时域鲁棒优化算法。依据其问题空间特征变化情况，找出了两个影响算法优化的重要指标：解在相邻环境下的目标函数的平均浮动值以及解在相邻环境下的目标函数的浮动值之和。算法在"生产时间"和"平均适应度"指标的基础之上，以当前动态环境下最优鲁棒解的值为度量基准，同时考虑相邻环境下解的目标函数平均浮动值以及浮动误差两个参数，由此来判断解的鲁棒性能好坏，从而达到减少误差的目的，从而更精确的获得符合实际工程要求的鲁棒解。

1.1 相邻环境下解的目标函数平均浮动值

定义相邻环境下解的目标函数平均浮动值计算公式如下：

$$\Delta f_{t(p:q)}^{a} = \frac{1}{p+q+1} \sum_{i=t-p}^{t+q} \left| f(x,\alpha_{i+1}) - f(x,\alpha_{i}) \right| \tag{1}$$

式中：$f(x,\alpha_i)$ 为第 i 个环境下的目标函数值；x 为决策变量；α_i 为时变参数；p,q,t 分别为历史环境个数、未来环境个数、当前环境时刻。当 $\Delta f_{t(p:q)}^{a}$ 较小时说明此时峰值坡度小，目标函数值变化慢；反之则表示目标函数值变化快。

1.2 相邻环境下解的目标函数浮动误差

$$\Delta f_{t(p:q)}^{+} = \sum_{i=t-p}^{t+q} \left(f(x,\alpha_{i+1}) - f(x,\alpha_{i}) \right) \tag{2}$$

当 $\Delta f_{t(p:q)}^{+}$ 为正时，说明目标函数值处于增长趋势；反之则表示目标函数值处于下降趋势。

1.3 问题特征变化引导的动态时域鲁棒优化算法

本课题所提算法根据求得的目标函数值 $f(x_t,\alpha_t)$，目标函数平均浮动误差 $\Delta f_{t(t_c-1:q)}^{a}$ 以及平均浮动值之和 $\Delta f_{t(t_c-1:q)}^{+}$，通过引入选择步骤，从而得到判断适应度函数 F 的选择策略，选择公式如下

$$
\begin{cases}
F = f\left(x_t, \alpha_t\right) - \dfrac{\eta(\Delta f^a_{t(t_c-1:q)} + E^{err})}{(t_c - 1)} & if \ \Delta f^+_{t(1:0)} < 0 \\[3mm]
F = f\left(x_t, \alpha_t\right) + \dfrac{\eta(\Delta f^a_{t(p:q)} - E^{err})}{(t_c - 1)} & if \ \Delta f^+_{t(1:0)} > 0 \\[1mm]
\&\& \ \Delta f^+_{t(0:q)} = q\Delta f^a_{t(0:q)} \\[2mm]
F = f\left(x_t, \alpha_t\right) - \dfrac{\eta(\Delta f^+_{t(t_c-1:q)} + E^{err})}{(t_c - 1)} & else
\end{cases}
\tag{3}
$$

算法步骤如下：

输入：动态单目标优化问题 $\max F(x) = f(x, \alpha_t)$

输出：每个环境 α_t 下的最优解 x_t 以及该解对应的目标函数值 $f(x_t, \alpha_t)$

Step1：设置粒子群算法种群规模 N，粒子维度 D，迭代次数 k，个体学习因子 c_1，群体学习因子 c_2，收缩因子 χ，粒子速度范围 $[-V_{\max}, V_{\max}]$；

Step2：初始化粒子群，获得初始化种群中每个粒子的位置和速度；

Step3：根据目标函数 $f(x_t, \alpha_t)$ 计算每个粒子在当前时刻 t_c 下的目标函数值 $f(x_{t_c}, \alpha_t)$ 以及前 t_i 个时刻下的函数值 $f(x_{t_i}, \alpha_{t_i})$，其中 $t_i \in [1, t_c-1]$；

Step4：判断当前时刻的目标函数值是否大于预先设定目标函数值的阈值 δ，若大于，则转至 Step5；否则，令适应度函数 F 为当前时刻对应的目标函数值，并转至 Step8；

Step5：由已知目标函数值计算出每个粒子在各相邻环境下的目标函数浮动值 Δf，该值由后一个环境下的目标函数值减去相邻前一个环境下的目标函数值计算；

Step6：用已知的 t_c-1 个历史目标函数平均浮动值作为训练数据来预测每个粒子在未来相邻动态环境下对应的目标函数平均浮动值 $\Delta f^a_{t(t_c-1:q)}$，并算出预测器的根的均方差 E^{err}；

Step7：根据求得的目标函数值 $f(x_t, \alpha_t)$，目标函数平均浮动值 $\Delta f^a_{t(t_c-1:q)}$ 及目标函数浮动值之和 $\Delta f^+_{t(t_c-1:q)}$，来判断适应度函数 F 选择策略，令 M=1,2,3 表示第①，②，③中策略，具体如下：

① $if \ \Delta f^+_{t(1:0)} < 0$，$F = f\left(x_t, \alpha_t\right) - \eta(\Delta f^a_{t(t_c-1:q)} + E^{err})/(t_c - 1)$；

② $else \ if \ \Delta f^+_{t(1:0)} > 0$ 且 $\Delta f^+_{t(0:q)} = q\Delta f^a_{t(0:q)}$，$F = f\left(x_t, \alpha_t\right) + \eta(\Delta f^a_{t(p:q)} - E^{err})/(t_c - 1)$；

③ $else \quad F = f(x_t, \alpha_t) - \eta(\Delta f^+_{t(t_c-1:q)} + E^{err})/(t_c - 1)$;

上式中 η 为差值调节算子，此处取 $\eta = 80$ ；

Step8：将 Step7 求得的适应度函数 F 代入粒子群算法中，计算每个粒子的适应度 P_fitness，保存每个粒子的最优位置 P_best，保存个体最佳适应度值 P_fitness 和群体最佳位置 G_best。

Step9：根据速度、位置更新公式更新 $V^{t_c+1}_{id}$ 和位置 $X^{t_c+1}_{id}$ ；

Step10：计算更新后每个粒子的适应度值 C_fitness，将每个粒子的当前适应度值 C_fitness 与其历史最优位置时的适应度 P_fitness 比较，如果较好，则将其当前的位置 C_best 作为该粒子的最优位置 P_best。

Step11：将每个粒子的最优位置对应的适应度值 P_fitness 与种群最佳适应度值 G_fitness 对比，如果更优，则更新种群最优位置 G_best 和最佳适应度值 G_fitness；

Step12：进行下一代进化，判断是否达到最大迭代次数，若达到则输出最优值，继续迭代，直到达到结束要求；

Step13：输出结果。

1.3 仿真与分析

为体现鲁棒解的平均性能，对求解结果计算平均值，并使用 Wilcoxon 符号秩对所有实验数据进行检查，表中对整体最优结果采用了阴影标记，对明显劣于最优结果的数据采用"*"标记，实验结果如下所示。

(a)阈值 40　　　(b)阈值 45　　　(c)阈值 50

图 1 M=1/不同阈值下生存时间

(a)阈值 40　　　(b)阈值 45　　　(c)阈值 50

图 2 M=2/不同阈值下生存时间

(a)阈值40　　　　(b)阈值45　　　　(c)阈值50
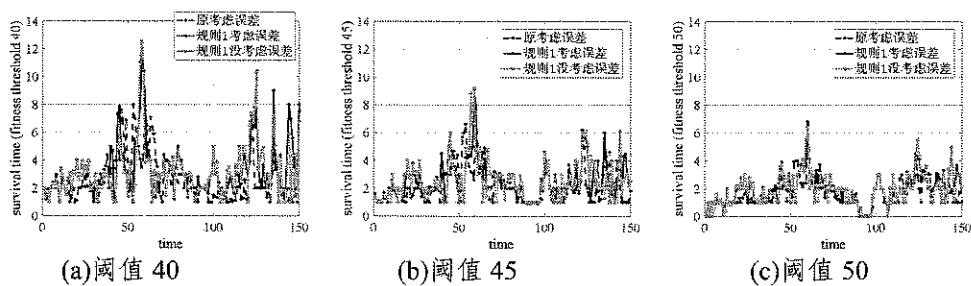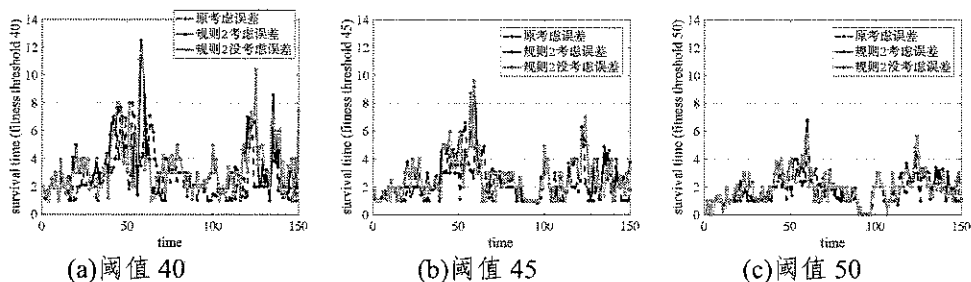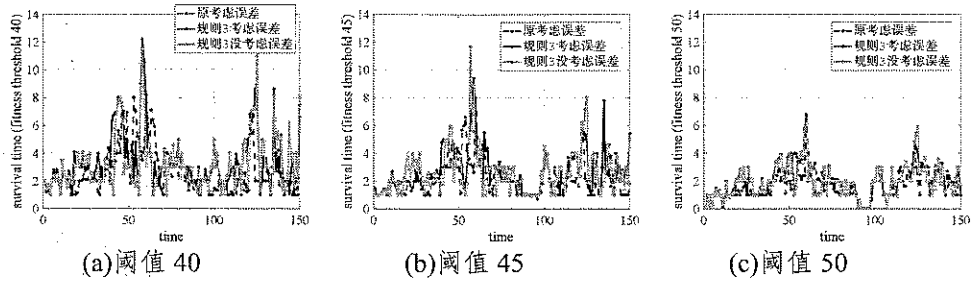
图 3 M=3/不同阈值下生存时间

表 1 不同算法的平均生存时间和平均适应度对比

算法	$\delta=40$	$\delta=45$	$\delta=50$	$T=2$	$T=4$	$T=6$
Jin's	1.53	1.11	0.69	25.32	22.20	18.46
Fu's($\theta=0$)	3.02	2.39	1.69	53.48	26.99	8.82
Fu's($\theta=1$)	3.01	2.49	1.72	50.15	4.91	-5.26
P's	1.35	1.21	1.02	48.88	45.31	40.58
Yazdani's	3.36	2.30	1.35	-	-	-
PCCG	3.78	3.01	2.05	50.16	27.29	25.68

针对其固定阈值下生存时间的性能度量，三种不同决策规则分别在阈值为40、45和50时，与Fu的算法进行比较的情况分别如图1、图2、图3。并在不同算法上进行平均生存时间和平均适应度性能对比，具体如表1所示，其生存时间性能具有明显提升。

2 考虑不确定性的含热电混合共享储能双层优化配置方法

2.1 含热电混合共享储能系统建立

冷热电联供系统(combined cooling heating and power, CCHP)能够实现冷热电能互补协同工作，提高能源利用率，在满足用户多种能源梯级利用的同时提高供能的经济性与可靠性。本文构建的CCHP系统结构如图4所示。
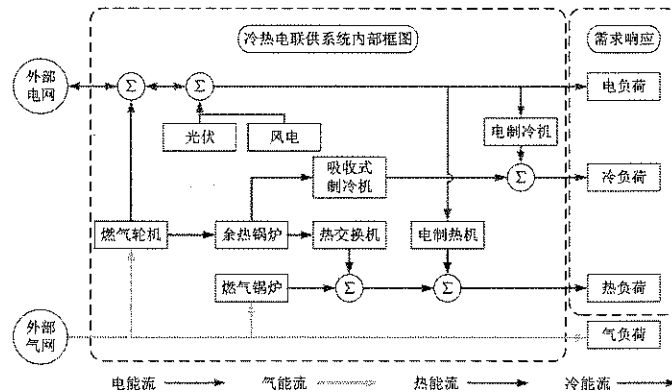
图 4 CCHP 系统结构图

CCHP与外部电网双向连接，即在电能不足时可以从外部电网购买电能，而在电能充裕时，可以将多余电能出售给外部电网。
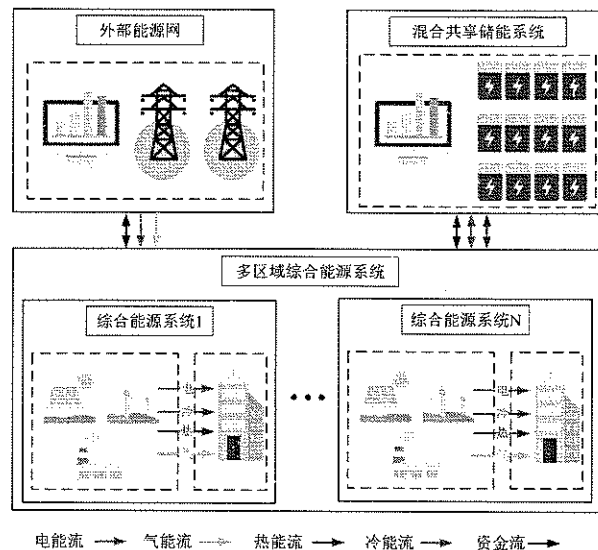
图5 含混合共享储能的多区域综合能源系统框架

如图5所示为含混合共享储能的区域综合能源系统框架，整个系统包含三个主体：外部能源网，混合共享储能系统以及多区域综合能源系统。各主体运营模式简述如下：外部能源网是系统中稳定的能源供应者，区域综合能源系统向外部能源网购买电、气等能源来保证自身稳定，同时根据能源交易量向外部电网支付购能费用，外部能源网与混合共享储能之间不产生能源交易行为。混合共享储能系统向区域综合能源系统提供储能容量租赁服务，通过能量购入/出售差价赚取自身收益，能源充裕的区域可将多余的电/热能源出售给混合共享储能，而能源匮乏的区域可以从混合共享储能系统处购买所需电/热能源。区域综合能源系统的目标是在保证自身负荷得到满足的情况下，实现自身运营成本最优。

2.2 双层优化配置模型建立

双层优化可以很好的解决不同主体在互相耦合的情况下同时寻求各自模型最优决策解的优化问题。本文双层规划问题结构如图6所示，其中上层模型以混合共享储能系统容量配置以及功率配置为决策变量，以年时间尺度运行成本为优化目标。下层模型以多区域综合能源系统各设备出力为决策变量，以日时间尺度运行成本最优为优化目标。上层模型依赖下层模型的决策解，而下层模型的决策解受到上层模型的决策变量影响。
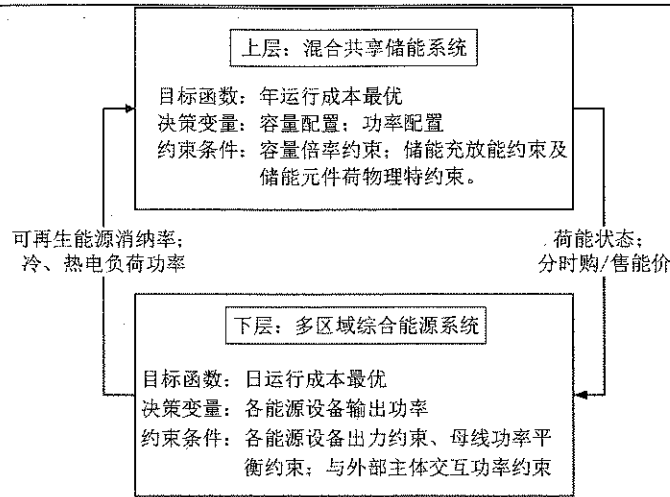
图 6 双层规划模型

2.2.1 上层混合共享储能系统规划模型

上层优化目标函数为混合共享储能系统年运营成本最，即

$$\min f_{HESS} = \sum_{w=1}^{W} \left[T_d \left(C_{inv,w} + C_{main,w} + C_{hess,b,w} - C_{hess,s,w} - C_{ser,w} \right) \right] \quad (4)$$

式中：$C_{inv,w}$、$C_{main,w}$、$C_{hess,b,w}$、$C_{hess,s,w}$、$C_{ser,w}$ 分别为混合共享储能系统每个典型日的平均投资成本、平均维护成本、从多区域综合能源系统购能成本、向多区域综合能源系统售能收益、混合共享储能服务费收益。

$$C_{inv,w} = \sum_{k=1}^{K} \left(\frac{\omega_{cap}^k W_{cap}^k + \omega_{pow}^k W_{pow}^k}{T_n} \right) \quad (5)$$

$$C_{main} = \sum_{k=1}^{K} \omega_{main}^k W_{pow}^k \quad (6)$$

$$C_{hess,b,w} = \sum_{t=1}^{T} \sum_{i=1}^{N} \sum_{k=1}^{K} \left[\delta_k(t) P_{hess,b,w}^{i,k}(t) \right] \Delta t \quad (7)$$

$$C_{hess,s,w} = \sum_{t=1}^{T} \sum_{i=1}^{N} \sum_{k=1}^{K} \left[\gamma_k(t) P_{hess,s,w}^{i,k}(t) \right] \Delta t \quad (8)$$

$$C_{ser,w} = \sum_{t=1}^{T} \sum_{i=1}^{N} \sum_{k=1}^{K} \left\{ \theta_k(t) \left[P_{hess,b,w}^{i,k}(t) + P_{hess,s,w}^{i,k}(t) \right] \right\} \Delta t \quad (9)$$

2.2.2 下层优化目标函数

下层优化目标为多区域综合能源系统年运行成本最优，即

$$\min C_{HIES} = \sum_{w=1}^{W} \left[T_w \left(C_{grid,w} + C_{fuel,w} - C_{mess,b,w} + C_{mess,s,w} + C_{serve,w} \right) \right] \quad (10)$$

式中：$C_{grid,w}$、$C_{fuel,w}$ 分别为多区域综合能源系统每个 类型典型日从外部能源网

购买电能的支出以及购买天然气的支出。

$$C_{grid,w} = \sum_{t=1}^{T} \sum_{i=1}^{N} \left[\alpha(t) P_{grid,w,s}^i(t) \right] \Delta t \tag{11}$$

$$C_{fuel,w} = c_{gas} \sum_{t=1}^{T} \sum_{i=1}^{N} \left\{ \left[\frac{P_{gt,w}^i(t)}{\eta_{gt}^i L_{ng}} + \frac{Q_{gb,w}^i(t)}{\eta_{gb}^i L_{ng}} \right] \right\} \Delta t \tag{12}$$

2.3 求解算法

由于区域综合能源系统内部的可再生能源出力具有随机性及波动性，因此上述双层模型中下层优化模型是动态的，基于期望值的优化方法在这种情况下不适用。以控制理论角度来看，可以将该问题视作是一个含时变参数的动态优化问题，因此引入时域鲁棒优化算法进行求解，然而下层优化问题由于涉及到可再生能源随机性，很难找到一个显示函数来评估解的适应度，因此本文在传统 ROOT 算法的基础上，提出了基于问题特征变化引导的改机时域鲁棒优化算法，算法详细内容见第一部分。

3 算例分析

3.1 算例描述

算例假设某地存在由 IES-1，IES-2，IES-3 三个区域综合能源系统组合而成的 MRIES，结构如图 5 所示。各 IES 之间互不相连，IES 内部结构如图 4 所示。各 IES 一年之中四个典型日的光伏、风电最大预测出力数据和冷热电负荷预测数据见图 7。
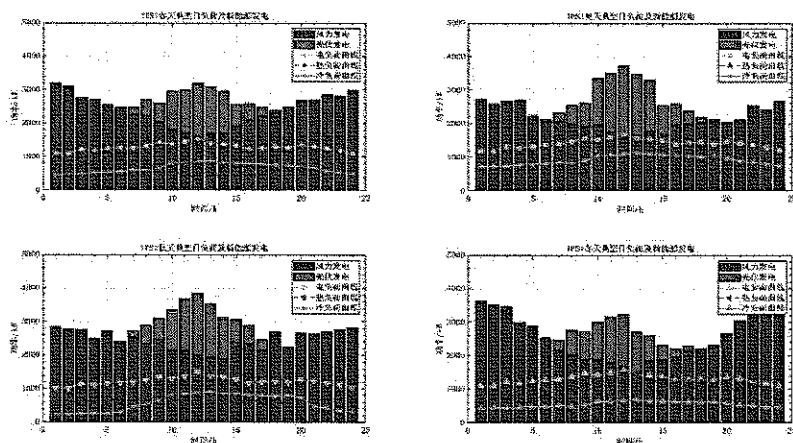
图（a）IES1 负荷功率曲线及可再生能源功率曲线
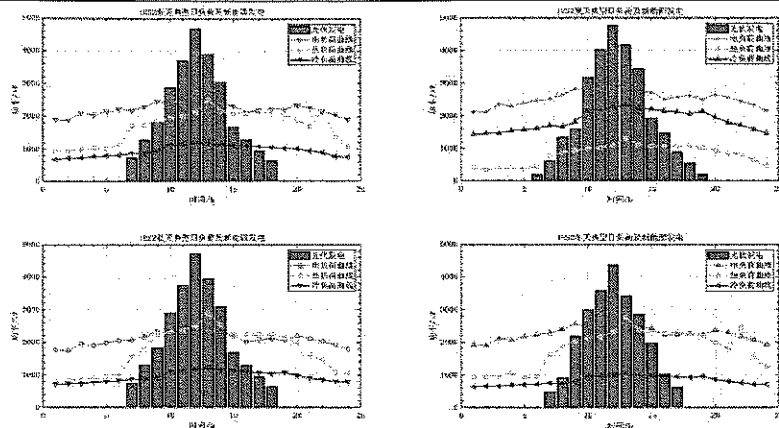
图（b）IES2 负荷功率曲线及可再生能源功率曲线
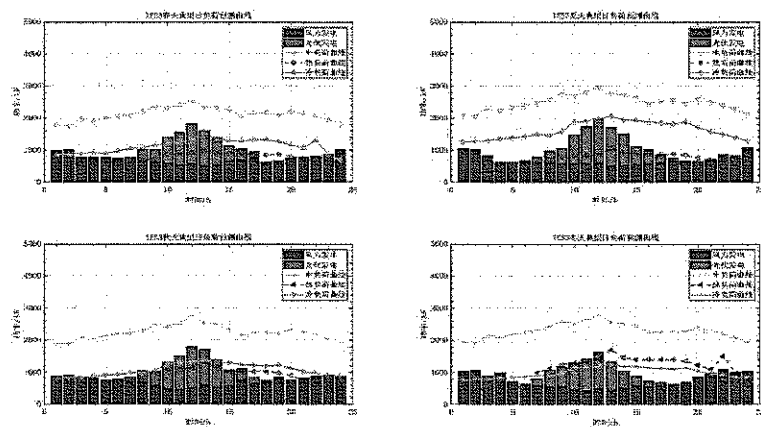
图（c）IES3 负荷功率曲线及可再生能源功率曲线

图 7 各 IES 各季节典型日负荷功率曲线及可再生能源功率曲线

3.2 结果分析

3.2.1 混合共享储能配置结果

为研究本项目所提算法对混合共享储能容量配置的影响，算例设置如下场景：

场景 1：不考虑本项目所提算法的情况下进行混合共享储能容量配置计算；

场景 2：考虑本项目所提算法的情况下进行混合共享储能容量配置计算；

以场景 2 为例进行说明，在考虑本项目所提算法的情况下，混合共享储能系统充放能优化结果如图 8(a)，8(b)所示。定义混合共享储能系统充入能量为正，表示此刻综合能源系统将能量存储进混合共享储能；混合共享储能系统释放能量为负，表示此刻综合能源系统将能量由混合共享储能系统取回。混合共享储能系统储电设备的配置结果：最大充放电功率为 6526.44kW，最大储电容量为 26117.36kW·h。由图 8(a)可知，混合共享储能系统夏季典型日中午 13:00 达到储电站最大充电功率，

在夏季典型日 17:00 达到储电站最大放电功率。混合共享储能系统蓄热设备配置结果为：最大蓄放热功率为 3550.71kW，最大蓄热容量为 8494.21kW·h，由图 8(b) 可知，混合共享储能系统在冬季上午 09:00 及 11：00 达到蓄热站最大蓄热功率，在冬季下午 13:00 达到蓄热站最大放热功率。
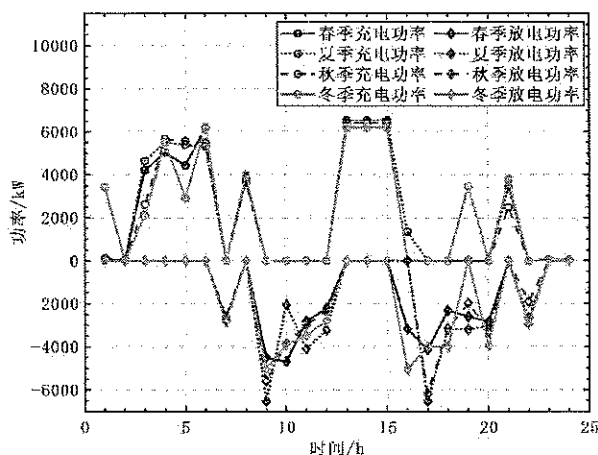
(a) HSESS 典型日充放电功率图
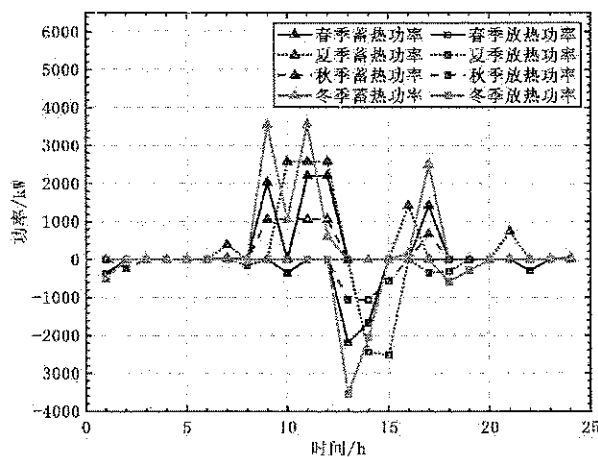
(b) HSESS 典型日充放热功率图

图 8 HSESS 电热储能容量配置优化结果

各场景下混合共享储能系统的容量配置结果，混合共享储能系统的年收益以及综合能源系统的年运行成本如表 2 所示。
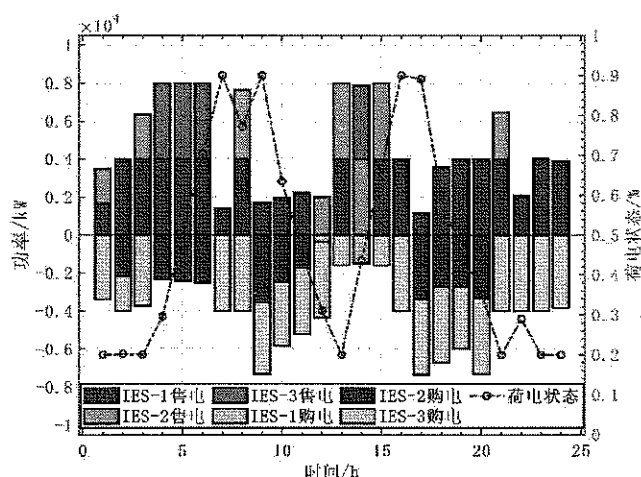
表 2 各场景下的对比结果

项目	场景 1	场景 2	变化率
储电设备容量配置结果	27031.66 kWh	26117.36kWh	-3.4%
储电设备功率配置结果	6754.92kW	6526.44kW	-3.4%

| 蓄热设备容量 配置结果	9116.13 kWh	8494.24 kWh	-6.8%
蓄热设备功率 配置结果	3810.09kW	3550.17kW	-6.8%
HSESS 年收益	843.21 万元	897.97 万元	+6.5%
MRIES 年运行成本	3678.19 万元	3606.16 万元	-4.3%

由表 2 可知，通过本项目所提算法对各综合能源系统内可再生能源出力的不确定性进行优化计算后，有效降低了混合共享储能系统的电/热储能配置容量，这对于混合共享储能系统来说，其初始投资成本以及日常维护成本得到优化，后期可以更快回收投资成本；对于综合能源系统来说，其向混合共享储能系统缴纳的电/热服务费减少，使自身运行成本得到降低，在满足负荷需求的前提下每日运行更经济。

3.2.2 混合共享储能运行结果分析

在秋季典型日下混合共享储能运行优化结果如图 9 所示。由图 9(a)荷电状态可知，在每个典型日下，混合共享储能系统都是在用能高峰期前尽可能的达到荷电峰值，以保证在综合能源系统用能高峰期时有能可供。由图 9(b)可知，由于 10:00-16:00 是每个典型日内气温较高的时段，此时其热负荷需求量较低，同时此时整个综合能源系统内部不仅有风电出力，而且此时光伏也达到了每个典型日内的出力峰段，因此此时综合能源系统尽可能多的使用电制热设备来产生热能并存储进混合共享储能系统，在减少使用燃气降低碳排放的同时，消纳自身可再生能源。

(a) 混合共享储能秋季典型日下充放电运行优化结果
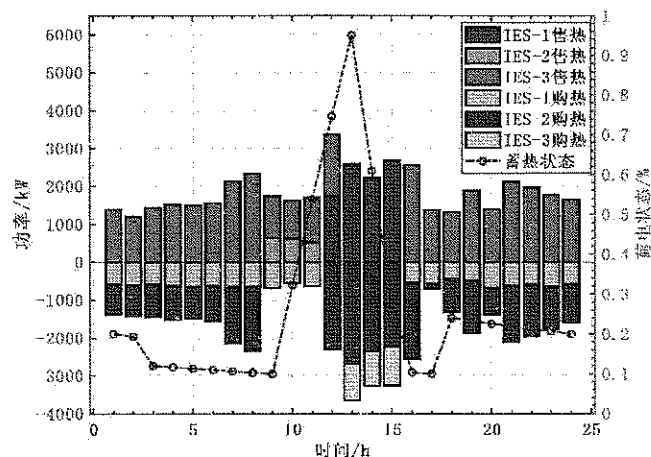
(b) 混合共享储能秋季典型日下充放热运行优化结果

图 9 混合共享储能秋季典型日下运行优化结果

为研究混合共享储能配置热储能设施对自身经济性的影响，算例设置如下场景：

场景 1：混合共享储能仅考虑配置电储能不考虑配置热储能；

场景 2：混合共享储能同时考虑配置电-热储能。

表 3 各场景下的对比结果

混合共享储能成本项目	场景 1	场景 2	变化率
典型日投资运维成本	11089.45 元	13500.95	+21.7%
典型日购能成本	53623.79 元	65358.27	+21.9%
典型日售能成本	67407.17 元	81546.34	+21.1%
典型日服务费	5112.26 元	6810.16	+33.2%
典型日最优收益	7869.19 元	9769.84	+24.2%

各场景下混合共享储能系统每日收益如表 3 所示，由表 3 可知，由于场景 2 相比场景 1 增加了热储能，因此其每个典型日的投资运维总成本上升 21.7%。但由于增加了热储能，通过合理使用热电耦合的手段，混合共享储能与综合能源系统交互的方式更加多样化，因此购售能差值由场景 1 的仅考虑电交互的 13846.38 元上升至场景 2 同时考虑电热交互的 16118.07 元，上升 16.9%。相比于仅配置电储能，同时配置电-热混合储能的最优收益上升 24.2%。目前热、冷储能技术已相对成熟，功率成本及容量成本低于电储能，而能源用户对于多种能源的需求却更加旺盛，因此多能源混合储能能够为运营商提供更加丰厚的收益回报。

二、受资助期间，取得的研究成果，包括发表或正式录用核心及以上刊物（正刊）科技论文、已完成创新性产品或实物模型、获奖情况及发明专利等

1、第十九届机器学习会议发表会议论文 1 篇；

2、《Lecture Notes in Electrical Engineering》期刊正式录用论文 1 篇；

三、项目全体成员（此项须与任务书保持一致）

姓名	职称	职务	身份证号	所在单位
周勃	工程师	项目负责人	620102198911135310	兰州理工大学
钟昕妤	工程师	算法编写	53030219990719002X	兰州理工大学
李双	工程师	模型建立	130682199903144222	兰州理工大学
吴煜	工程师	理论分析	620123200008092125	兰州理工大学

三、项目经费支出情况（单位：万元）

购置设备费：0.2

差旅费：0.1

会议费：0.1

出版/文献/信息传播费：0.4

项目导师意见	同意结题 签字：李□□ 2023年11月21日
学院（部）意见	同意结题 主管领导签字（公章）：李□□ 2023年11月21日
研究生院意见	同意结题 负责人签字（公章）： 2023年2月1日

备注：本结题报告一式三份。